UNIVERSITÀ
DI PAVIA
PhD IN BIOMEDICAL SCIENCES
DEPARTMENT OF BRAIN AND BEHAVIORAL SCIENCES
UNIT OF NEUROPHYSIOLOGY

A DEEPER INSIGHT INTO THE CEREBELLAR NETWORK FUNCTION: EXPLORING THE INPUT PROCESSING AND ITS LEVEL OF COMPLEXITY

PhD Tutor: Prof. Egidio D'Angelo

PhD Tutor: Dott.ssa Lisa Mapelli

PhD dissertation of
Monteverdi Anita

Academic year: 2020-2021

... A Massimo ...

“Ogni uomo è una scintilla nel buio,

che ci sia concesso di splendere”

,

Contents

1. Introduction

In humans the cerebral cortex represents 82% of total brain mass holding 16 billion neurons. The cerebellum covers 10% of total brain mass, holding 69 billions neurons (Herculano-Houzel 2009). Thus, despite the volumetric preponderance of the cerebral cortex, the 80% of all brain neurons in humans is located in the cerebellum. This neuronal fraction is maintained across species (from rodents to primates), and an increase in brain size is accompanied mainly by an increase of the cerebral cortex relative size. The cerebellum in fact keeps a constant relative size across species, but it has been demonstrated that the numerosity of neurons in the cerebral and cerebellar cortices varies together, presenting a ratio of 3-4 neurons in the cerebellum for every neuron in the cerebral cortex (Herculano-Houzel 2010). This coordinated scaling supports the joint evolution of the two structures, highlighting the importance of their functional relationship not only for sensorimotor control. Indeed, an increased amount of studies is recently suggesting a cerebellar involvement in higher cognitive functions (D'Angelo 2019). A deeper investigation of cerebellar network functioning and its level of complexity can shed new light on the neuronal mechanisms underlying its processing as a motor controller and beyond.

1.1 Cerebellar anatomy and network organization.

The cerebellum is located in the posterior fossa and connected to the brainstem through three pairs of peduncles (inferior, middle and superior). It consists of an outer layer of tightly folded gray matter surrounding a highly branched white matter in which three deep cerebellar nuclei (DCN) are embedded. Several fissures originate ten transverse lobules identified by Roman numerals (Fig. 1.1). Two of these fissures, the primary fissure and the posterolateral fissure, are deeper than the others and divide the cerebellum into three lobes: the anterior lobe, the posterior lobe and the flocculonodular lobe (Fig. 1.1). In addition, three other regions can be identified longitudinally on each side of the midline: the vermis, the paravermis and the hemisphere.

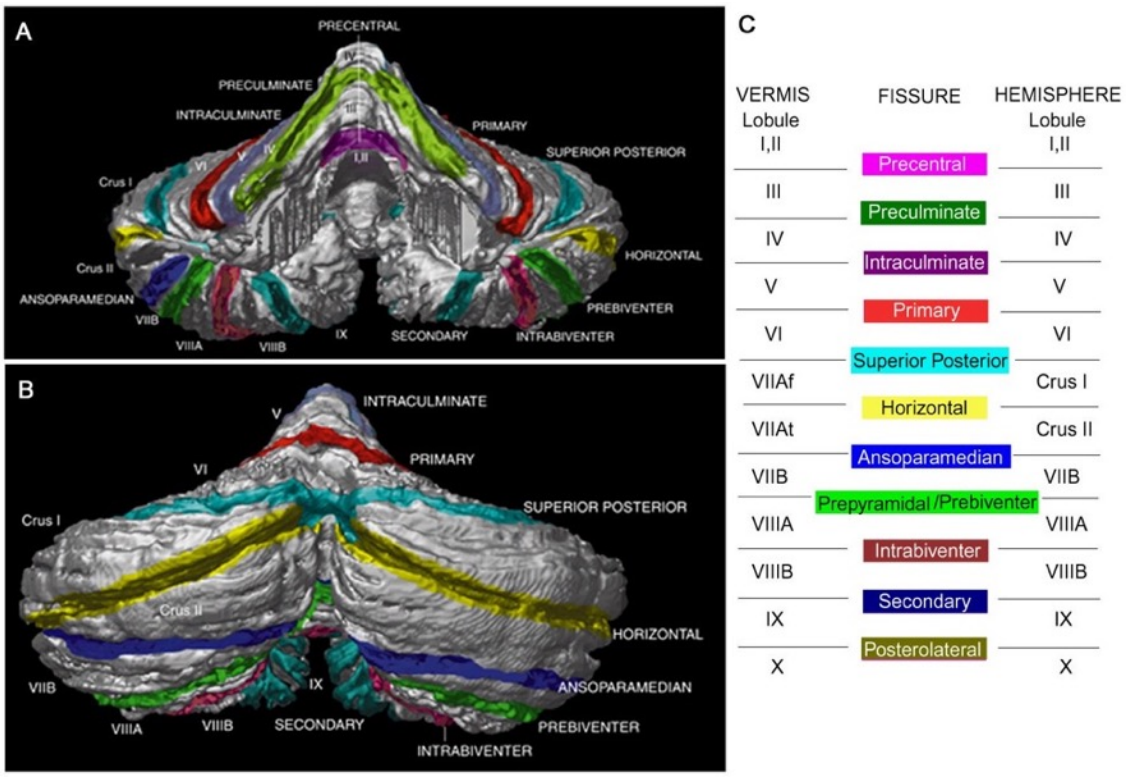

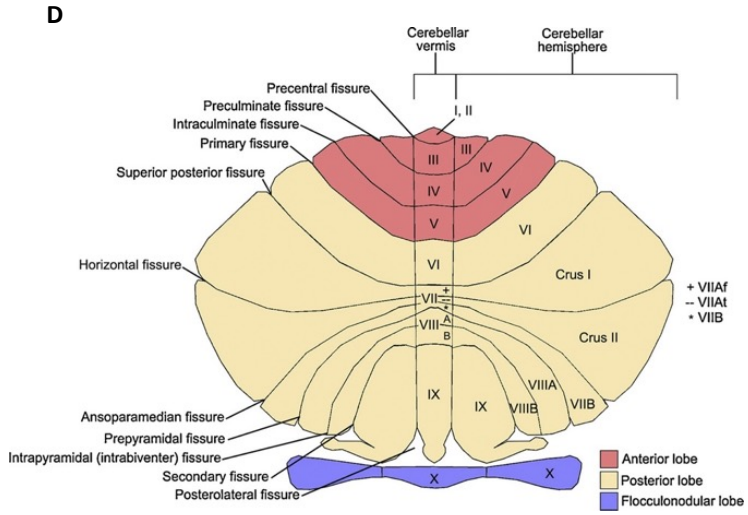

Fig. 1.1| Cerebellar anatomy. Figures A and B show a three-dimensional reconstruction of human cerebellum from MRI (A=anterior view; B=posterior view) highlighting with different colors all the fissures characterizing its external surface. Table C contains the color-code used in figures A and B adding the Roman numerals for lobules identification (Stoodley and Schmahmann 2010). In figure D the cerebellum with its major fissures, lobes and lobules is represented in a flattened and schematic view. Its longitudinal subdivision (vermis and hemispheres) is specified, too (Schmahmann 2019).

These regions are functionally segregated, presenting different afferent projections. The vermis and the paravermis in fact, regarded as the spinocerebellum, receive extensive somatosensory information from the trunk and limbs through the spinocerebellar tract, and from the head and face through the trigeminocerebellar tract (Roostaei et al. 2014). In particular, the spinocerebellar tract terminates in lobule VIII, while the trigeminocerebellar tract primarily projects to lobule V and VI (Stoodley and Schmahmann 2010). These lobules receive connections from the motor cortex. The prefrontal cortex mainly targets the so called cerebrocerebellum, composed by the cerebellar hemispheres (Fig. 1.2). In particular, physiological studies confirm a significant connection with cerebellar lobules CrusI and CrusII (Kelly and Strick 2003). The cerebellar connections to nonmotor areas seem to be more extended than the ones involved in sensory-motor control, in humans (Palesi et al. 2015).

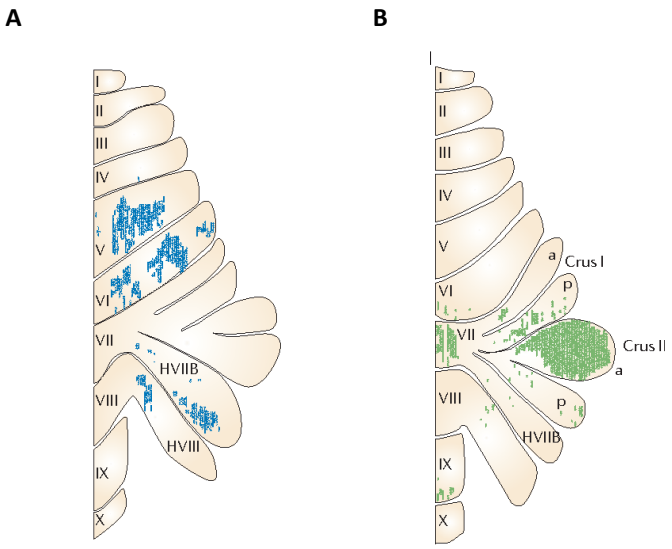

Fig. 1.2| Different afferent projections to cerebellar vermis and hemispheres. A) Motor cortex connections with cerebellar lobules V and VI, with some extension into hemispheres lobule VIIB and VIII. **B)** Prefrontal cortex main connection with cerebellar lobules CrusI and CrusII (Ramnani 2006).

At the microscopic level, the cerebellum presents a similar microcircuit structure across the entire cortex (D'Angelo and Casali 2012). The cerebellar cortex is composed by three layers: the molecular layer (ML), the Purkinje cell layer (PCL) and the granular layer (GL) (Fig. 1.3).

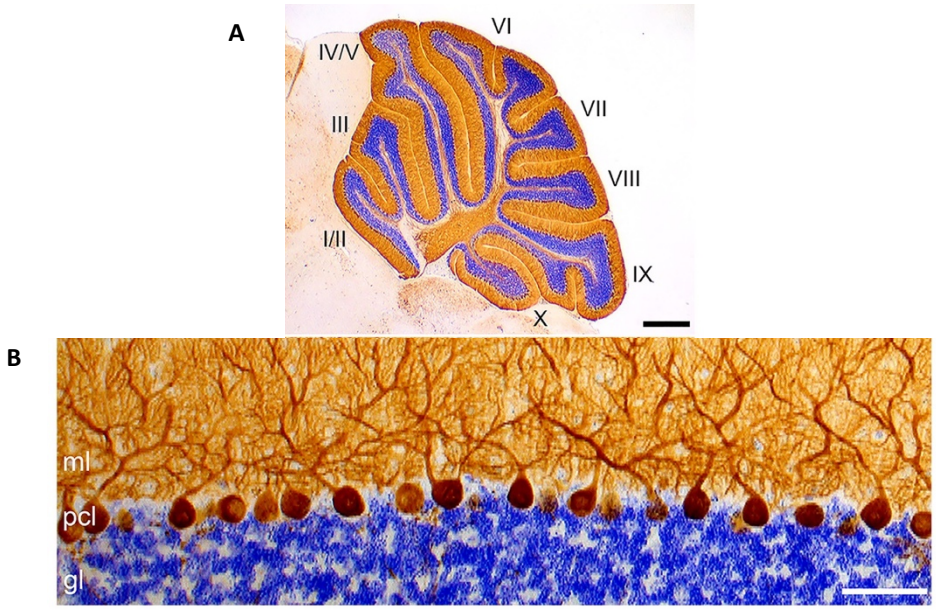

Fig. 1.3| Cerebellar cortical layers (Lackey, Heck and Sillitoe 2018). **A)** An example of a sagittal histologic section from a mouse cerebellum showing the layers of the cerebellar cortex. Granule cells are labeled using Nissl stain, while Purkinje cells are labeled using calbindin immunohistochemistry. **B)** A magnified view of A (scalebar shift from 500 μm to 50 μm) highlighting the granular layer (gl), the Purkinje cells layer (pcl) and the molecular layer (ml).

Mossy fibers (MFs) and climbing fibers (CFs) convey the primary inputs to the cerebellum both using glutamate as neurotransmitter. The GL contains three main types of neurons: the granule cells (GrC), the Golgi cells (GoC) and the Lugaro cells (LC). Another type of excitatory cell is called Unipolar Brush cells (UBC), present mainly in the vestibulocerebellum (flocculonodular lobe) GL. MFs contact GrC, which send their excitatory output into the ML and receive inhibition from GoC both in a feedforward and a feedback loop (Prestori, Mapelli and D'Angelo 2019). GoC are typically autorhythmic, generating spikes in the range of 1-10Hz, communicate with each other through gap junctions (D'Angelo 2018), and use both GABA and glycine as neurotransmitters. Their activity can be modulated by LC GABA/glycine outputs (Prestori et al. 2019). LC are normally silent in the GL, but especially in presence of serotonine, they become intensively active determining GoC inhibition and the modulation of molecular layer interneurons (MLI) in the ML. LC probably receive an excitatory input through MFs, but this kind of connection is not yet well defined (D'Angelo 2011).
The signal processed by the GL is then conveyed to the ML. GrC axons pass radially the PCL, reach the ML and branch transversally originating the parallel fibers (PFs). These fibers contact and activate

numerous Purkinje cells (PC), conveying the signals generated by GrC (D'Angelo 2011). PC show an autorhythmic activity at about 50Hz, and receive other two excitatory inputs in addition to the PFs one: the first from the GrC ascending axon (Walter, Dizon and Khodakhah 2009), and the second from CFs coming from the Inferior Olive (IO). While a massive number of PFs inputs reach PC generating simple spikes, each PC generates complex spikes in response to the activity of a single climbing fiber (D'Angelo 2011). PCs are GABAergic, and inhibits DCN neurons, which originate the cerebellar output to other brain areas. The activity of PC can be inhibited by the MLI: stellate cells (SC) and basket cells (BC). These cells are both GABAergic and can be excited by PFs activity. The SC are located in the outer part of the ML, are characterized by an autorhythmic activity (about 10Hz) and inhibit PC dendrites. BC instead are positioned in the deeper ML, inhibiting PC soma and parainitial segment (D'Angelo 2018). Moreover, PFs activated GoC, determining a feedback inhibition onto GrC (Fig. 1.4).

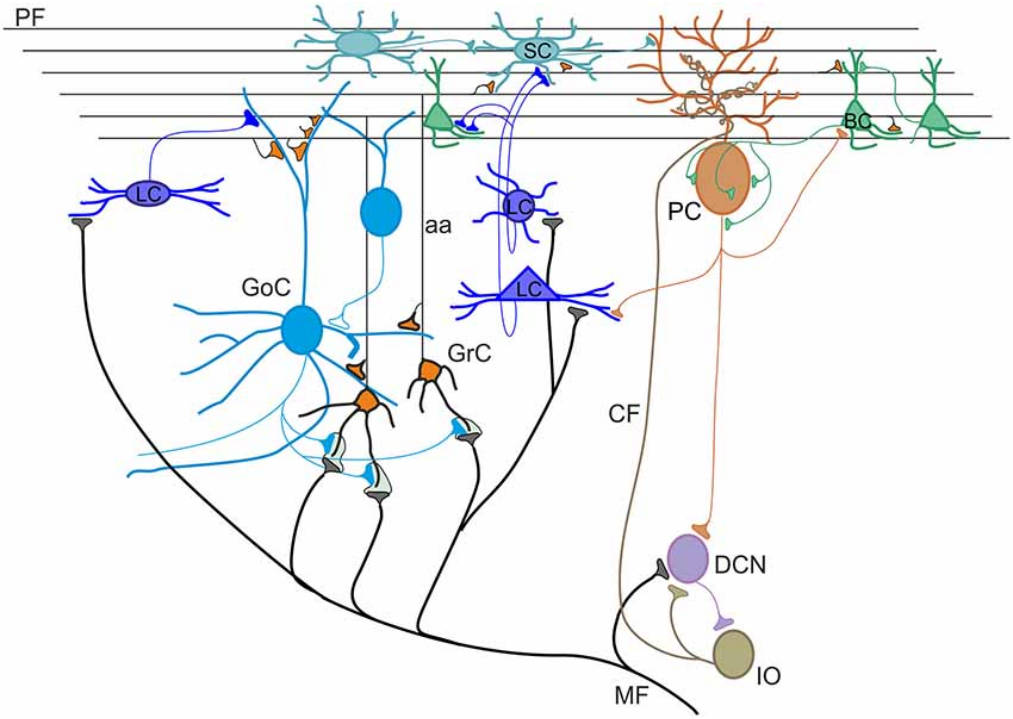

Fig. 1.4| The cerebellar microcircuit (Prestori et al. 2019). Mossy fibers (MF) convey an excitatory input in the granular layer, contacting granule cells (GrC), Golgi cells (GoC) and Lugaro cells (LC). GoC exert a feedforward and a feedback inhibition onto GrC, while Lugaro cells can inhibit GoC and Molecular layer interneurons (MLI) (stellate cells (SC) and basket cells (BC)). GrC axon (aa) passes vertically the Purkinje cells layer and reaches the molecular layer originating parallel fibers (PF). These fibers make excitatory synapses onto Purkinje cells (PC), which consequently inhibit Deep Cerebellar Nuclei (DCN). PC receive a massive number of parallel fibers synapses and one single climbing fiber (CF) synapse originating from the inferior olive (IO). The activity of PCs is under the inhibitory control exerted by SC and BC. From DCN the cerebellar output is conveyed to other brain areas.

In this multi-neuronal chain, both excitation and inhibition appear to cooperate in order to determine the cerebellar output. However, several aspects of this complex signal processing still need further investigation.

1.2 Cerebellar cortex input processing.

MFs usually convey bursts of frequency-modulated discharges to the cerebellum (Rancz et al. 2007, Chadderton, Margrie and Häusser 2004). Incoming signals are processed at first in the granular layer microcircuit, which is located at the cerebellar input stage and integrates inputs showing multiple dynamic properties (D'Angelo et al. 2009, Courtemanche, Robinson and Aponte 2013). The simultaneous activation of GrC and GoC allows the spatio-temporal reconfiguration of the incoming input (D'Angelo 2011). As a whole, the main mechanisms to exert this kind of control are: the time-window effect, the regulation of signal transmission gain, the center-surround organization, the combinatorial rearrangement of granular layer activity and the impact of synaptic plasticity at the mossy fibers-granule cells relay.

The time-window effect is strictly dependent on GoC feedforward inhibition (D'Angelo and De Zeeuw 2009). MFs bursts in fact determine the simultaneous activation of GrC and GoC engaging the feedforward inhibitory loop, but the combination of multiple transmission delays along the mossy fiber-Golgi cell-granule cell pathway generates a permissive "time window" of 5 ms. This enables GrC to fire 1-3 spikes before GoC inhibition prevalence.

Long-term synaptic plasticity can contribute, together with the time-window mechanism, to shape GrC responsiveness. Long-term potentiation (LTP) and long-term depression (LTD) in fact play a pivotal role in the control of GrC first spike delay (Nieus et al. 2006). Thus, LTP and LTD at the mossy fibers-granule cells relay cooperate in setting the number of spikes emitted by GrC in the permissive time window. This kind of mechanism is commonly referred to as window-matching effect (D'Angelo et al. 2009).

The coordination of time-window and window-matching operations have a profound impact on bursts retransmission toward the molecular layer, favoring short bursts for information transfer (Arleo et al. 2010).

Both the components of GoC inhibition, called phasic and tonic (Fig.1.5) (Mapelli, Solinas and D'Angelo 2014), play a role in shaping granular layer activity. The first component is based on vesicular γ-aminobutyric acid (GABA) release from GoC pre-synaptic terminal, and regulates the delay and precision of GrC firing (Nieus, Mapelli and D'Angelo 2014). The second component depends on the level of tonic GABA, present at the synaptic cleft and able to activate extra-synaptic GABA-A receptors, and exerts a control on synaptic transmission gain at the mossy fibers-granule cells connection (Mitchell and Silver 2003). Acting together, these mechanisms of synaptic inhibition are able to tune the excitability of GrC and improve the information transfer. In addition, burst transmission shows a marked frequency-dependence, and the granular layer acts as an high-pass filter enhancing the retransmission to the molecular layer of high-frequency bursts (above 50Hz) (Mapelli, Gandolfi and D'Angelo 2010b). In this operation, NMDA receptors appear to be involved (D'Angelo and Rossi 1998, Mapelli et al. 2010b, Solinas, Nieus and D'Angelo 2010), suggesting that excitation concurs in balance with inhibition in the regulation of the temporal dynamics of input processing.

The innerving territories of GoC axons determine lateral inhibition, which plays a critical role in the center-surround organization of granular layer responses (Mapelli and D'Angelo 2007). Stimulation of MFs results in the activation of the granular layer showing a center-surround organization, in which excitation prevails in the core while inhibition prevails in the surrounding areas, in a classic "Mexican hat" profile (Mapelli and D'Angelo 2007, Gandolfi et al. 2014). Interestingly, this organization allows particular signal transmission properties: the center enhances spike bursts with an higher frequency and a shorter delay compared to the surround (Fig. 1.6) (Solinas et al. 2010), with strong excitation

in the core favoring long-term potentiation and weak excitation in the surround favoring long-term depression (D'Angelo et al. 2013). In addition to the center-surround structure, the variable arrangement of synaptic contacts provides the basis for combining responses in the granular layer (Mapelli, Gandolfi and D'Angelo 2010a). The different convergence of MFs onto GrC or GoC gives rise to areas of combined excitation and combined inhibition after MFs stimulation, which additionally configure the topological organization of granular layer activity.

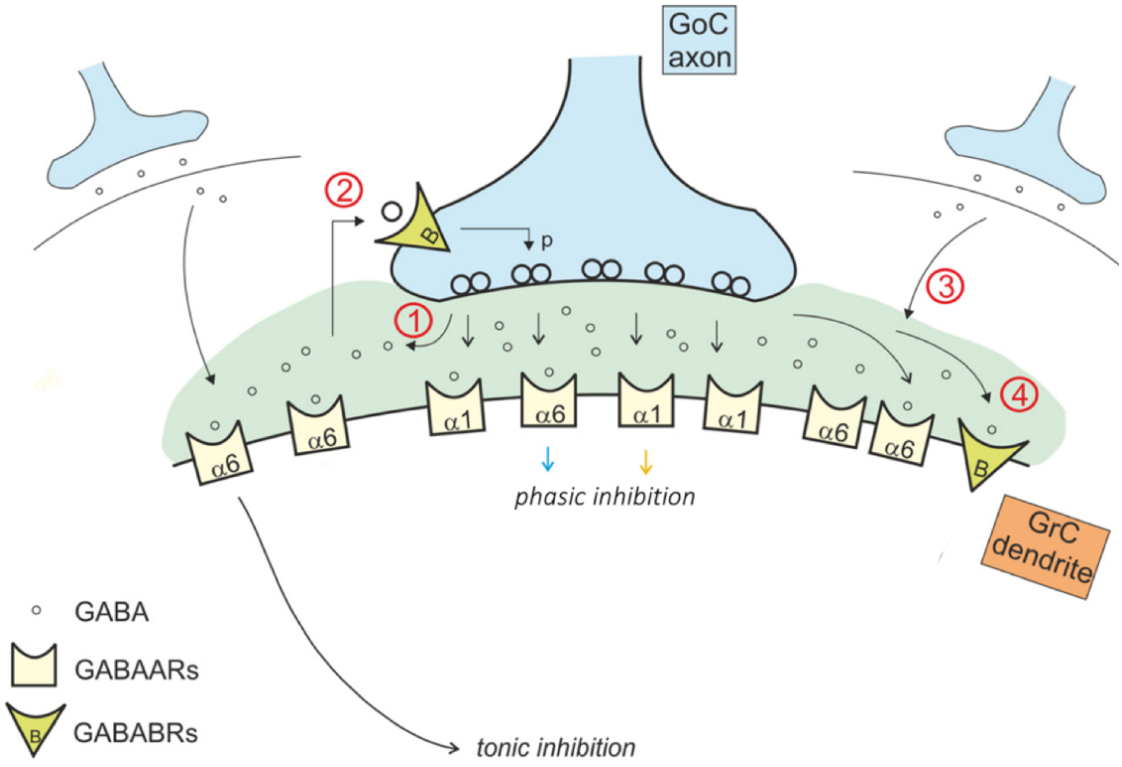

Fig. 1.5| Schematic representation of phasic and tonic inhibition mechanisms (Mapelli et al. 2014). 1) Direct release of GABA from Golgi cell terminals during phasic inhibition activates α1 and α6 subunits containing GABA-A receptors. 2) The tonic level of GABA affects α6 extra-synaptic GABA-A receptors and pre-synaptic GABA-B receptors, modulating the release probability. 3) The spillover from neighboring synapses contributes to tonic GABA level. 4) Tonic and phasic sources of GABA can activate GABA-B post-synaptic receptors and influence granule cells excitability.
As a whole, the granular layer enhances signals transmission through the control of the balance between all these inhibitory mechanisms and the excitatory ones.

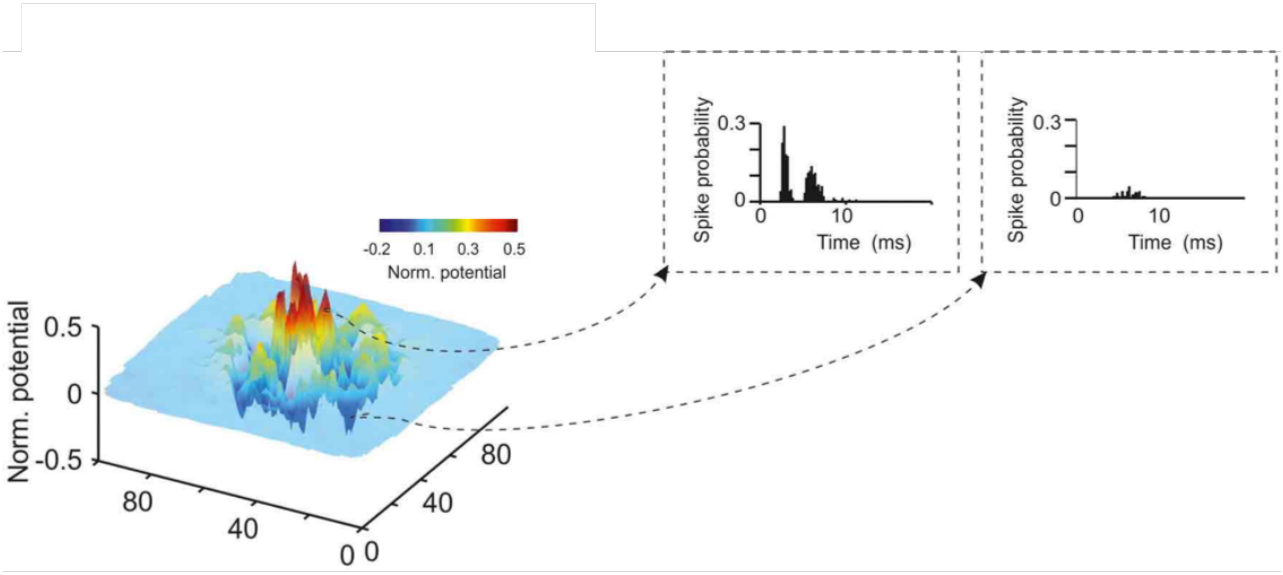

Fig. 1.6| The center surround organization of granular layer activity (D'Angelo et al 2013). Mossy fibers stimulation generates a center-surround structure, due to Golgi cells lateral inhibition. The spatial organization of the excitatory/inhibitory balance (on the left) reveals that inhibition especially reduces excitation around the core of the activated area, determining a Mexican hat profile. Interestingly, this network topology impacts on granular layer responses (on the right). As it can be observed, granule cells responses in the center present a shorter latency and a higher number of spikes than in the surrounding area.

A further contribution to this complex input processing comes from synaptic plasticity at the mossy fibers-granule cells relay (D'Angelo et al. 2009). A bidirectional synaptic plasticity has been indeed demonstrated at the cerebellum input stage, modulated by MFs discharge rates (D'Errico, Prestori and D'Angelo 2009), and correlated with the duration of the stimulus train (Gall et al. 2005). Additionally, both LTP and LTD occurring at the mossy fibers-granule cells synapses have been associated with changes of GrC intrinsic excitability (Sola et al. 2004, Gall et al. 2005, Nieus et al. 2006), supporting the role of plasticity in shaping the network activity and impact on the timing of GrC responses.

In addition to all these mechanisms, the granular layer is able to organize inputs processing following specific cellular properties of its components. This layer in fact appears to be well equipped for the development and maintenance of rhythmic low-frequency activity (mainly in the theta band), presenting coherent oscillations and resonance (Fig. 1.7) (D'Angelo et al. 2009). GrC and GoC act as multiple resonators (D'Angelo et al. 2013): on one side the granular layer resonance reflects intrinsic properties of GrC (D'Angelo et al. 2001) and amplifies GrC responses to input currents at around 6Hz (Gandolfi et al. 2013); on the other side GoC show pacemaker activity (Forti et al. 2006) and phase reset (Solinas et al. 2007) at the same frequencies, being strongly electrically coupled and displaying low-frequency oscillations (Dugué et al. 2009). Theta-frequency oscillations have been observed during resting state activity *in vivo* (Courtemanche et al. 2013), and a synchronization has been found between this rhythmic activity and cerebro-cortical up and down states (Ros et al. 2009, O'Connor, Berg and Kleinfeld 2002). Therefore, the granular layer circuit appears to be appropriately designed to respond when inputs occur in high-frequency bursts organized in theta patterns (2-10 Hz).

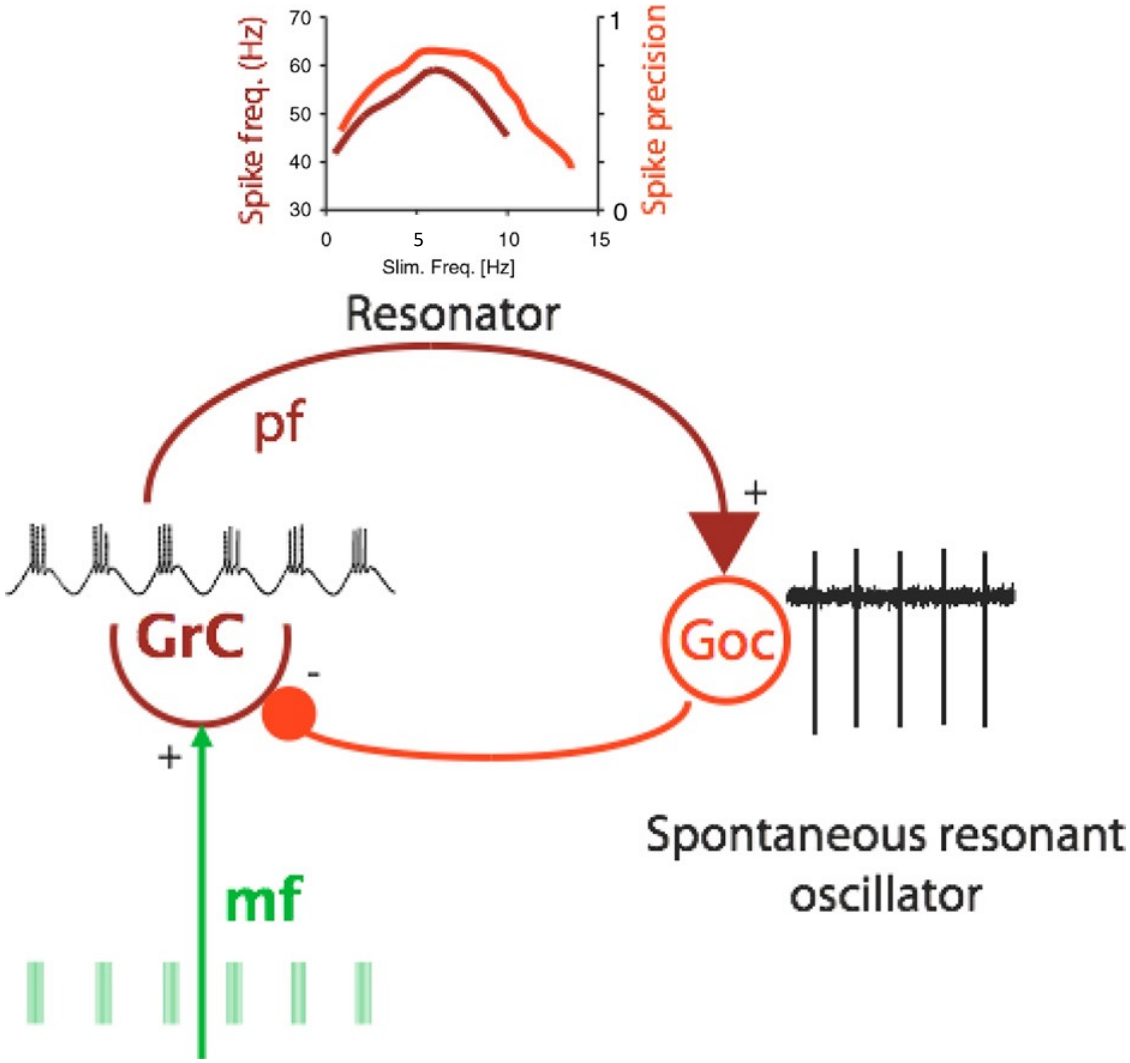

Fig. 1.7| Cellular properties supporting rhythmic low-frequency activity in the granular layer (D'Angelo et al. 2009). Granule cells and Golgi cells act as multiple resonators: granule cells show theta-frequency resonance (left side) and are coupled to Golgi cells (right side) which act as spontaneous resonant oscillators. Due to these properties, both the neuronal elements of the granular layer respond maximally to burst patterns organized in the theta band (2-10Hz), enhancing spike generation and improving spike-timing precision (graph on top).

Extracellular field recordings in freely behaving animals have shown that the granular layer can be also entrained in synchronous oscillations encompassing the beta frequency (7-25 Hz) (Courtemanche et al. 2013). This frequency band has been recorded *in vivo* as a "background activity" within the granule cell layer (Pellerin and Lamarre 1997), and subsequent studies have revealed its relevance for sensorimotor processing (Courtemanche and Lamarre 2005, Courtemanche, Chabaud and Lamarre 2009) and vestibulo-ocular reflex performances (Rössert et al. 2014). The granular layer response to inputs in the beta band has not been locally characterized yet. Actually, only a computational model has been developed to investigate granular layer activation in this case, predicting an increase in the responsiveness of GrC and GoC and a coherent organization of the emergent activity (Solinas et al. 2010).

An *ex vivo* investigation has been conducted to reconstruct the excitation of the granular layer and signal transmission towards the molecular layer at higher frequencies (50Hz and 100Hz) (Mapelli et al. 2010b). This paper shows the frequency-dependence of signals retransmission in the cerebellar cortex, originating a cascade of two high-pass filters. The first is the granular layer itself, which cuts off signals below 50Hz. The second is located at the PC synaptic stage, enhancing PC responses to PFs activity elicited by MFs activations at 100Hz. Interestingly, this effect is lost along the PFs, suggesting an amplification of bursts responses along the vertical axis. This vertical transmission is in line with the spot-like activation of PC observed *in vivo*, following MFs bursts with frequencies over 100Hz (Bower 2010).

To further complicate the picture, the molecular layer ability to sustain synchronous oscillations in the gamma band (30-80 Hz) and higher (80-160 Hz) has been demonstrated both *in vivo* (de Solages et al. 2008) and *in vitro* (Middleton et al. 2008). Even if the contribute of these high-frequency oscillations to signal processing in the cerebellar system has been already hypothesized (De Zeeuw, Hoebeek and Schonewille 2008), their specific role in concert with low-frequency patterns still remains unknown.

Although the coexistence of all these mechanisms is needed to enable pattern recognition and information processing in the cerebellum, a comprehensive study of the cerebellar cortex responsiveness at different input frequencies is still missing and deserves experimental assessment.

1.3 Short-term plasticity in the cerebellar network.

Synaptic plasticity is actually known to occur at several sites in the cerebellar network (D'Angelo 2014, Gao, van Beugen and De Zeeuw 2012, Le Guen and De Zeeuw 2010, Hoxha et al. 2016, De Zeeuw et al. 2011). While long-term synaptic plasticity typically contributes to cerebellar motor learning (D'Angelo et al. 2016, Mapelli et al. 2015), various forms of short term plasticity (STP) occur at multiple synapses within the cerebellar network and are crucial determinants of input processing. Both presynaptic and postsynaptic mechanisms coexist in regulating neurotransmission dynamics, especially during a train of stimuli.

At the mossy fibers-granule cell relay, these mechanisms endow the cerebellar cortex with the ability to process incoming inputs in the time and frequency domain (D'Angelo and De Zeeuw 2009). In particular, in the mouse vestibulocerebellum, the physiological diversity of MFs inputs converging onto GrC has been recently demonstrated (Chabrol et al. 2015). This diversity has been correlated with distinct presynaptic and STP related behaviors, depending on the type of input conveyed by MFs. Performing a k-mean clustering analysis on AMPA receptor mediated synaptic currents measured in the vestibulocerebellum, five groups of MFs inputs can be identified presenting significant differences in the number of release sites and in the release probability. Moreover, the characterization of the type of input conveyed by MFs belonging to each group leads to the demonstration that distinct classes of MFs with distinct presynaptic behaviors can be reconducted to a different sensory input pathway. Depending on the input combination GrC show a different output firing. This evidence supports the important role of STP in information processing at this level. Nevertheless, the molecular underpinnings of MFs synaptic release heterogeneity still remain unclear.

The evaluation of the effect of short stimulus trains of MFs activity on GrC responses reveals a composite process involving presynaptic events (influencing neurotransmitter release), and changes in postsynaptic excitability. Cerebellar mossy fibers-granule cells synapses appear to be characterized by a relatively high release probability (Sargent et al. 2005, Sola et al. 2004) and a rapid reloading of

presynaptic release sites, especially during high-frequency stimulation (Saviane and Silver 2006). These properties exert a large control over the glutamate concentration in the synaptic cleft, consequently shaping the synaptic response to bursts. In particular, at the mossy fibers-granule cells relay, short-term depression (STD) is primary observed (Gao et al. 2012). STD during repetitive stimulation is not only due to high release probability and vesicle depletion, but also to postsynaptic receptors desensitization. Differences in postsynaptic receptors kinetics and intense glutamate spillover play a central role in determining this phenomenon. During short input bursts, AMPA and NMDA receptors show a different behavior and NMDA receptors tend to saturate (Nieus et al. 2006). Thus, the short-term plasticity observed is mainly related to AMPARs desensitization (Wall 2005, DiGregorio et al. 2007). GrC dendrites, GoC axonal collaterals and MFs rosettes generate complex interactions in structures called glomeruli. The particular architecture of the cerebellar glomerulus (Xu-Friedman and Regehr 2003) favors glutamate spillover from release sites onto neighboring GrC (DiGregorio, Nusser and Silver 2002, Nielsen, DiGregorio and Silver 2004). The elevated glutamate concentration in the synaptic cleft derived by both quantal release and spillover determines receptors desensitization and gives rise to STD (DiGregorio et al. 2007).

Another effect mediated by glutamate spillover is heterosynaptic plasticity. Glutamate released from neighboring MFs terminals can activate mGluRs (metabotropic glutamate receptors) on GoC decreasing the efficacy of inhibitory transmission onto GrC (Mitchell and Silver 2000b). This effect is mirrored by presynaptic activation of GABA-B receptors on MFs terminals, which induces a decrease in glutamate release probability (Mitchell and Silver 2000a, Mapelli et al. 2009). The overall glomerular crosstalk additionally contributes to the control of GrC responses. Moreover, the lack of STP and the highly synchronous vesicular release at mossy fibers-Golgi cells relay increases the effectiveness of input processing modulation (Kanichay and Silver 2008). MFs-GoC synaptic connections in fact appear to be characterized by a high temporal precision and a rapid time course of quantal presynaptic release. These quantal properties allow MFs to rapidly reset GoC firing, consequently shaping GrC responses, especially at low input frequencies.

An additional level of complexity is added to cerebellar signaling by ascending axons synapses. Interestingly, these synapses present an higher release probability than PFs (Sims and Hartell 2005), but don't show the capability to sustain plastic changes (Sims and Hartell 2006). This suggests that two segments of the same axon play different roles in information processing: whereas ascending axons behave like event detectors, PFs selectively filter input signals (Isope and Barbour 2002) and are more susceptible to a dynamic regulation (Sims and Hartell 2006).

Moreover, it has been recently demonstrated that PC firing rate can be strongly affected by GrC bursts duration (Grangeray-Vilmint et al. 2018), suggesting a further contribution to signals coding coming from short term dynamics at the parallel fibers-Purkinje cells synapses. After granular layer processing, signals reach the molecular layer where other forms of short-term synaptic plasticity operate a fine tuning of incoming inputs. PFs synapses show different types of plasticity depending on the target neuron (PC or MLI) and the stimulation frequency (Isope and Barbour 2002, Valera et al. 2012, Sims and Hartell 2005, Beierlein, Fioravante and Regehr 2007, Carter and Regehr 2000, Bao, Reim and Sakaba 2010).

At the parallel fibers-Purkinje cells relay, synapses present a low release probability (Isope and Barbour 2002, Valera et al. 2012, Sims and Hartell 2006) and show a prominent facilitation (Atluri and Regehr 1996, Kreitzer and Regehr 2000, Valera et al. 2012, Le Guen and De Zeeuw 2010). Presynaptic calcium dynamics play a central role in the control of this process (Atluri and Regehr 1996, Dittman, Kreitzer and Regehr 2000, Valera et al. 2012): the small number of vesicles ready for

the release typical of these synapses (Xu-Friedman, Harris and Regehr 2001) can be increased by local calcium concentration (Valera et al. 2012), especially at high frequencies stimulations (Doussau et al. 2017). In addition, a calcium-dependent mechanism has been suggested to operate during bursts determining a rapid recovery of the ready releasable vesicles at the presynaptic terminals (Dittman et al. 2000).

NMDA receptors are not expressed on PC and synaptic transmission is consequently mediated by AMPARs (Häusser and Roth 1997). The facilitation observed during bursts does not appear to be particularly limited by AMPARs desensitization (Valera et al. 2012) or saturation (Foster, Crowley and Regehr 2005). However, their simultaneous activation with mGluR1 postsynaptic receptors can trigger the release of endocannabinoids by PC, regulating synaptic strength in a retrograde fashion (Brown, Brenowitz and Regehr 2003). Endocannabinoids activate presynaptic CB1 receptors and reduce neurotransmitter release, ensuring a continuous regulation of short-term plasticity (Beierlein et al. 2007, Brenowitz and Regehr 2005). This retrograde inhibition can be further enhanced by the activation of extrasynaptic mGluR1 by glutamate spillover (Beierlein and Regehr 2006).

PFs are endowed of presynaptic GABA-A and GABA-B receptors, which can contribute to the control of synaptic strength: while GABA-A activation usually increases glutamate release and potentiates synaptic transmission, GABA-B activation reduces synaptic strength inhibiting presynaptic calcium channels (Dittman and Regehr 1996, Kreitzer and Regehr 2000, Le Guen and De Zeeuw 2010). The activation of both these presynaptic receptors is induced by the elevated concentration of GABA following MLI activation, characterizing an heterosynaptic pathway (Dittman and Regehr 1997, Le Guen and De Zeeuw 2010).

The control of action potentials timing in PC is in large part achieved by the feed-forward inhibition (FFI) mediated by both BC and SC. The tuning of this FFI pathway is complex, due to the presence of other forms of short-term dynamics shaping MLI activities. Following high frequency stimulation of GrC, parallel fibers-stellate cells synapses show facilitation while parallel fibers-basket cells synapses show depression (Carter and Regehr 2000, Bao et al. 2010). Considering the location of the synapses of SC and BC on the PC, their different behavior suggests a frequency-dependent inhibition exerted on different PC compartments (soma or dendrites). In addition, STP heterogeneity has been demonstrated at parallel fibers-molecular layer interneurons synapses (Dorgans et al. 2019). According to the Principal Component Analysis and the k-means clustering analysis performed on excitatory postsynaptic currents recorded in cerebellar slices, four different profiles of STP can characterize parallel fibers-molecular layer interneurons synapses. These profiles differ by the quantity of neurotransmitter released and the depression or facilitation of glutamate release exhibited during high frequencies stimulation trains. Glutamate release behavior act as a major determinant of firing frequencies and delays in MLI responses. Thus, heterogeneous profiles of STP shape the spike output pattern of interneurons consequently expanding their coding range. Similarly to parallel fibers-Purkinje cells synapses, parallel fibers-molecular layer interneurons synaptic strength can be reduced by endocannabinoid-mediated inhibition (Beierlein and Regehr 2006). Importantly, in contrast with the parallel fiber - Purkinje cells connection, synaptic transmission at parallel fibers – molecular layer interneurons synapses shows an NMDA component (Carter and Regehr 2000) and endocannabinoids release from interneurons requires NMDARs activation (Beierlein and Regehr 2006). NMDA receptors are expressed postsynaptically with AMPARs both on BC and SC, and glutamate spillover largely contributes to their activation especially upon PFs sustained activity (Carter and Regehr 2000). Interestingly, a pure spillover connection has been confirmed also between climbing fibers and BC / SC (Szapiro and Barbour 2007). However, the effect of glutamate spillover at this level is

actually controversial: on one side, climbing fibers activity can lead to an increased spike firing of both interneurons causing a potentiation of PC inhibition (Szapiro and Barbour 2007); on the other side, high-frequency stimulation of climbing fibers can suppress GABA release from interneurons through AMPARs-mediated presynaptic inhibition (Satake et al. 2004).

These heterosynaptic effects of climbing fibers activity concur with the direct modulation exerted by climbing fibers on PC firing (De Zeeuw et al. 2011). Climbing fibers synapses are characterized by high release probability and multivesicular release (Foster et al. 2005, Wadiche and Jahr 2001). Despite their structural similarity with parallel fibers-Purkinje cells synapses (Xu-Friedman et al. 2001), a different kind of STP occurs at the climbing fibers-Purkinje cells relay. Climbing fibers shows a prominent short term depression (Dittman and Regehr 1998), with no physiological evidence of spillover (Wadiche and Jahr 2001, Zucker and Regehr 2002) and are generally unaffected by AMPARs desensitization (Xu-Friedman and Regehr 2003). Combined activation of climbing fibers and PFs can exert a double control on PC activity, either improving endocannabinoids retrograde inhibition (Brenowitz and Regehr 2005) or enhancing the potentiation of mGluR-mediated excitation at PFs synapses (Batchelor and Garthwaite 1997, Kim et al. 2008). Together, these forms of depression and potentiation allow climbing fibers supervision of PC spiking.

The coordination of all these plastic behaviors at the successive stages of cerebellar computation is essential to process incoming signals and generate the output ultimately consolidated in the deep cerebellar nuclei. Thus, with its disparate forms of plasticity, the cerebellar cortex is able to compute multiple types of information in a fast and precise manner, thereby efficiently subserving motor control and higher cognitive functions.

1.4 Functional aspects of cerebellar physiology.

The functional aspects of cerebellar physiology have been classically evaluated in a motor control perspective (D'Angelo 2018). The processing pillars of the cerebellar circuit can be summarized in a triad: *timing*, *learning* and *prediction*. The ability to elaborate temporal information on the millisecond time scale determines a cerebellar reaction to inputs 1-2 order of magnitude faster than the cerebral cortex (D'Angelo 2011). Thus, the cerebellar control of movements reaches a precision unfeasible in cerebro-cortical circuits, and the cerebellum can be described as a *timing machine* (D'Angelo 2011). *Learning* emerges as an integrated process involving multiple plasticity sites along the circuit (Mapelli et al. 2015). The main hypothesis is that the cerebellar cortex processes the faster component of memory while deep cerebellar nuclei elaborate and consolidate the slower component (D'Angelo and Casali 2012). As a site of procedural memory, the cerebellum can be defined as a *learning machine* (Mapelli et al. 2015). The critical role played by the cerebellum in sensory prediction can be explained looking at its characteristic connectivity with central and peripheral structures (Fig.1.8) (D'Angelo 2011). The multiple pathways connecting the cerebellum with other brain areas enable the circuit to compare cortical and sensory patterns and elaborate a *prediction* of sensory consequences of motor actions.

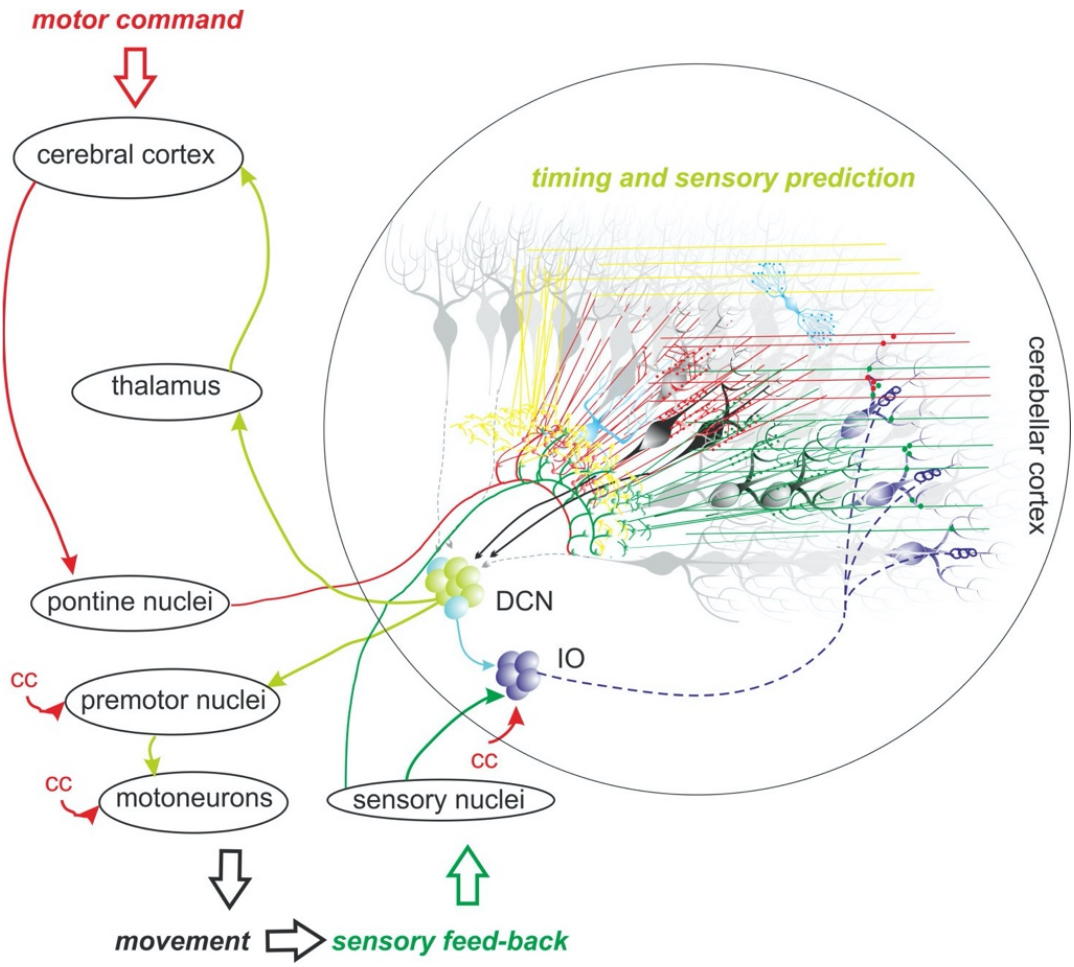

Fig. 1.8| General connectivity of the cerebellum with other brain areas (D'Angelo 2011). Multiple pathways reach various parts of the cerebellar cortex delivering sensory and cognitive signals. In this scheme a motor command is sent from the cerebral cortex through the pontine nuclei and enters the cerebellum through mossy fibers. After processing, the output signal is transmitted to deep cerebellar nuclei and sent to the thalamo-cortical circuit and to the premotor nuclei. Movement generates a sensory feed-back, which reaches the cerebellum directly or passing through the inferior olive.

These concepts are at the core of the internal model hypothesis (Ito 2008). This theory implies the ability of the cerebellum to generate internal models and behave as an adaptive control system (Fig. 1.9). Two types of internal models have been proposed: the forward model and the inverse model. In the first case, a copy of the motor command generated by the cortex is sent to the cerebellum which uses its internal model to elaborate a prediction of the sensory consequences of actions. This prediction is compared with the sensory feedback and in case of deviations from prediction the cerebellum produces sensory corrective signals and is able to learn how to modify the internal model itself (Fig. 1.9B). In the second case the cerebellum receives sensory inputs and delivers motor corrective terms to the cortex, implementing an inverse model of movement. Learning processes in this scheme are derived from discrepancies between the aimed action and command signals generated by the motor cortex (Fig. 1.9C). Both forward and inverse models might operate in combination and can be seen as inter-related: motor control would require a forward model while the inverse model lodged in the cerebellum would allow unconscious skilled movements (Manto et al. 2012).

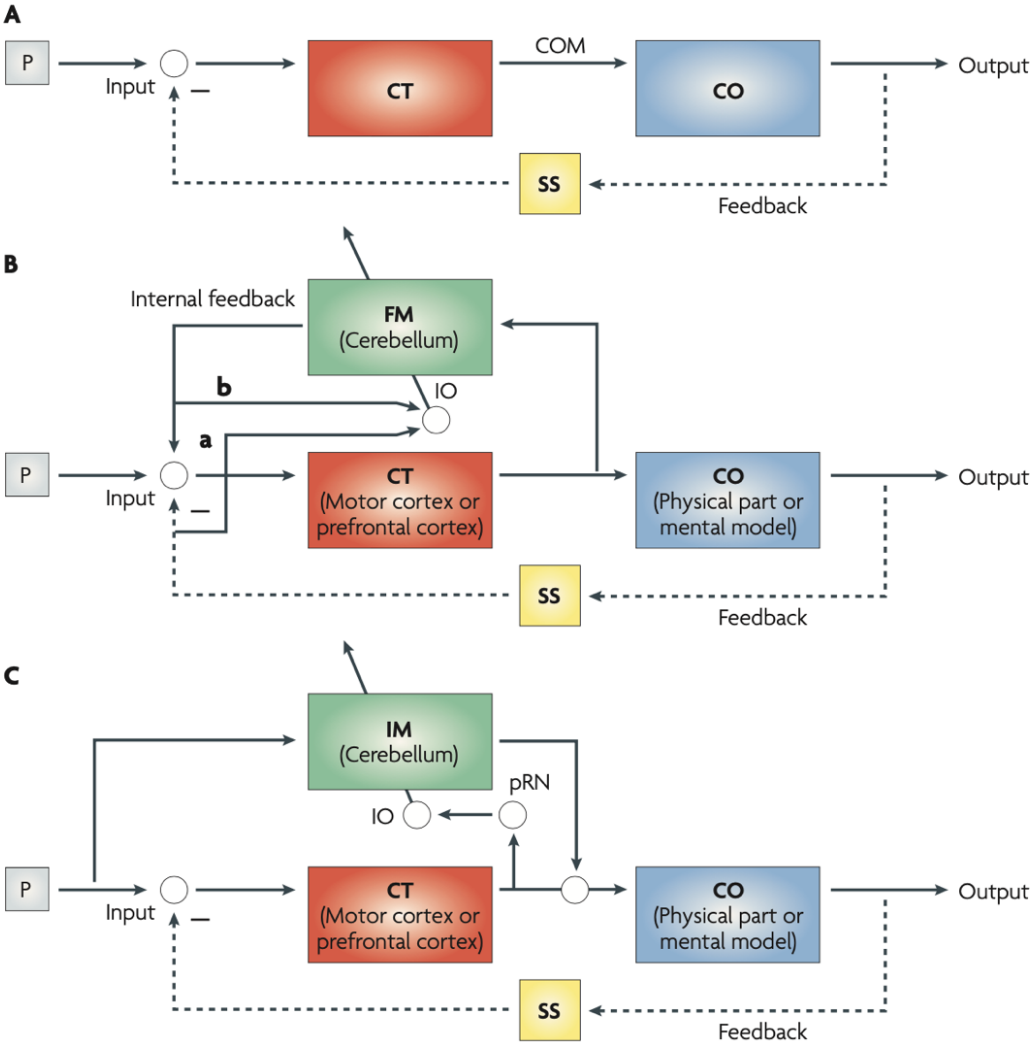

Fig. 1.9| Diagrams explaining the internal-model hypothesis (Ito 2008). **A)** The basic structure of a control system includes a controller (CT) which sends commands to a controlled object (CO) and receives instruction from an instructor (P) and feedback signals from a sensory system (SS). In the case of voluntary movement, the motor cortex would act as the controller, the body part would be the control object, and the premotor cortices and anterior cingulate gyrus would provide the instructions. **B)** Diagram of a forward model system in which error signals can be derived comparing the outputs of the controlled object (b) with those of the forward model (a). The inferior olive (IO) would be the site of this kind of comparison. **C)** Diagram of an inverse model system in which error signals can be derived from discrepancies between command signals generated by the motor cortex and signals coming from the instructor.

Given the strong connection between the cerebellar hemispheres and cortical associative areas (Palesi et al. 2015) and the observation of cerebellar activation during cognitive tasks (Stoodley and Schmahmann 2009), there is general agreement among recent studies on the extended role of internal models in regulating non-motor functions (Koziol et al. 2014). The ability of the neuronal circuit of the cerebellum to support different types of processing using the same computational scheme would depend on the connectivity of its regions with other brain areas (D'Angelo and Casali 2012). The reciprocal connection between the cerebellar hemispheres and the prefrontal cortex might provide an

internal forward model for mental activity, while the common input received by cerebellar hemispheres and prefrontal cortex from the anterior cingulate gyrus supports an inverse model scheme (Ito 2008). Therefore, according to anatomical data, either type of internal model can be used *in vivo*. In the case of cognitive processing, thoughts and cognitive processes would be treated as controlled objects and this kind of models would be manipulated to provide the solution to novel problems without reaching conscious awareness. Thus, the cerebellum would be the site of implicit thought (Ito 2006, Ito 2008) and a co-processor for cognitive functions. A direct cerebellar involvement in the development of conscious representations cannot be inferred from clinical evidences (Tononi and Edelman 1998). However, this lack of ability in generating consciousness does not mean that the cerebellum is completely extraneous to conscious processing. In fact, thanks to its fast spatio-temporal integration of inputs it could contribute to the perception of reality as *instantaneous* and *continuous*. Moreover, behaving as a forward controller, it would take part in the generation of an *anticipatory* virtual reality predicting possible environmental configurations (D'Angelo and Casali 2012).

Motor and non-motor functions present a particular pattern of organization within the cerebellum. The mapping of cognitive and motor functions shows a medial-to-lateral gradient, with sensory-motor regions located in the anterior lobe and lobules VI and VII and cognitive areas distributed laterally in the posterior lobe (Klein et al. 2016). This kind of gradient also applies to the deep cerebellar nuclei (Fig. 1.10).

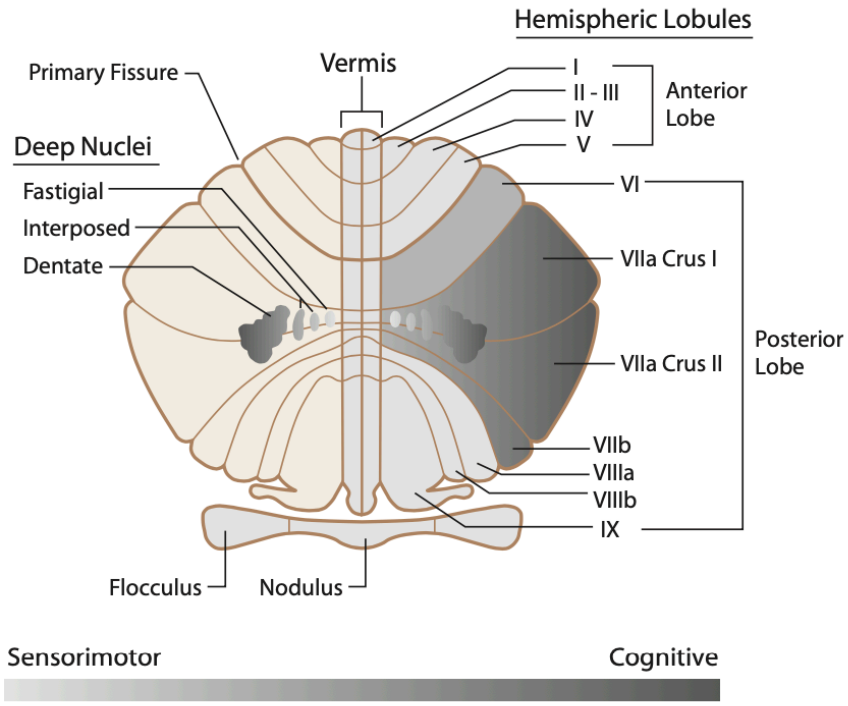

Fig. 1.10| Functional map of the cerebellum (Klein et al. 2016). Motor and non-motor functions in the cerebellum present a specific pattern of organization with sensorimotor functions more distributed toward the midline and cognitive functions located more laterally in the cerebellar hemispheres. The same kind of gradient can be seen in the cerebellar nuclei.

Finally, several studies are actually supporting a cerebellar activation during imitation learning (Casiraghi et al. 2019) and emotional processing (Adamaszek et al. 2017). While the circuit underlying actions understanding appears to engage the same cerebellar areas devoted to cognitive functions, the vermis appears to play a pivotal role in perceiving and evaluating emotions. Thus, a third well-delineated cerebellar zone involved in key aspects of emotion should be added in functional maps (Fig. 1.11).

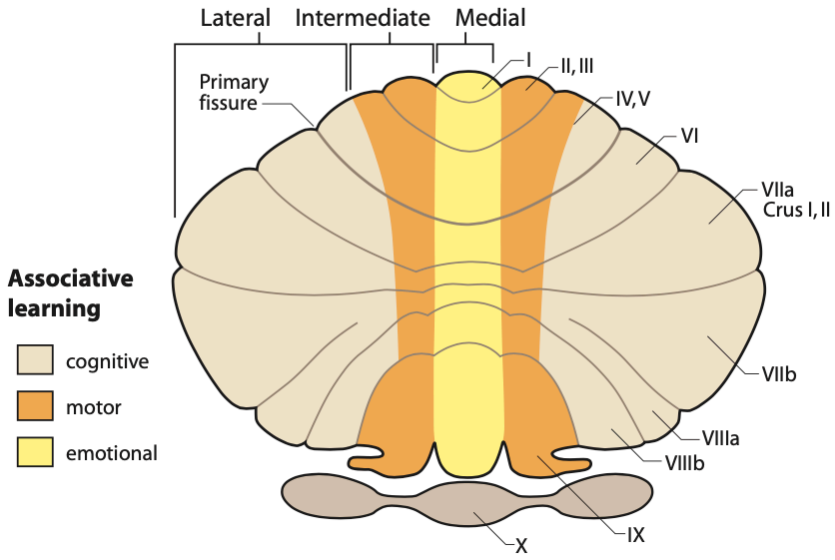

Fig. 1.11| The "emotional" cerebellum. Mapping the cerebellar areas mainly involved in associative learning in the motor, emotional, and cognitive domains (Timmann et al. 2010), it is possible to confirm the pivotal role played by the vermis in emotional processing, while motor and cognitive functions maintain the medial-to-lateral cerebellar distribution.

All these evidences support that the narrow view of the cerebellum solely operating as a co-processor of movement has been actually abandoned. However, a deeper insight into cerebellar processing is still needed and the understanding of its contribution to cognitive functions represents a remarkable challenge that is far from being completed.

2. Materials and Methods.

2.1 Cerebellar slices preparation.

The investigation of the cerebellar circuit has been conducted recording extracellular signals in acute parasagittal or coronal slices (220µm) obtained from the cerebellar vermis or hemisphere, according to the experimental settings, of 18 to 23-days-old C57BL/6 mice. Animals were anesthetized with halothane and killed by decapitation. The whole procedure was performed in cold and oxygenated Krebs solution and slices were recovered for 1 hour in the same solution before recording. Krebs solution contained (in mM): 120 NaCl, 2 KCl, 1.2 $MgSO_4$, 26 $NaHCO_3$, 1.2 KH_2PO_4, 2 $CaCl_2$,11 glucose, pH 7.4 equilibrated with 95% O_2–5% CO_2.

2.2 Extracellular signals recordings.

The reconstruction of a realistic picture of neurons functioning within intact networks is a primary aim of modern neuroscience. Beside the investigation of single neurons properties through intracellular or membrane level approaches, the need of a deeper understanding of neuronal ensembles activity and connectivity is actually emerging. This kind of question can be addressed with extracellular signals recordings, which might lose single neurons information but enable a comprehensive assessment of circuits dynamics in physiological conditions.
The summation of all ionic processes coming from excitable membranes into brain tissues gives rise to an extracellular field. Currents flowing in the extracellular space around active neurons determine a voltage deflection of this electric field, which can be measured by extracellular microelectrode arrays. The biophysics underlying this type of measurements is well known, and the most common mathematical approach explaining the contribute of transmembrane currents to extracellular fields potentials is the *volume conductor theory* (Heinricher 2004). In this approach, the neuron is envisioned as surrounded by a purely homogeneous, isotropic and ohmic extracellular medium and currents flowing from the extracellular medium to the intracellular space are referred to as current *sinks*, while positive currents entering the extracellular medium are termed as current *sources* (Einevoll et al. 2013) (Fig. 2.1).

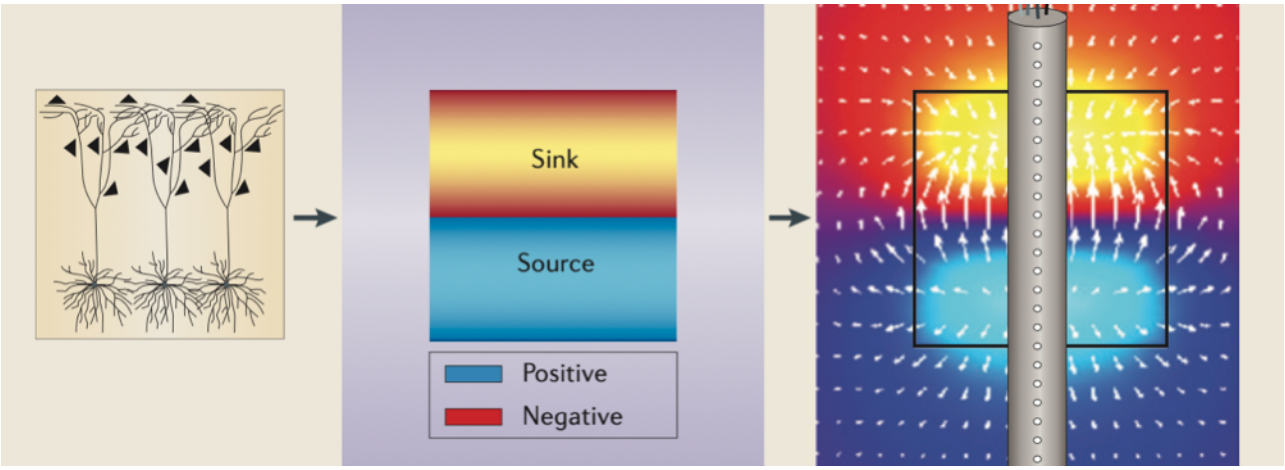

Fig. 2.1| The *sink-source* pattern generation (Einevoll et al. 2013)**.** The activity of a population of neurons (on the left) gives rise to a typical *sink-source* pattern (in the middle) in which the *sink* represents currents flowing from the extracellular space to the intracellular one while the *source* represents currents entering the extracellular medium. The resulting deflection of the extracellular field can be measured with multielectrode arrays (a laminar multielectrode is represented as an example in the right panel).

The potential recorded by extracellular electrodes is defined with the following equation:

$$V_e = \frac{I}{4\pi\sigma r} \qquad (Eq.\,2.1)$$

in which I denotes the transmembrane current, σ is the conductivity of the medium and r the distance between the recording electrode and the source of the transmembrane current (Obien et al. 2014). This equation implies that the contribution of a source to an extracellular potential is inversely proportional to the distance between the electrode and the neuron. Indeed, the amplitude of detected signals rapidly decays increasing the distance between electrodes and neurons (Buzsáki, Anastassiou and Koch 2012) (Fig. 2.2)

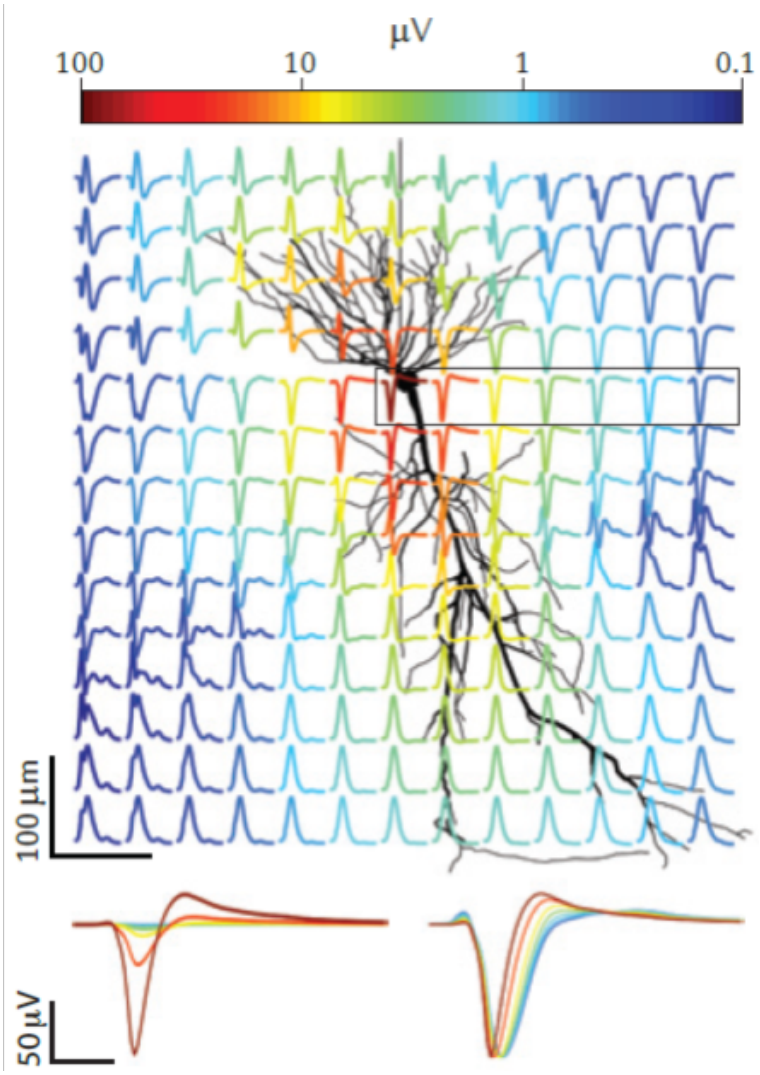

Fig. 2.2| Extracellular signals amplitude dependence on neuronal distance from the recording electrode (Buzsáki et al. 2012)**.** Extracellular signals present a different sign, shape and amplitude according to the position of the recording electrode. In particular, increasing the distance between the recording electrode and neurons, the extracellular signals amplitude is markedly decreased (represented in the image with different colours).

In single neurons extracellular recordings, the depolarization sustained by fast sodium currents entering the neuronal membrane is detected by microelectrodes as an action potential, or "spike". Due to the fact that the initial segment of neuronal axons usually presents the lowest threshold for spike generation, most commonly neuronal initial segment acts as a current *sink* while inactive regions of the axon act as current *sources*. Therefore, a detected spike presents a negative overshoot when electrodes are close to neuronal soma/initial segment, and a positive deflection moving down the axon. However, many neuronal dendrites in the nervous system are electrically excitable and sometimes can act as a *sink* giving rise to the opposite pattern. These evidences support the fact that not only neuronal distance from electrodes influences the shape of recorded extracellular potentials, but also the position of the electrode relative to the cell body significantly impacts on the detected signal (Lindén, Pettersen and Einevoll 2010) (Fig. 2.3).

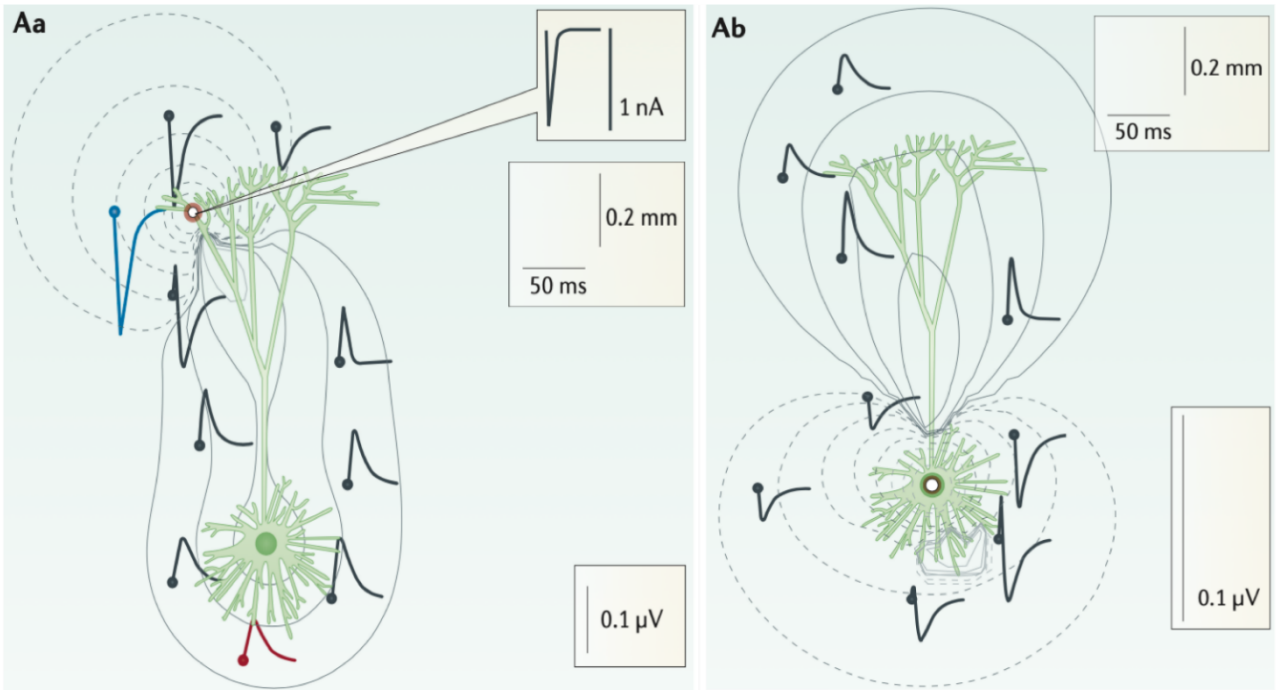

Fig. 2.3| Extracellular signals shape dependence on the recording position (Einevoll et al. 2013)**.** Extracellular signals shape changes according to the position of the electrode with respect to the soma, the axon or dendrites, and according to the position of the active synapse. Near a synaptic input (represented with a white dot in both images) the extracellular signal recorded shows a negative deflection, while near inactive regions it usually presents a positive shape.

Besides the recording of spiking activity, electrodes can sample Local Field Potentials (LFPs). The origin of this kind of signal is harder to discern than spikes because multiple neuronal processes concur in its generation.

Synaptic activity is surely one of the main contributors. Extracellular *sink* is determined by transmembrane fluxes of sodium and/or calcium ions following the activation of AMPA and NMDA receptors. The extracellular *sink* is balanced by an extracellular *source*, which represents the opposite ionic currents entering the cell in order to grant the electrical equilibrium required for correct neuronal functioning. Cells morphology can strongly influence LFPs generation. Neurons presenting a considerable spatial separation between apical dendrites and soma, such as pyramidal cells, are thought to have an *open-field* configuration and significantly contribute to the recorded extracellular signal. This kind of morphology in fact determines a considerable spatial separation of the *sink* from the *source* and favours the rise of a sizeable current dipole. On the other hand, neurons with a spherical structure, such as thalamocortical ones, can be considered as *close-field* generators. This kind of cells are not expected to give rise to significant extracellular signals, because dipole formation is counteracted by their symmetric morphology which can exert a cancellation effect on multiple extracellular contributors and consequently on the resulting LFP (Lindén et al. 2010) (Fig. 2.4).

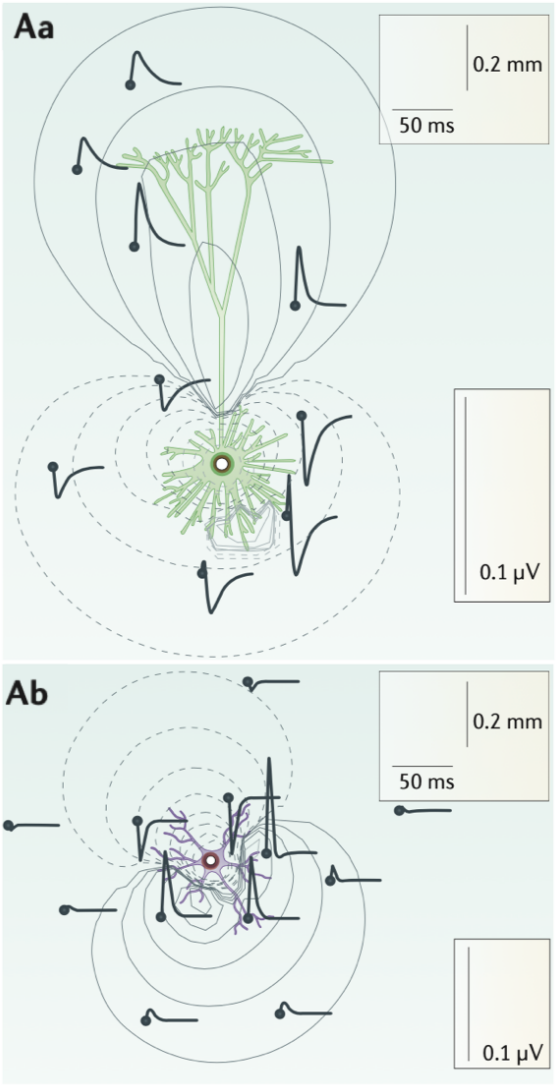

Fig. 2.4| Extracellular signals dependence on neuronal morphology (Einevoll et al. 2013)**. Aa)** An *open-field* dendritic structure implies a sizeable current dipole and consequently favors the rise of a sizeable LFP. **Ab)** A *close-field* configuration can determine a cancellation effect on the resulting LFP and neurons presenting this kind of morphology contribute less to LFPs generation.

LFPs signals are not only determined by geometric factors, but also neuronal synchrony appears as an important component. Action potentials from multiple neurons firing synchronously provide a contribution to extracellular fields generation (Buzsáki et al. 2012). This kind of synchrony can be facilitated by electrical synapses such as gap junctions, which consequently can indirectly impact on the extracellular signal. Additionally, it is important to point out that the homogeneous, isotropic, and ohmic extracellular medium assumed by the *volume conductor theory* is unlikely in physiological conditions, and the synchronous activation of a significant number of neurons can increase a phenomenon known as *ephaptic coupling.* In this case one cell excitation can influence the transmembrane potential of another cell without any synaptic or direct contact: the spread of extracellular currents in the extracellular space impacts on the extracellular field which consequently affects the transmembrane potential of each neuron.

Therefore, the simple picture derived from theory is deeply complicated by several factors and the reconstruction of the mechanisms underlying extracellular signals is not always straightforward. Advanced analysis tools need to be implemented or developed in order to account all the possible information that can be obtained from this type of recordings.

2.2.1 Extracellular recordings in the cerebellar cortex.

In the cerebellum, both spikes and LFPs can be recorded.

The autorhythmic activity of Purkinje cells, Golgi cells, and molecular layer interneurons can be detected by extracellular electrodes. Each electrode can record both action potentials coming from a single neuron and action potentials of multiple neurons. In the second case, the signal is called “multi-unit activity” (MUA), and a further analysis of the shape of the spikes is needed in order to discern all the units contributing to the total signal.

The LFP is common in the cerebellar granular layer and is derived from the simultaneous activation of granule cells following mossy fibers inputs. Granule cells are silent at rest and therefore do not give rise to signals that can be detected by extracellular electrodes. The activation of mossy fibers determines granule cells simultaneous firing in a narrow time window, which can be recorded as a large-amplitude Local Field Potential propagating through the granular layer. According to theoretical models reconstructions, the LFP elicited in the granular layer usually presents the current *sink* in granule cells clusters and the current *source* in their axons (parallel fibers). Therefore, the signal detected from an electrode close to granule cells would present the negative deflection relative to the current *sink*, while the signal detected from an electrode located into the axon bundle would present a positive shape typical of the *source* (Diwakar et al. 2011). In addition, spike doublets generation in granule cells are expected to give rise to two main waves characterizing the LFP signal and respectively called N_{2a} and N_{2b} (Fig. 2.5).

These predictions are effectively in line with the main properties of the LFPs recorded experimentally, though just few investigations have been conducted sampling this kind of signal (Maffei et al. 2002, Mapelli and D'Angelo 2007). Different positions of the extracellular electrodes with respect to the neuronal source of activity determine a positive (Maffei et al. 2002) or a negative sign (Mapelli and D'Angelo 2007) of the LFPs recorded. Nevertheless, in all the experiments, the LFP showed a typical N1-N2-P2 complex (Fig. 2.6) in which N1 corresponds to presynaptic volley activation, N2 can be split into N2a and N2b components and P2 represents the currents returning from the molecular layer. It has been demonstrated that not only spike generation in granule cells is the major determinant of N_{2a} and N_{2b}, but also N_{2a} peak amplitude is proportional to the synaptic current derived from AMPA receptor activation and N_{2b} wave is regulated by synaptic inhibition and NMDA receptors activation (Mapelli and D'Angelo 2007).

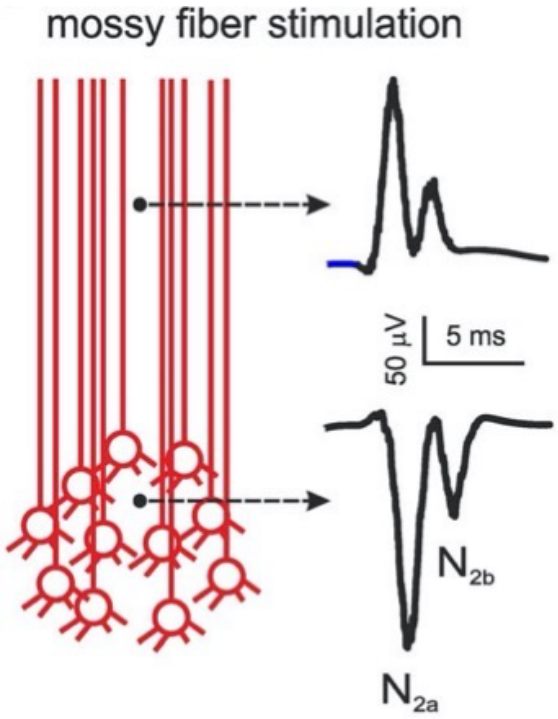

Fig. 2.5| Theoretical reconstruction of the LFP in the granular layer (Diwakar et al. 2011)**.** In the granular layer, the *sink* is expected to be positioned in granule cells clusters while the *source* is expected to be in their axons. Thus, the positioning of a recording extracellular electrode near the parallel fibers would determine the detection of a positive LFP while the positioning of an extracellular electrode near granule cells would determine the detection of an LFP with a negative deflection. In both cases the LFP detected in the granular layer is characterized by two main peaks named N_{2a} and N_{2b}.

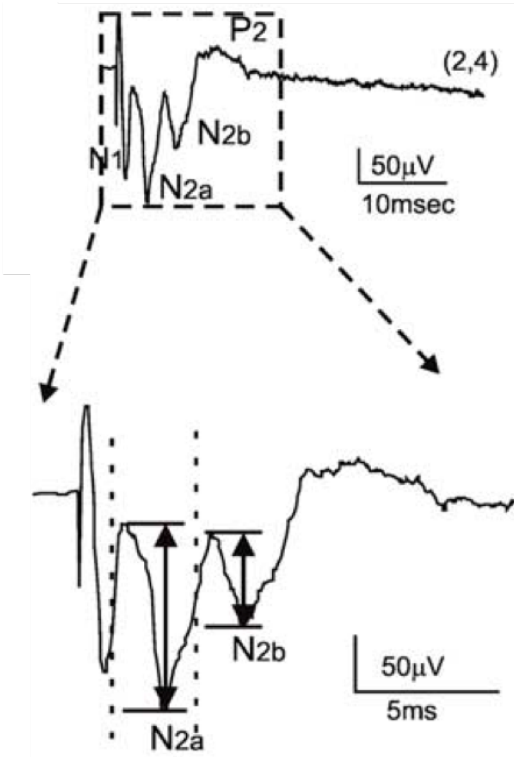

Fig. 2.6| Experimental recording of an LFP in the granular layer (Mapelli and D'Angelo 2007)**.** The experimental recording of LFPs in the granular layer leads to the observation of a typical N_1-N_{2a} -N_{2b} -P_2 shape, in which N_1 represents presynaptic volley activation, N_{2a} and N_{2b} correspond to granule cells spiking activity and P_2 is relative to the current returning from the molecular layer.

2.2.2 The High-Density Multi Electrode Array (HD-MEA).

In order to better understand network functioning in the cerebellum, a Multi Electrode Array (MEA) system can be used. This kind of system allows the recording of extracellular activity from multiple electrodes with an extremely high temporal resolution, allowing to simultaneously record spiking activities and LFPs. The most recent improvement of this kind of technology is the High-Density Multi Electrode Array (HD-MEA), in which the increased electrodes density enables the recording of neuronal activity with unprecedented detail. The complementary metal-oxide- semiconductor (CMOS) based HD-MEA (Biocam X, 3Brain AG) (Fig. 2.7) has been used for the *ex-vivo* investigations conducted in this work. In this system, the microelectrodes array integrates 4096 recording electrodes arranged in a 64 x 64 matrix on a small and compact area (2.67mm x 2.67mm). These electrodes have a size of 21µm x 21µm with a pitch of 42 µm (Biochip Arena) (Fig. 2.8). The whole chip is packaged onto a substrate together with a glass reservoir with a diameter of 25mm and 7mm in height.

Fig. 2.7| The BioCam X used for cerebellar slices extracellular recordings. The BioCam X is the station of the HD-MEA in which BioChips are plugged into. This station contains the electronics and hardware needed to control the HD-MEA chips, acquire electrophysiological data, and is embedded with a stimulation unit.

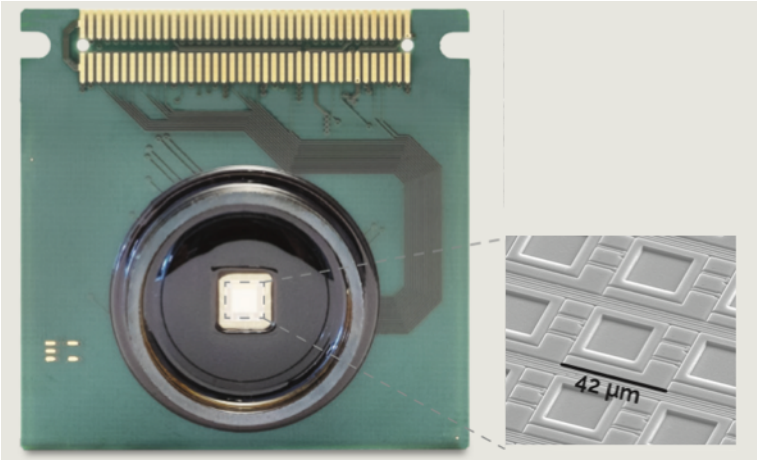

Fig. 2.8| Arena BioChip. The Arena BioChip integrates 4096 recording electrodes arranged in a 64x64 matrix on an area of 2.67x2.67mm. Electrodes have a size of 21µm x 21µm with a pitch of 42 µm and the whole chip is arranged onto a substrate together with a glass reservoir (diameter 25mm; heigh 7mm).

Extracellular signals were acquired using Brainwave X software (3Brain AG) and sampled at 18kHz/electrode with a high pass filtering set at 100Hz. For the recording (Fig. 2.9), cerebellar slices were gently positioned on the MEA chip and fixed with a nylon mesh attached to a platinum wire, to improve tissue coupling with the electrode array. Krebs solution (2-3 ml/min) was continuously perfused in the glass reservoir during the whole recording session, using a perfusion system consisting of an external peristaltic pump (ISMATEC). Krebs solution had the following composition (in mM): 120 NaCl, 2 KCl, 1.2 $MgSO_4$, 26 $NaHCO_3$, 1.2 KH_2PO_4, 2 $CaCl_2$,11 glucose, pH 7.4 equilibrated with 95% O_2–5% CO_2. When electrical stimulation was needed, a bipolar tungsten electrode was positioned on the mossy fibers bundle, delivering current pulses of 50 µA (pulses duration 200 µs).

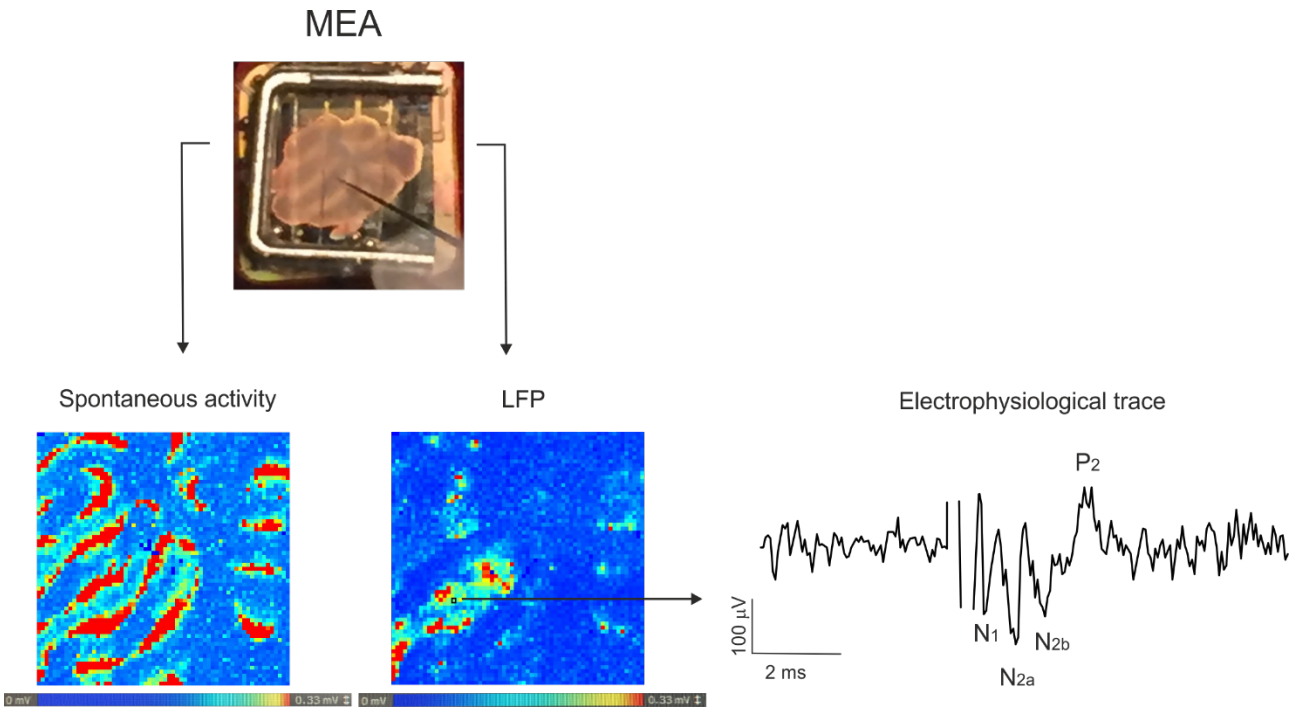

Fig. 2.9| Typical HD-MEA recording. On top, a cerebellar slice on the HD-MEA chip, stabilized with a platinum ring with nylon wires and presenting a stimulating electrode positioned on the mossy fibers. On bottom left, Purkinje cells spontaneous activity (in red) is recorded from the same slice using the BrainWave X software. On bottom right, mossy fibers stimulation evokes an LFP response propagating through the granular layer. At right, the electrophysiological trace showing the typical LFP with the N1– N2a - N2b –P2 complex, as recorded by the channel indicated by the arrow.

2.3 Experimental settings.

The experimental settings were as following:

- When the aim of the study was to investigate differences between cerebellar vermis and hemisphere neural activity, slices were stimulated with one train lasting 35 seconds at 6Hz, 20Hz, 50Hz and 100Hz (in mixed combinations and starting every 4 minutes) recording the neuronal activity at physiological temperature (37°C)

- When the aim was to investigate the cerebellar processing of inputs at different frequencies, parasagittal and coronal slices from cerebellar vermis were used, recordings were performed at 32°C and 30 single stimuli were delivered at 0.1 Hz, followed by 30 trains of 5 impulses at 6Hz, 20Hz, 50Hz and 100Hz (in mixed combinations) repeated every 10 seconds.

2.4 Data analysis.

The analysis of granular layer responses to mossy fibers activation at different frequencies was performed using *ad-hoc* routines written in MATLAB. The analysis of Purkinje cells firing was performed using Brainwave 4 software (3Brain AG) and *ad-hoc* routines written in MATLAB.

2.4.1 LFP analysis.

LFP signal presented the typical N_1-N_{2a} -N_{2b} -P_2 complex in agreement with previous reports in similar experimental conditions (Fig. 2.10).

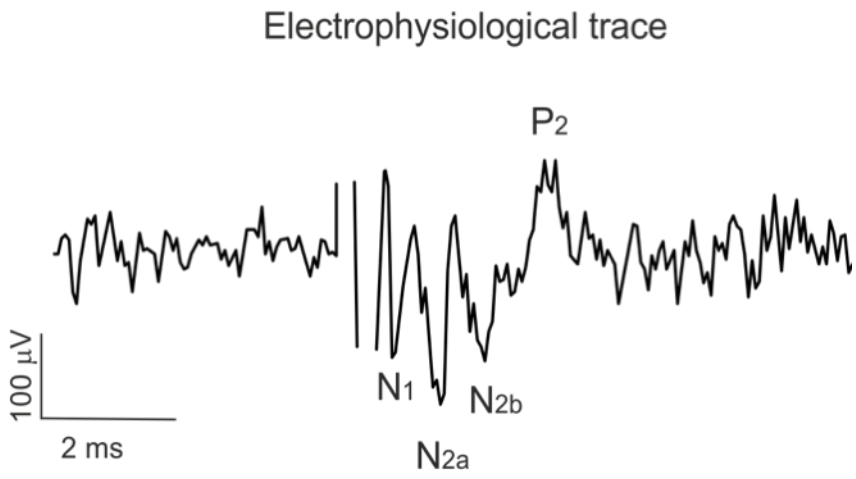

Fig. 2.10| Example of an LFP electrophysiological trace recorded from one channel of the HD-MEA. This Figure shows the typical LFP complex recorded from a single channel of the HD-MEA.

To characterize this response, the analysis has been focused on N_{2a} and N_{2b} peaks amplitude. For each experiment, peak amplitudes were calculated subtracting the negative peaks in the appropriate time window (1.9ms±1.1 ms and 4.5ms±1.2 ms from the stimulus artifact, for N_{2a} and N_{2b}, respectively) to the baseline derived from the averaged signal in 300 ms before stimulus onset. Only peak values that exceeded 3 times (for N_{2a}) and 2.5 times (for N_{2b}) the standard deviation calculated from the baseline period were considered for the subsequent analysis. A compensation of baseline drifting was not necessary. The HD-MEA system in fact calibrates automatically the signal after the stimulation. Signal calibration starts 1 μs after the stimulation and lasts 100 μs.

2.4.2 Purkinje cells firing analysis.

The high density of the HD-MEA commonly leads to the detection of MUAs in each single electrode. In order to discriminate the contribution of single neurons and characterize Purkinje cells responses at different frequencies, a multi-step processing of spike data (Fig. 2.11) was necessary.

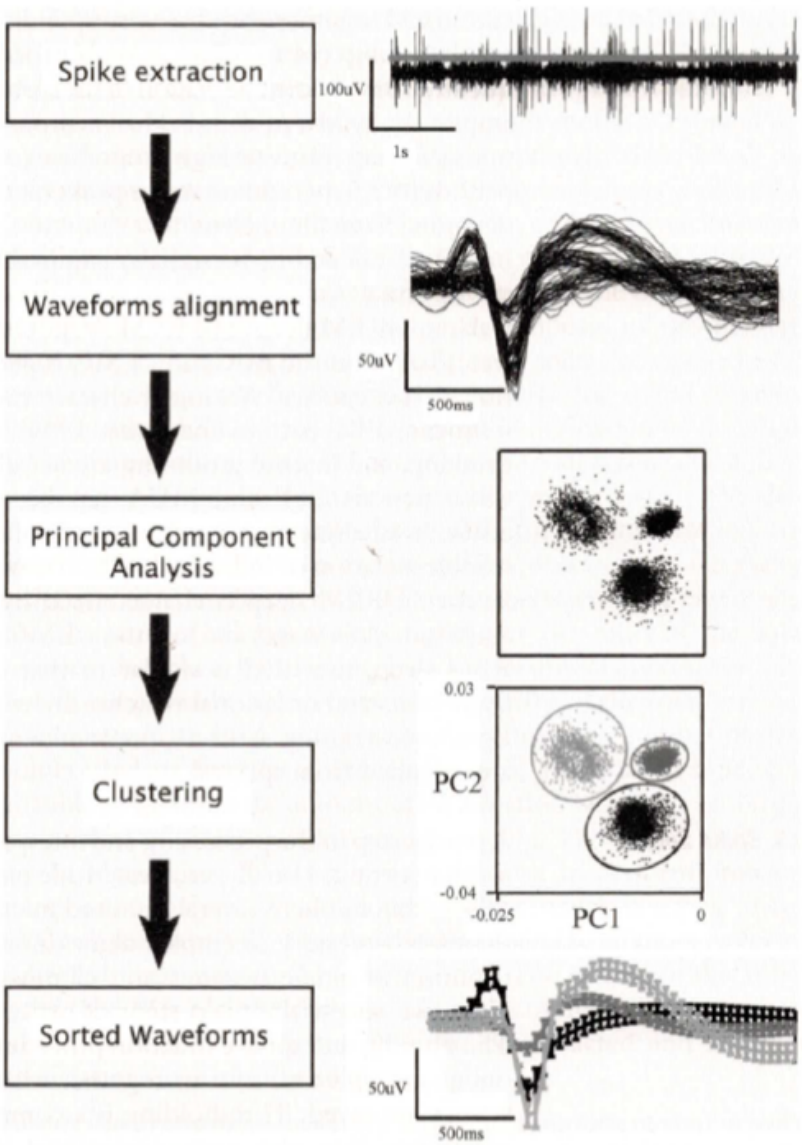

Fig. 2.11| Main steps of extracellular spikes analysis (Vyazovskiy Vladyslav V., Olcese U. and Tononi G. 2012)**.** Spike detection has been performed at first considering the events exceeding in amplitude a threshold of -100 μV. Then, waveform feature extraction has been performed on the identified spikes in order to detect different units contributing to extracellular signals. The use of the Principal Component Analysis (PCA) followed by a clustering algorithm allowed the discrimination of different groups of waveforms presenting similar features and originating from different Purkinje cells. The resulting sorted waveforms were treated separately for subsequent analysis.

First of all, spike detection was performed in Brainwave 4 software using the hard threshold algorithm (-100µV / refractory period of 1 ms) (Fig. 2.12).

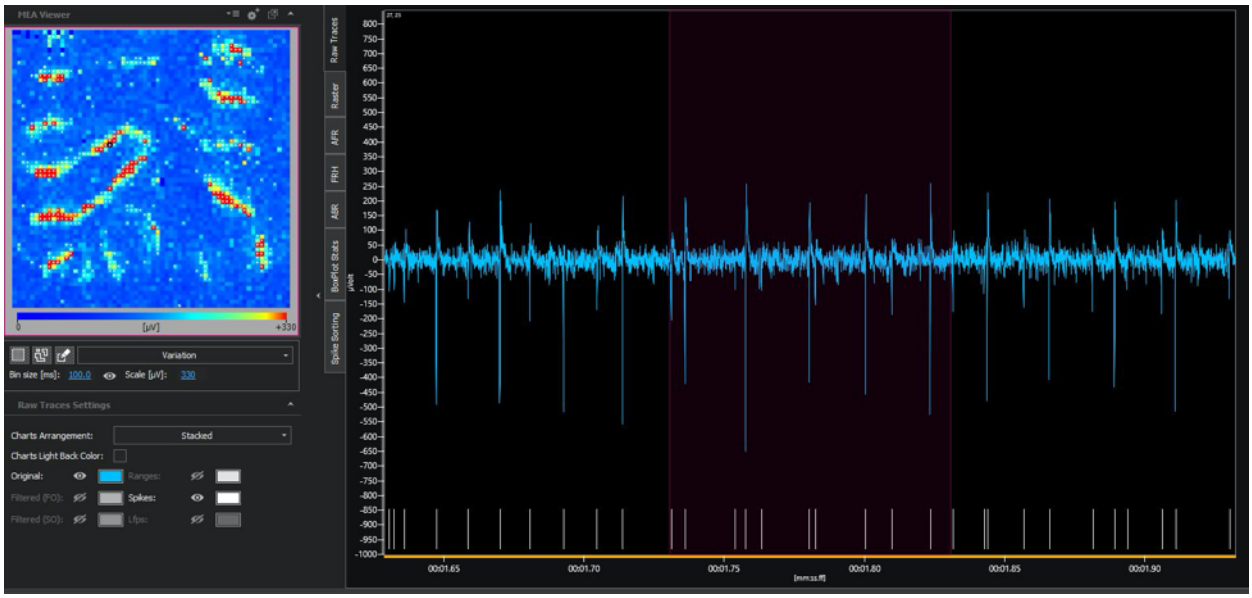

Fig. 2.12| Example of spike detection performed with the Brainwave 4 software. The picture shows a screenshot of the analysis software used: on the right, the electrophysiological trace of the Purkinje cell detected by the channel selected in the plot at left, where activity is reported with a color scale shifting to red. Notice that the detected spikes are marked with white bars in the original trace, allowing a direct control on the software operations by the user.

Spike detection was followed by spike sorting, again performed with the Brainwave 4 software. In the first step of spike sorting, spike waveforms were extracted in a temporal window of 0.5 ms pre-spike and 3 ms post-spike. Then, Principal Component Analysis was chosen to perform waveforms features extraction. For neuronal spikes, three components are commonly enough to describe over 70% of the total sample variance. PCA performed on Purkinje cells firing took into account spikes slope, and the maximum and minimum values of peaks amplitude. Feature extraction was followed by a clustering procedure. The clustering algorithm used was the k-mean & PBM index, resulting in one or more clusters of spikes for each electrode recording a spiking activity (Fig. 2.13).

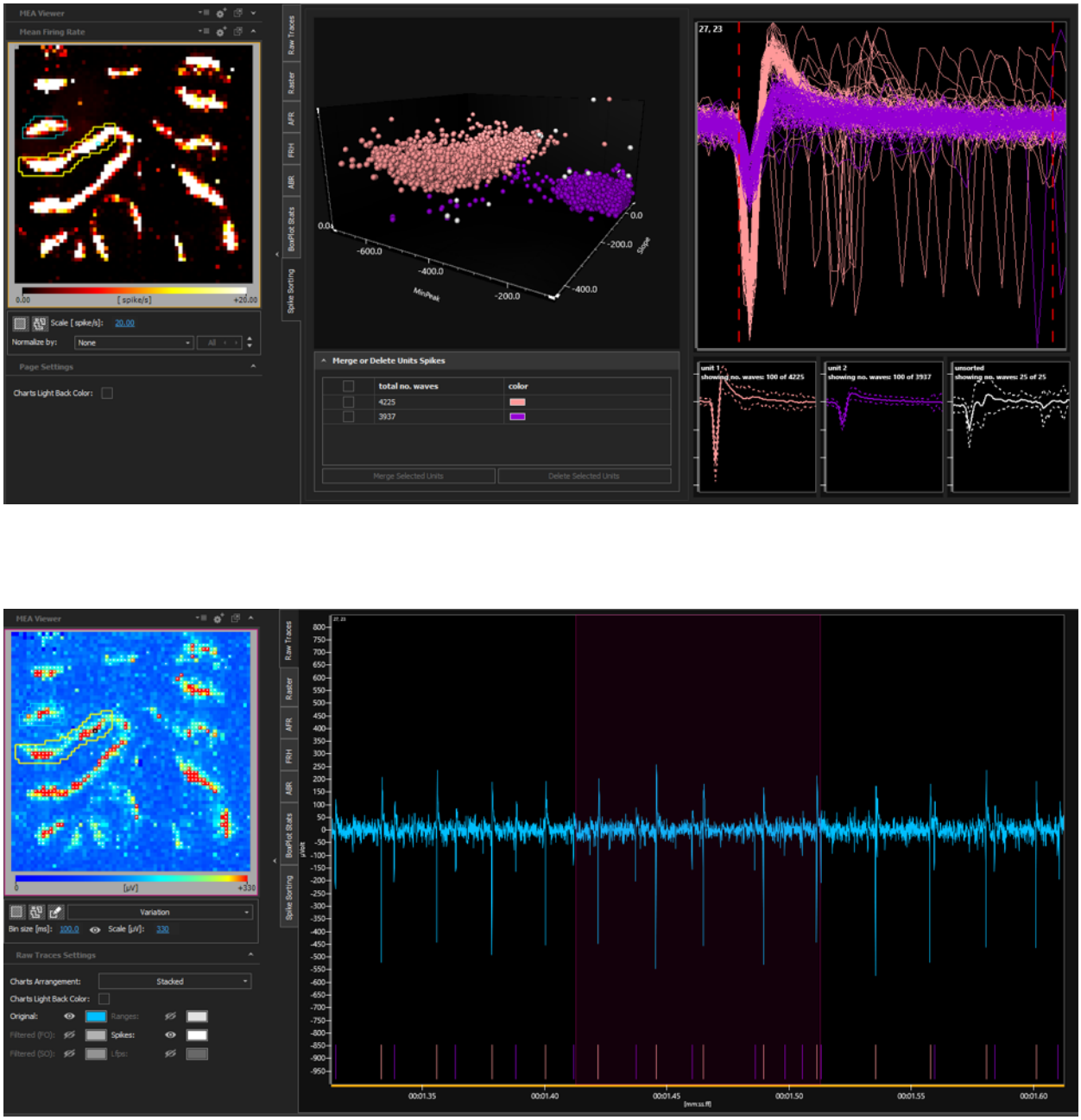

Fig. 2.13| Example of spike sorting performed with the Brainwave 4 software. Spike sorting leads to the definition of different clusters of spikes in each electrode recording a spiking activity. This figure reports an example of a channel presenting two waveforms with different features (one in pink, the other in violet). Spike markers in the raw trace of the same channel present the same colors used to display the clusters after spike sorting.

Finally, in order to avoid considering the same Purkinje cell multiple times in different electrodes, the software identified common units in nearby channels and retained the signal only in the channel showing the spikes with the largest amplitude (Fig. 2.14). Each step of this procedure was checked by user's supervision.

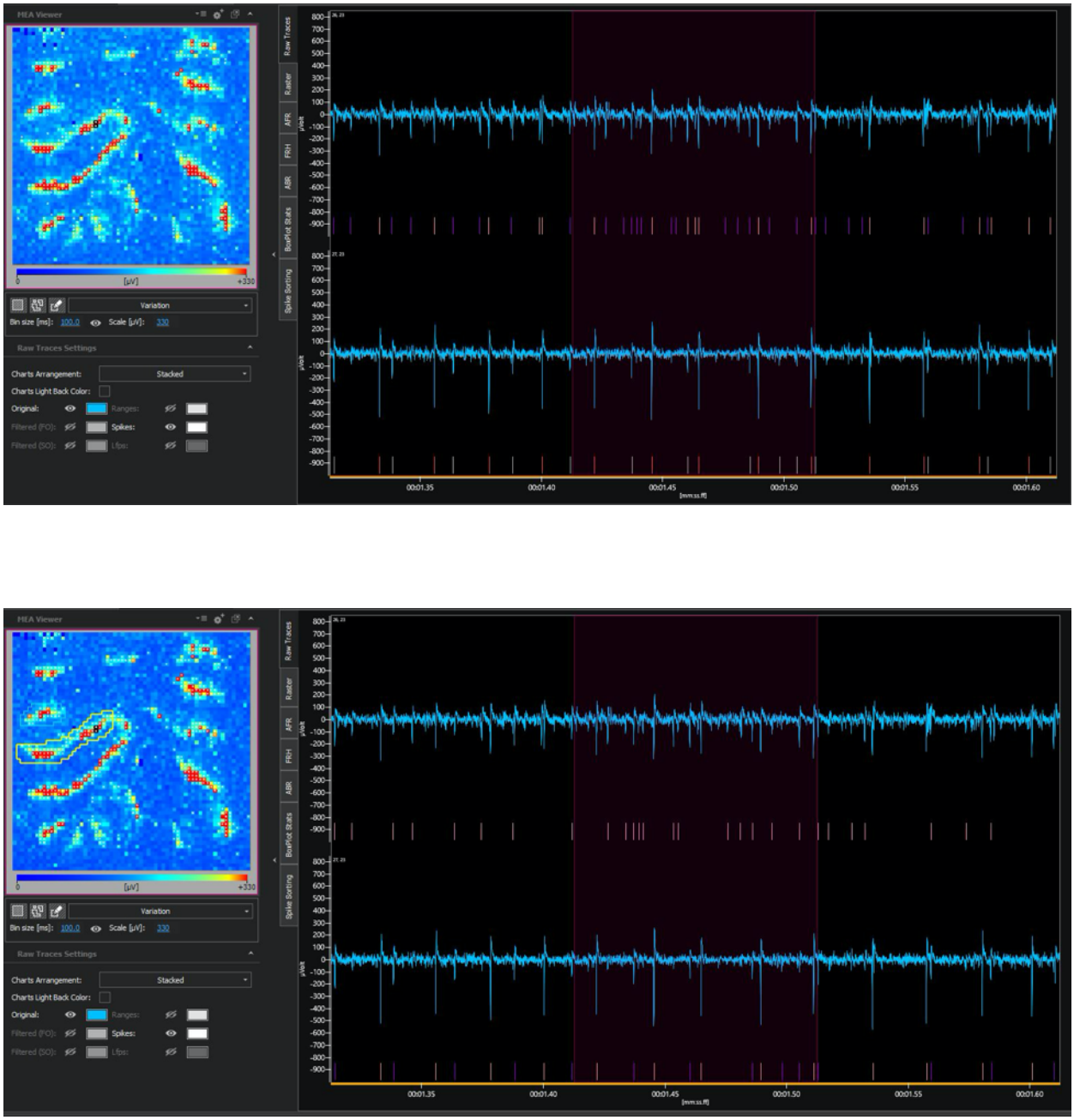

Fig. 2.14| Example of the elimination of common units in nearby channels performed by the BrainWave 4 software. On top, the picture shows two nearby channels detecting the same unit. After the elimination of common units performed with the Brainwave 4 software, each channel retained only the signal with the largest spike amplitude. In this way, the same Purkinje cell is not considered multiple times in different electrodes.

2.4.3 Raster plots, PSTHs and statistical analysis.

For each Purkinje cell detected a raster plot was reconstructed. This kind of plot was obtained aligning the spikes sorted for each channel from 30 consecutive trials on the stimulus onset. The x axis showed the duration of each trial (with 0 when stimulus was delivered), while the y axis showed the number of trials (Fig. 2.15).

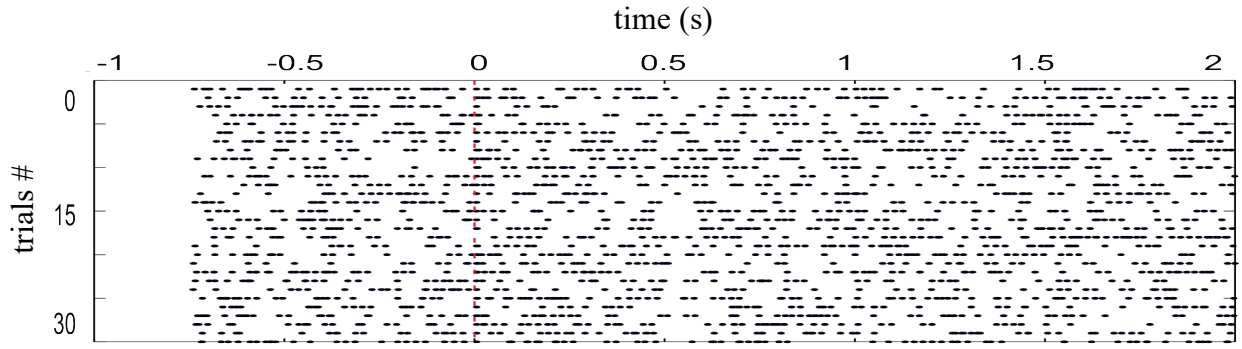

Fig. 2.15| Example of a Raster Plot of a channel in the region of interest. This graph shows all the spikes generated from a Purkinje cell recorded by one channel of the HD-MEA. The spikes are represented as dots.

In order to quantify Purkinje cells activity and their response to stimulation, Peri-Stimulus Time Histograms (PSTHs) were generated for each channel. PSTHs were reconstructed by binning the time period and calculating the number of spikes detected in every time-bin in every trial. Each bin in the PSTH represents the firing frequency in that time point of the Purkinje cell recorded (Fig. 2.16). In response to a stimulation, a Purkinje cell can show three different patterns:

- no change in firing frequency (not affected by stimulation);
- An increase in firing frequency (generating a peak in the PSTH emerging from the background discharge);
- A decrease in firing frequency (generating a pause in the PSTH).

In order to optimize PSTHs resolution, in this work a 5ms bin width was used to analyze peaks and a 20ms bin width was chosen for pauses.

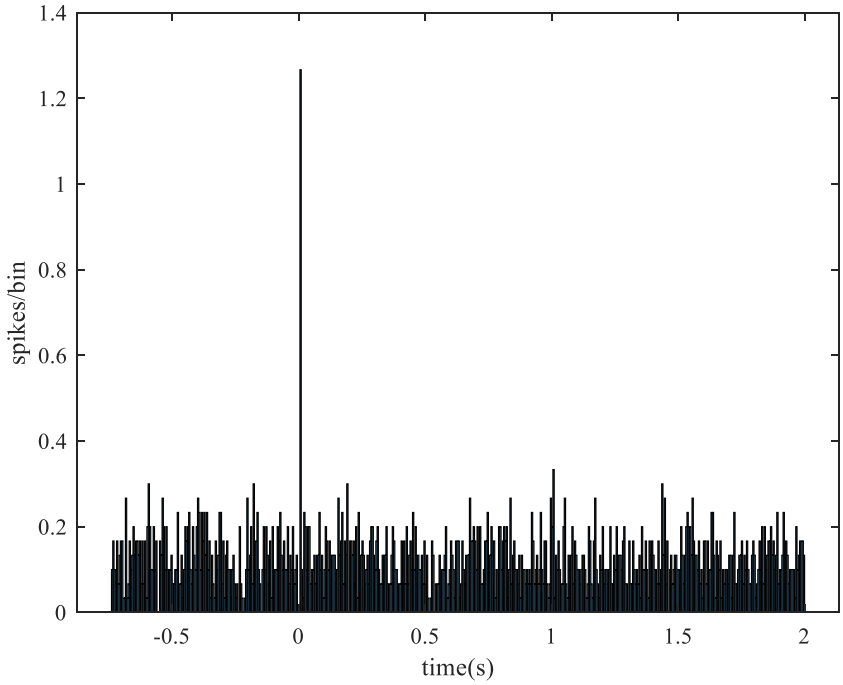

Fig. 2.16| Example of a Peristimulus Time Histogram. The histogram shows the firing frequency of a Purkinje cell recorded by one channel of the HD-MEA. Each bin represents a time period of 5 ms in which the average number of spikes detected in each trial for that time window is reported. The x axis shows the trial length with the stimulation time at 0, while the y axis shows the firing frequency in spikes/bin. An increase in firing frequency immediately after the stimulus originates a PSTH peak.

One tailed permutation test was used for peaks and pauses detection. The permutation test was restricted to increased Mean Firing Rate (MFR) for peaks and to decreased MFR for pauses. In both cases, it was followed by a False Discovery Rate (FDR) correction with alpha at 0.01. FDR correction was chosen to control probability of having at least one false positive result given the set of the reported positive results.

3. Aim of the thesis.

The primary aim of this thesis is to deepen our knowledge of cerebellar network input processing. For years the highly ordered cerebellar structure has incorrectly led to the idea that anatomical considerations would be sufficient to understand the underlying circuit dynamics. However, experimental data indicate that the cerebellum operates in a much more complex manner than predicted and that new experimental and computational tools are needed to investigate cerebellar network function and dynamics (D'Angelo et al. 2011). In **chapter 1** of this thesis, a complete description of the cerebellar network is provided, focusing on its ability to process incoming inputs bearing several frequencies and highlighting the essential role of the granular layer in performing spatio-temporal reconfiguration of signals. In **chapter 2**, a recent advanced technology is presented. The high-density multi-electrode array (HD-MEA) has been used to record neuronal activity with unprecedented detail respect to previous electrophysiological recording techniques. Being characterized by 4096 electrodes simultaneously recording, this technique opens a new perspective in the study of neuronal activity in an intact network with high temporal and spatial resolutions, allowing the investigation of the interaction of neuronal ensembles during whole network activation. The attention has been focused on two key points: the reconstruction of the spatio-temporal profile of the spread of activity in the network depending on input frequencies (**chapter 4**) and the investigation of the neurophysiological mechanisms underlying region and frequency dependence of vascular responses in the cerebellum (**chapter 5**).

Though some partial investigation of cerebellar input processing has already been performed, a thorough analysis of the frequency dependence of cerebellar cortical processing is still lacking. A characterization of cerebellar input processing would help to better understand cerebellar contribution not only in sensori-motor integration but also in complex brain states related processes. For all these reasons, in **chapter 4** an investigation performed stimulating mossy fibers at different input frequencies, in order to mimic different brain states, is reported. The activity was recorded from parasagittal and coronal slices, reconstructing a map of granular layer and Purkinje cells layers activation in a frequency-dependent manner. Taking into account the high level of geometry characterizing the organization of neuronal elements in the cerebellar cortex (D'Angelo 2018), the use of both parasagittal and coronal slices was fundamental in order to reconstruct input spreading throughout the "real" network. The results provided by this analysis appear to be a new starting point for the development of computational models taking into account the influence of frequency variations on cerebellar network functioning and for clarifying its contribution in higher cognitive functions (D'Angelo 2019).

In **chapter 5** the attention has been focused on differences between neuronal activity in cerebellar vermis and hemisphere. This difference has never been investigated *ex-vivo*, though fMRI studies in humans have shown a different activation of cerebellar vermis and hemisphere performing the same motor task (Alahmadi et al. 2017). The region and frequency dependence of vascular responses has been confirmed through an investigation of capillaries motility in cerebellar vermis and hemisphere slices (Gagliano et al., *in preparation*), but the description of the neurophysiological basis of these differences is still lacking. Therefore, in this second part of the thesis HD-MEA recordings of cerebellar vermis and hemisphere granular layer activity were performed while activating mossy fibers at different input frequencies. This led for the first time to the observation of a frequency dependence and a region dependence of the neuronal response, supporting the ability of cerebellar regions to differentiate neurovascular responses. Moreover, a computational model of granular layer activity (Casali et al. 2020) has been used to unravel the correlation between neuronal activity and

capillaries motility. Taken together the results achieved in this study led to a novel detailed description of neurovascular mechanisms in the cerebellum, taking into account their frequency and region dependence.

In **chapter 6** a general discussion is proposed, in order to summarize and discuss the findings reported in previous chapters.

4.

Spatio-temporal reconstruction of the spread of activity in the cerebellar network exploring its frequency dependence.

Monteverdi A.[1], Di Domenico D. [1], Mapelli L[1]. and D'Angelo E.[1*]*

[1] Dept of Brain and Behavioral Sciences, University of Pavia, 27100 Pavia, Italy

AUTHOR CONTRIBUTIONS: L.M. and E.D. designed research; A.M. performed HD-MEA recordings and data analysis; D.D.D. contributed to data acquisition and analysis; A.M., L.M., and E.D. wrote the paper.

* Lisa Mapelli and Egidio D'Angelo are co-senior authors

In preparation

4.1 ABSTRACT

The cerebellar cortex receives extensive inputs from motor and non-motor areas of the cortex and from the brain stem. Therefore, the cerebellum is likely to receive inputs at different frequency ranges. Nevertheless, a thorough investigation of the frequency-dependence of cerebellar cortical processing is still missing. The characterization of cerebellar processing at different input frequencies shed new light on cerebellar contribution not only in sensori-motor integration, but also in complex brain states related processes. Thus, the main aim of this work is to perform a comprehensive study of cerebellar cortex responsiveness at different input frequencies, reconstructing the spread of activity in cerebellar sagittal and coronal slices. Thanks to the extremely high spatial and temporal resolution of an HD-MEA (4096 electrodes simultaneously recording), it was possible to record the simultaneous activation of cerebellar granular and molecular layers highlighting frequency dependent mechanisms and the spatial distribution of activity with unprecedented details. Different brain activity ranges were mimicked stimulating mossy fibers at different frequencies (5 pulses at 6Hz, 20Hz, 50Hz and 100Hz). Focusing the attention on granular layer activity, the spatial organization of short-term plasticity mechanisms and their frequency dependence was reconstructed, suggesting a possible frequency-dependent involvement of inhibitory mechanisms in sagittal and coronal slices. Then, the high spatial resolution of recordings allowed to reconstruct the precise spatial location of Purkinje cells in the stimulated lobule, showing a zebrin-like distribution pattern of Purkinje cells in the coronal plane. Mossy fibers stimulation elicited different Purkinje cells responses in sagittal and coronal slices likely due to the activation of two distinct pathways involving ascending axons or parallel fibers. Several units were analyzed in the sagittal and coronal plane (n=1953 in 9 parasagittal slices and 9 coronal ones), reconstructing the whole network activation at different input frequencies. This eventually led to the evaluation of the correlation levels between granular and Purkinje cells layers activation, taking into account its frequency-dependence. Taken together these results open a new perspective for the

evaluation of the computational power of the cerebellar cortex, allowing levels of details never obtained before.

4.2 INTRODUCTION

A deeper understanding of neuronal ensembles activity and connectivity within intact networks has become a primary aim of neuroscience. The overcoming of previous technical limitations makes this kind of investigations now feasible. Considering the organization of the cerebellar network and the available information about its spatio-temporal distribution of activation, the cerebellum appears to be an ideal candidate for a circuit dynamics assessment. The cerebellar network is characterized by a well-organized modular structure repeating itself almost identically along the whole cortex (D'Angelo 2018). This led for years to the incorrect idea that anatomical considerations will be sufficient to understand the underlying circuit dynamics. However, an increasing amount of experimental data in the last decade suggests that cerebellar processing is more complex than predicted, and its network complexity still deserves a deeper investigation. The granular layer plays a central role in cerebellar processing receiving inputs at different frequencies from several brain areas. The granular layer exerts multiple dynamic properties for inputs integration, from oscillations to resonance (D'Angelo et al. 2009), and allows the spatio-temporal reconfiguration of incoming signals (D'Angelo 2011) which are then conveyed to the molecular layer. To further complicate the picture, several forms of synaptic plasticity occur at multiple sites of the cerebellar network and contribute to shape the final output of cerebellar cortex computation (D'Angelo 2014). A detailed investigation of cerebellar network functioning and its modulation during different ranges of activity is needed to understand its role in complex processing. For years, the functional aspects of this highly ordered network have been evaluated in a motor control perspective, highlighting the essential role of cerebellum in motor learning and coordination (D'Angelo 2018). Recently though, an increased amount of studies is suggesting a cerebellar involvement in higher cognitive processes (D'Angelo 2019). In humans, a diffusion magnetic resonance imaging (MRI) tractography study has been able to map the connections between the cerebellum and cerebral cortex, revealing a more extended cerebellar connection with areas involved in cognitive functions than with areas involved in sensori-motor control (Palesi et al. 2015). Moreover, functional MRI studies showed the cerebellar engagement in an extended Action Execution-Observation Network, supporting its role in complex processing (Casiraghi et al. 2019). Thus, the primary aim of this work is to investigate the role of different neuronal components of the cerebellar cortical circuit, in order to gain a deeper insight into frequency-dependent cerebellar elaboration of incoming stimuli and its role in complex input processing. Cerebellar cortical activity is known to be frequency dependent: the granular layer appears to be well equipped for the development and maintenance of rhythmic low-frequency activity (theta band, 2-10Hz), presenting coherent oscillations and resonance (D'Angelo et al. 2009); when basal activity of mossy fibers is around 20Hz, an increase in the responsiveness of granule cells and Golgi cells and a coherent organization of the granular layer emergent activity has been predicted (Solinas et al. 2010); mossy fibers burst above 50Hz are efficiently transmitted by granule cells, optimally reaching the molecular layer (Mapelli et al. 2010); mossy fibers stimulation around 100Hz maximally evokes Purkinje cells response located over the excited granular layer area (Mapelli et al. 2010). However, the influence of frequency variation and the spatial distribution of activity on the entire cerebellar network are still not fully understood and need a deeper investigation.

Herein, we took advantage of a high-density multielectrode array (HD-MEA) device, to simultaneously record activity from 4096 electrodes, covering all the cortical layers. Mossy fibers were stimulated in sagittal and coronal cerebellar slices at different frequencies (6Hz, 20Hz, 50Hz,

100Hz), to mimic different ranges of brain activity. The sagittal plane is more suited to study the ascending connections among granule cells and PCs located above, in a radial manner (mainly through granule cells ascending axons synapses). The parallel fibers (PF), granule cells axons, travel in the coronal plane. This plane is then ideal to investigate the processing along the PF axis, most likely involving molecular layer interneurons (MLI). Granule cells and Purkinje cells responses have been characterized in a frequency-dependent manner, reconstructing a map of the spatial distribution of granular and Purkinje cell layers activation and correlating the activity in these two regions. Taken together, data coming from both sagittal and coronal slices led to the reconstruction of the cerebellar cortex processing and its modification during different regimes of activity with unprecedented spatial and temporal resolution. Compelling differences have been highlighted in sagittal and coronal slices granular layer and Purkinje cells responses, unraveling a strict frequency dependence of cerebellar network activity. All the information on the granular and molecular layers gained with these analyses pointed out the importance of frequency variations on cerebellar network functioning and consequently will be fundamental for the development of future advanced computational models.

4.3 MATERIALS AND METHODS

4.3.1 Slice preparation and maintenance.

Acute parasagittal or coronal cerebellar slices (220 μm thick), according to the experimental settings, were obtained from 18 to 23-days-old C57BL/6 mice of either sex. Animals were anesthetized with halothane (Aldrich, Milwaukee, WI) and killed by decapitation. The cerebellum was gently removed in order to isolate the vermis, fixed with cyanoacrilic glue on the specimen support of a vibroslicer (LEICA VT1200S), used to obtain the slices. The whole procedure was performed in cold and oxygenated Krebs solution which contained (in mM): 120 NaCl, 2 KCl, 1.2 $MgSO_4$, 26 $NaHCO_3$, 1.2 KH_2PO_4, 2 $CaCl_2$,11 glucose, pH 7.4 equilibrated with 95% O_2–5% CO_2. Slices were recovered for 1 hour in the same solution before recording. In order to record cerebellar activity, slices were gently positioned on the HD-MEA chip improving the coupling with the electrodes array using a platinum ring with a nylon mesh. Oxygenated Krebs solution (2-3 ml/min) was continuously perfused in the glass reservoir during the whole recording session and maintained at 32 ºC with a Peltier feedback temperature controller (TC-324B; Warner Instrument Corporation). HD-MEA recordings are described in detail below.

4.3.2 HD-MEA recordings.

The investigation of the cerebellar circuit was conducted using a complementary metal-oxide-semiconductor (CMOS) based high-density multielectrode array (HD-MEA; Biocam X, 3Brain AG). This device performs extracellular recordings from 4096 electrodes and allows to monitor neuronal activity with unprecedented detail compared to previous electrophysiological recording techniques. Electrodes are arranged in a 64x64 matrix on an area of 2.67mm x 2.67mm and have a size of 21μm x 21μm with a pitch of 42 μm (Biochip Arena). The whole chip is packaged onto a substrate together with a glass reservoir with a diameter of 25mm and 7mm in height. Signals were sampled at 18kHz/electrode, with a high pass filter at 100Hz. Electrical stimulation was provided using a bipolar tungsten electrode positioned on the mossy fibers bundle (pulses of 50 μA with a duration of 200 μs). In order to investigate cerebellar processing of inputs at different frequencies, 30 single stimuli were delivered at 0.1 Hz, followed by 30 bursts of 5 impulses at 6Hz, 20Hz, 50Hz and 100Hz (in mixed combinations) repeated every 10 seconds.

4.3.3 Data analysis.

4.3.3.1 Local Field potential analysis.

Mossy fibers stimulation elicited granule cells response observed in the form of Local Field Potentials (LFP) propagating through the granular layer. This kind of signal was characterized by a typical N_1-N_{2a}-N_{2b}-P_2 complex, in agreement with previous reports in similar experimental conditions ((Mapelli and D'Angelo 2007). In this complex, N_1 derives from the activation of the presynaptic volley, N_{2a} and N_{2b} are informative of granule cells synaptic activation, and P_2 represents the current returning from the molecular layer. Data were displayed on-line and stored using the BrainWave X Software (3Brain AG) and data analysis was performed using *ad-hoc* routines written in MATLAB (Mathworks). In order to investigate granule cells synaptic activation, the attention was focused on N_{2a} and N_{2b} peaks amplitudes. Peaks amplitudes were calculated subtracting the negative peaks found in the appropriate time window (1.9ms±1.1 ms and 4.5ms±1.2 ms from the stimulus artifact, for N_{2a} and N_{2b}, respectively) to the baseline derived from the averaged signal in 300ms before the stimulus onset. LFP signals were considered for the analysis only when peaks amplitudes exceeded 3 times (for N_{2a}) and 2.5 times (for N_{2b}) the standard deviation calculated over the baseline period, in response to at least the 75% of trials. The LFP spread through the granular layer and could range up to several tens of micrometer along the stimulated lobule. Only channels showing LFP signals that remained stable during the entire duration of the experiment were considered for the analysis (using unpaired Student's t-test, $p<0.05$). Then, N_{2a} and N_{2b} amplitude changes during the stimulation trains at different input frequencies were reconstructed. The percent change between the first and the last response peak within each stimulation pattern was calculated both for N_{2a} and N_{2b}, and then used to generate colormaps to represent the corresponding spatial distribution. The signals showing a statistically significant change (unpaired Student's t-test, $p<0.05$) in N_{2a} and N_{2b} peak amplitudes at the end of the 5 pulses stimulation compared to the first response in the train were considered undergoing short-term plasticity (STP).

4.3.3.2 Purkinje cells firing analysis.

Purkinje cells auto-rhythmic spiking activity was recorded using the BrainWave X software. The analysis of Purkinje cells firing was performed using BrainWave 4 software (3Brain AG) and *ad-hoc* routines written in MATLAB (Mathworks). Spike detection of Purkinje cells activity was performed in BrainWave 4 using the hard threshold of -100μV (refractory period of 1 ms). Spike detection was followed by the waveform extraction in a temporal window of 0.5 ms pre-spike and 3ms post-spike and the spike sorting using the Principal Component Analysis followed by a clustering k-mean algorithm. Pakhira-Bandyopadhyay-Maulik (PBM) index was used for validating clustering results. Due to the inter-electrode tip distance of 42μm and the large Purkinje cell soma (25-40μm diameter), commonly more than a unit was detected by each single electrode of the HD-MEA. The BrainWave 4 software was used to eliminate common units in nearby channels and retain the signal only in the channel presenting spikes with the largest amplitude. In this way the same Purkinje cell was not considered multiple times in different electrodes. User's supervision of every step of this procedure was performed. Then peri-stimulus time histograms (PSTHs) and raster plots were used for the analysis of Purkinje cells responses to stimulation, normally consisting of peaks and pauses emerging from background discharge. An increased in firing frequency was defined as a peak in PSTHs, while a decrease in firing frequency was defined as a pause. In order to optimize PSTHs resolution, a 5ms bin width was used to analyze peaks and a 20ms bin width was chosen for pauses. One tailed

permutation test was used for peaks and pauses detection. The permutation test was restricted to increased Mean Firing Rate (MFR) for peaks and to decreased MFR for pauses. In both cases, it was followed by an FDR correction with alpha at 0.01. For each Purkinje cell detected, the MFR was calculated on the 500ms pre-stimulus and used to generate colormaps. Then the % change of the MFR within each stimulation pattern was calculated comparing the MFR at the beginning of the trains at different input frequency with the MFR at the end of the trains at different input frequencies. This % change was used to generate colormaps together with the % change of N_{2a} peak amplitude obtained from the previous analysis.

4.3.3.2 Correlation matrix.

In order to unravel possible correlations between granular and Purkinje cells layer activations and their frequency-dependence, two different types of correlation matrices were reconstructed. In the first case, for each channel of the granular layer the N_{2a} peak amplitudes detected after 30 single stimuli delivered at 0.1 Hz were taken into account and normalized for the largest amplitude detected. For each channel detecting a Purkinje cell activity, the MFR was calculated in the 20ms after each of the 30 single stimuli delivered at 0.1 Hz, subtracted for the MFR calculated in the 500ms pre-stimulus and normalized for the maximum MFR detected. The normality of data distribution was confirmed with 10 different normality tests (Öner and Kocakoç 2017). The Pearson correlation coefficient was calculated between these two samples of channels, retaining for each channel the maximum and the minimum value of correlation found. Then a threshold of 0.5 (or -0.5) was set looking at the significance of the Pearson correlation (values with a coefficient higher than 0.5, or lower than -0.5, always presented $p<0.01$). In the second type of correlation matrices, for each channel of the granular layer at each frequency of stimulation the percent change of N_{2a} peak amplitude within each of the 30 bursts of 5 pulses was considered. On the other hand, for each channel detecting a Purkinje cell the percent change of the MFR within each of the 30 bursts at different frequency was considered. The Pearson correlation coefficient was computed for each stimulation frequency between the two samples of channels, retaining for each channel the maximum and the minimum value of correlation found and setting a threshold of 0.5 ($p<0.01$).

4.4 RESULTS

4.4.1 Spontaneous and evoked cerebellar cortical activity.

Recording of slices spontaneous activity (Fig. 1) revealed the presence of autorhythmic firing in Purkinje cells. As expected, the granular layer was silent at rest. Mossy fibers stimulation evoked granule cells response, recorded as an LFP propagating through the granular layer of the stimulated lobule both in parasagittal and coronal slices (Fig. 1). LFPs showed the typical N_1-N_{2a}-N_{2b}-P_2 complex in agreement with previous observations (Mapelli and D'Angelo 2007, Maffei et al. 2002). The analysis was focused on N_{2a} and N_{2b} peaks as a measure of postsynaptic granule cells activation (see Methods for details). Over the large sample obtained (9 parasagittal slices, 804 channels and 9 coronal slices, 1649 channels) (Table1), average peak delays and amplitudes values for N_{2a} and N_{2b} peaks were as follows: N_{2a}, 1.6 ± 0.02 ms, -233.29 ± 21.37 μV in parasagittal slices and 1.55 ± 0.04 ms, -214.04 ± 19.58 μV in coronal slices; N_{2b}, 4.5 ± 0.09 ms, -76.79 ± 3.85 μV in parasagittal slices and 4.25 ± 0.16 ms -71.80 ± 1.9 μV in coronal slices. These data are in agreement with previous reports (Mapelli and D'Angelo 2007). N_{2a} and N_{2b} peaks amplitudes and delays did not present a

significant difference in sagittal and coronal slices (unpaired Student's *t* test, p>0.05). Channels in which the stability of LFP signals was confirmed during the whole experiment were taken into account for the evaluation of short-term plasticity (STP) in the granular layer. In the same slices, Purkinje cells activity was taken into account (1859 channels in parasagittal slices and 1809 channels in coronal slices) (Table1). Spike detection and spike sorting operations found 858 units in parasagittal slices and 1095 in coronal ones (Table1). The Mean Firing Rate (MFR) of the detected units was 58.11 ± 2.83 Hz in parasagittal slices (n=9) and 85.51 ± 8.02 Hz in coronal slices (n=9). Units detected in coronal slices showed higher MFR compared to the ones detected in sagittal slices (unpaired Student's *t* test, p=0.001).

For simplicity, the detailed analysis of cerebellar cortical responses to different frequencies of mossy fibers stimulation is reported separately for the experiments performed in sagittal and coronal slices. The comparison between these two conditions is highlighted in a devoted paragraph (see below).

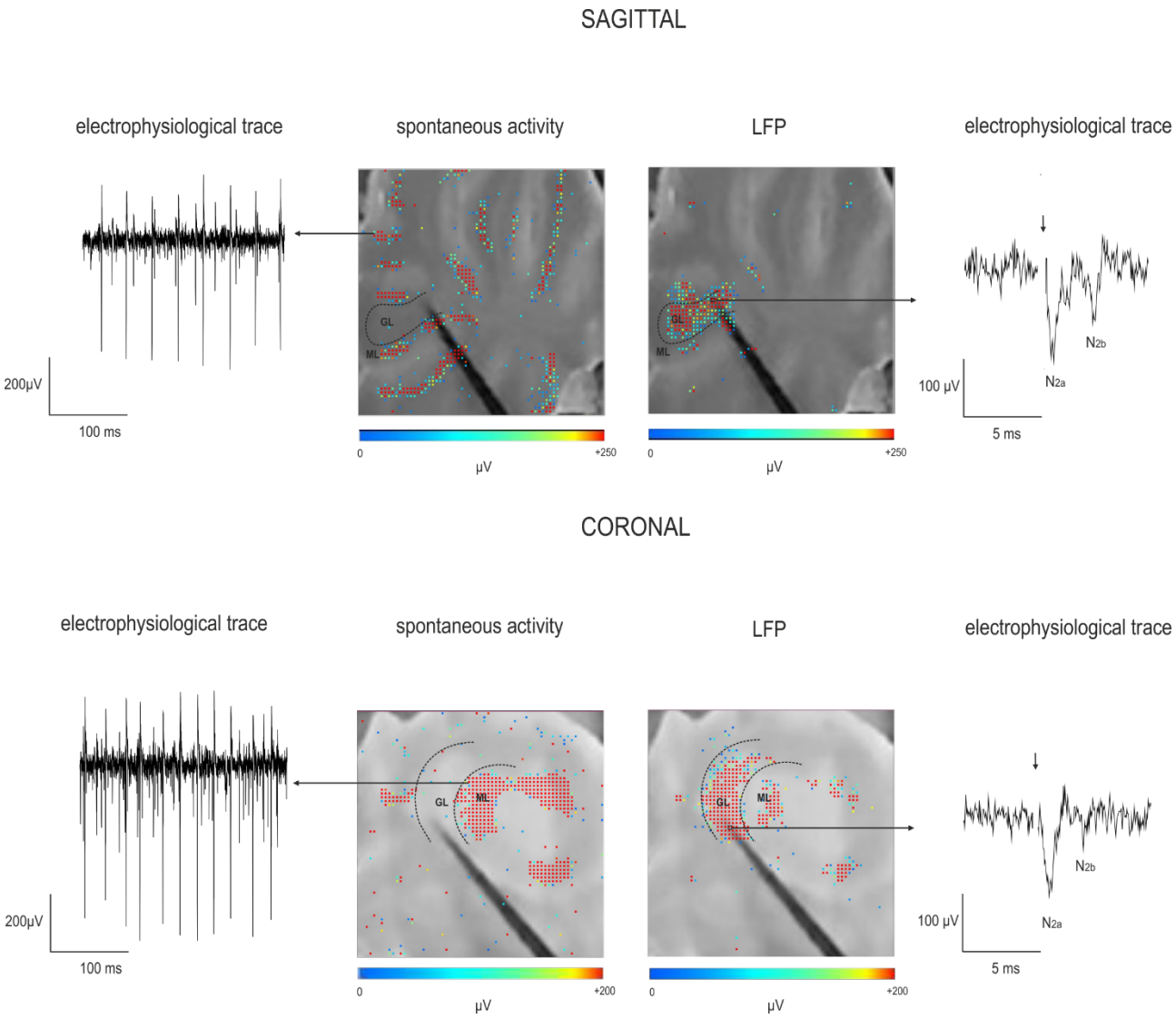

Fig.1| Typical HD-MEA recording. A classical recording using the HD-MEA chip leads to the observation of Purkinje cells spontaneous activity (in red) both in sagittal and coronal slices (gray area on background). Purkinje cells are autorhythmic at around 50Hz, as it can be observed selecting one of the recording channels in the molecular layer (indicated by the arrow on the left). Mossy fibers stimulation evoked a Local Field Potential (LFP) propagating through the granular layer both in sagittal and coronal slices. The LFP electrophysiological trace in the recording channels (indicated by the arrow on the right) presented the typical N1-N_{2a}- N_{2b} -P2 complex. The analysis was focused on the main peak of the LFP, N_{2a} and N_{2b}, as representative of granule cells activity (Mapelli and D'Angelo 2007).

	SAGITTAL	CORONAL	
	n=9	n=9	tot
ch granular layer	804	1649	2453
ch Purkinje cells	1859	1809	3668
detected units	858	1095	1953

Table 1| Recording channels and detected units. This table shows the number of channels in 9 parasagittal and 9 coronal slices detecting an LFP signal in the granular layer and Purkinje cells firing (ch=channels). Moreover, the number of units detected in sagittal and coronal slices after spike detection and spike sorting operations is reported. Finally in the last column this table contains the total amount of channels and units of all cerebellar slices.

Sagittal slices

4.4.2 Granular layer responses at different input frequencies.

4.4.2.1 N_{2a} and N_{2b} amplitude changes at different input frequencies.

In order to characterize granular layer response at different ranges of activity, the % change of N_{2a} and N_{2b} peaks amplitudes at the end of the 5 pulses stimulation compared to the first response in the train was calculated at different input frequencies (6Hz, 20Hz, 50Hz, 100Hz). The results showed a trend to decrease of N_{2a} peak amplitude while N_{2b} presented a more complex behavior increasing or decreasing its amplitude during the stimulation trains (Table 2A). However, while the percentage of channels showing a significant change of N_{2a} peak amplitude was always high in the granular layer (more than 70% of the recording channels), the percentage of channels detecting a significant change of N_{2b} was more than 40% only at high input frequencies (Table 2B).

A

	6Hz	20Hz	50Hz	100Hz
N_{2a}	-13.60±0.99	-15.58±1.45	-19.87±1.41	-27.37±1.92
N_{2b} +	12.33±1.68	13.89±2.01	17.13±2.83	20.09±3.18
N_{2b} -	-10.59±2.42	-13.36±3.08	-17.24±1.85	-13.48±2.10

B

	6Hz	20Hz	50Hz	100Hz
%ch N_{2a}	75.82±4.63	72.34±6.48	83.92±3.85	88.82±3.03
%ch N_{2b} +	11.83±3.61	16.94±5.74	25.74±5.88	40.09±9.05
%ch N_{2b} -	16.57±9.41	15.15±8.86	22.81±7.61	13.56±4.49

Table 2| N_{2a} and N_{2b} peak changes at different input frequencies. A) The table shows the percent change of the last response peak compared to the first one within each stimulation pattern. **B)** The table shows the percentage of channels in the granular layer recording a significant N_{2a} or N_{2b} peak amplitude change.
In both these tables N_{2b} + stands for N_{2b} amplitude increase during the stimulation trains while N_{2b} – refers to N_{2b} amplitude decrease during the stimulation trains.

The reconstruction of N_{2a} and N_{2b} peak amplitude changes for each pattern of stimulation led to the observation of different degrees of N_{2a} and N_{2b} changes inside the input trains (Fig. 2). Short-term depression was mainly detected for N_{2a} peak amplitude while N_{2b} appeared to weakly tend to increase especially at higher input frequencies. STP was identified for each channel showing a response every time that N_{2a} peak amplitude showed a statistically significant change (unpaired Student's *t* test, $p<0.05$) at the end of the 5 pulses stimulation compared to the first response in the train. As expected considering the mechanisms at the basis of STP (Sola et al. 2004), the decrease of N_{2a} peak amplitude became more evident increasing the stimulation frequency.

6Hz

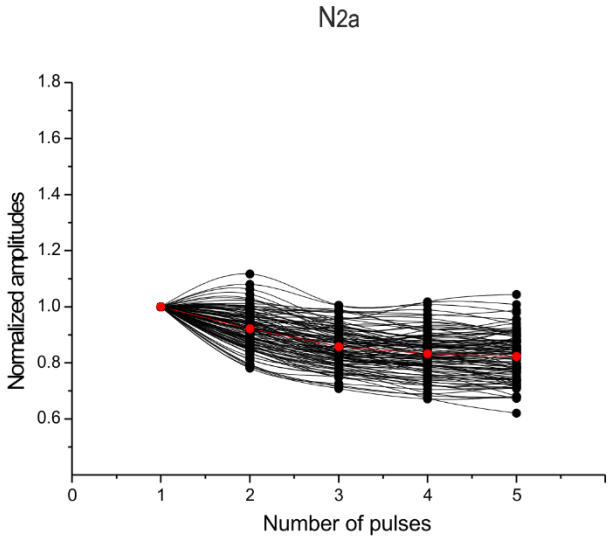
N2a
Normalized amplitudes
Number of pulses

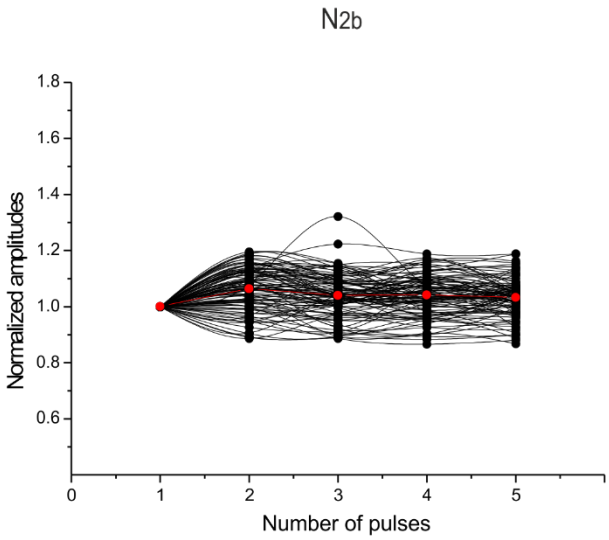
N2b
Normalized amplitudes
Number of pulses

20Hz

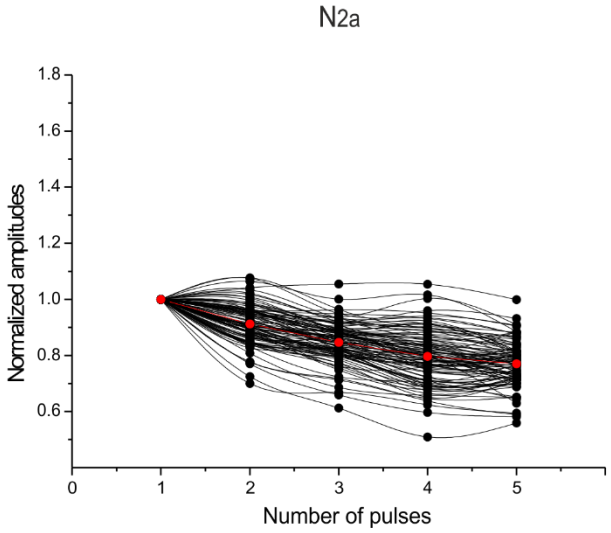
N2a
Normalized amplitudes
Number of pulses

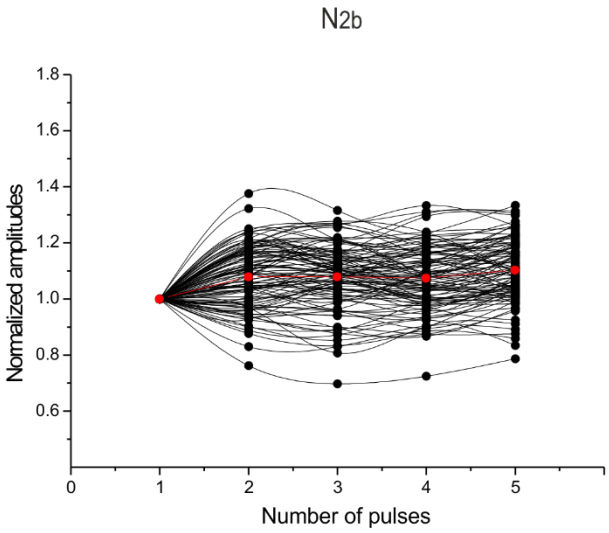
N2b
Normalized amplitudes
Number of pulses

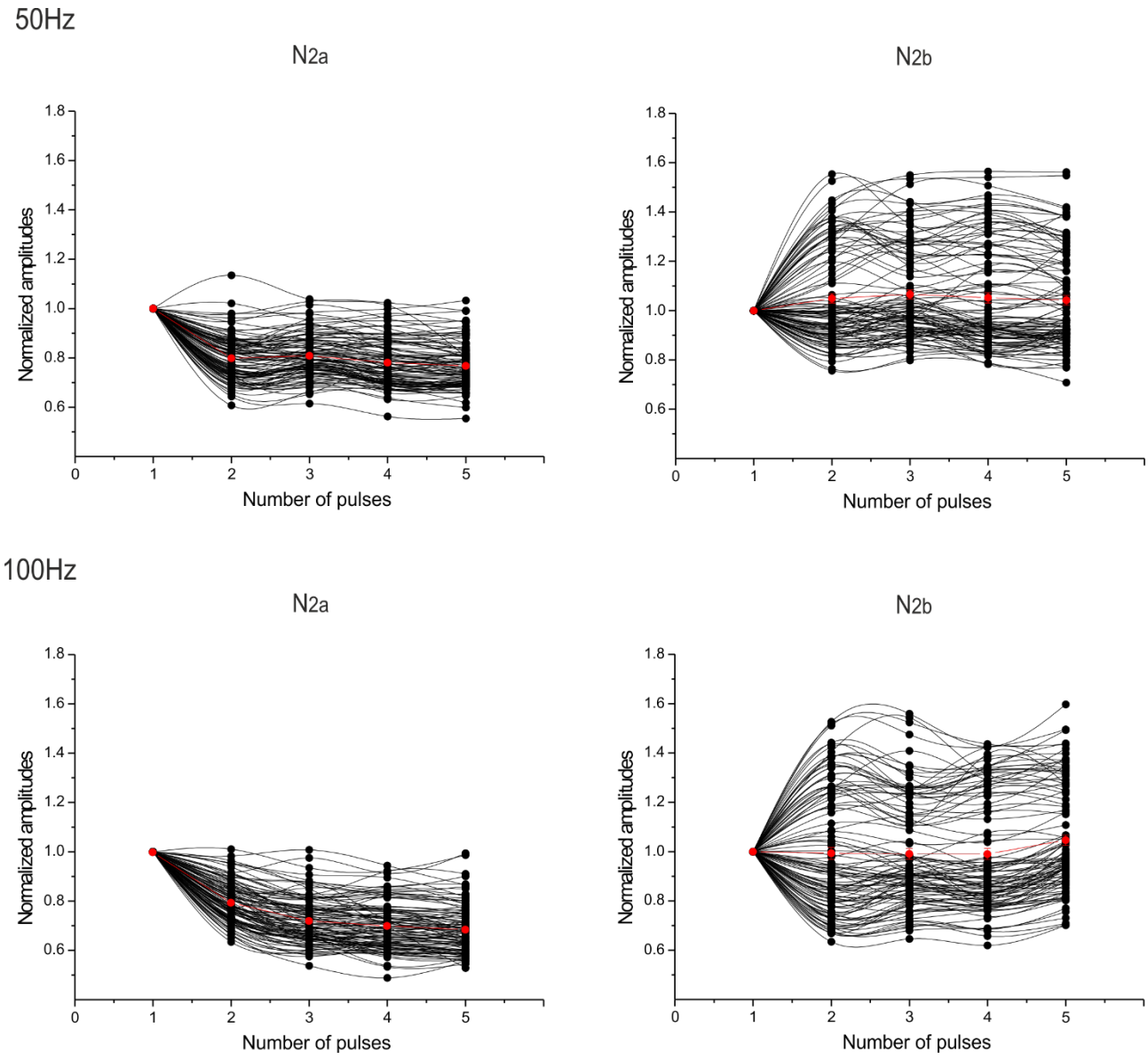

Fig. 2| Normalized N_{2a} and N_{2b} peak amplitudes during the stimulus train at different frequencies. N_{2a} and N_{2b} peak amplitudes were reconstructed in response to each of the five stimulation pulses in the train and normalized to the first response. Each line in the plot represents a channel considered for the analysis. The red line represents the average trend (a decrease of N_{2a} peak and an increase of N_{2b} peak).

4.4.2.2 The spatial organization of Short-Term Plasticity in the granular layer.

The percent change of N_{2a} and N_{2b} peaks was used to generate colormaps, showing the position of the channels in the cerebellar lobule originating the response. Colormaps constructed with N_{2a} peak percent change seemed to show a spatial organization of STP in the granular layer (Fig. 3). In particular, short-term depression appeared to be more pronounced in the center of the granular layer and this spatial organization became more evident increasing the stimulation frequency.

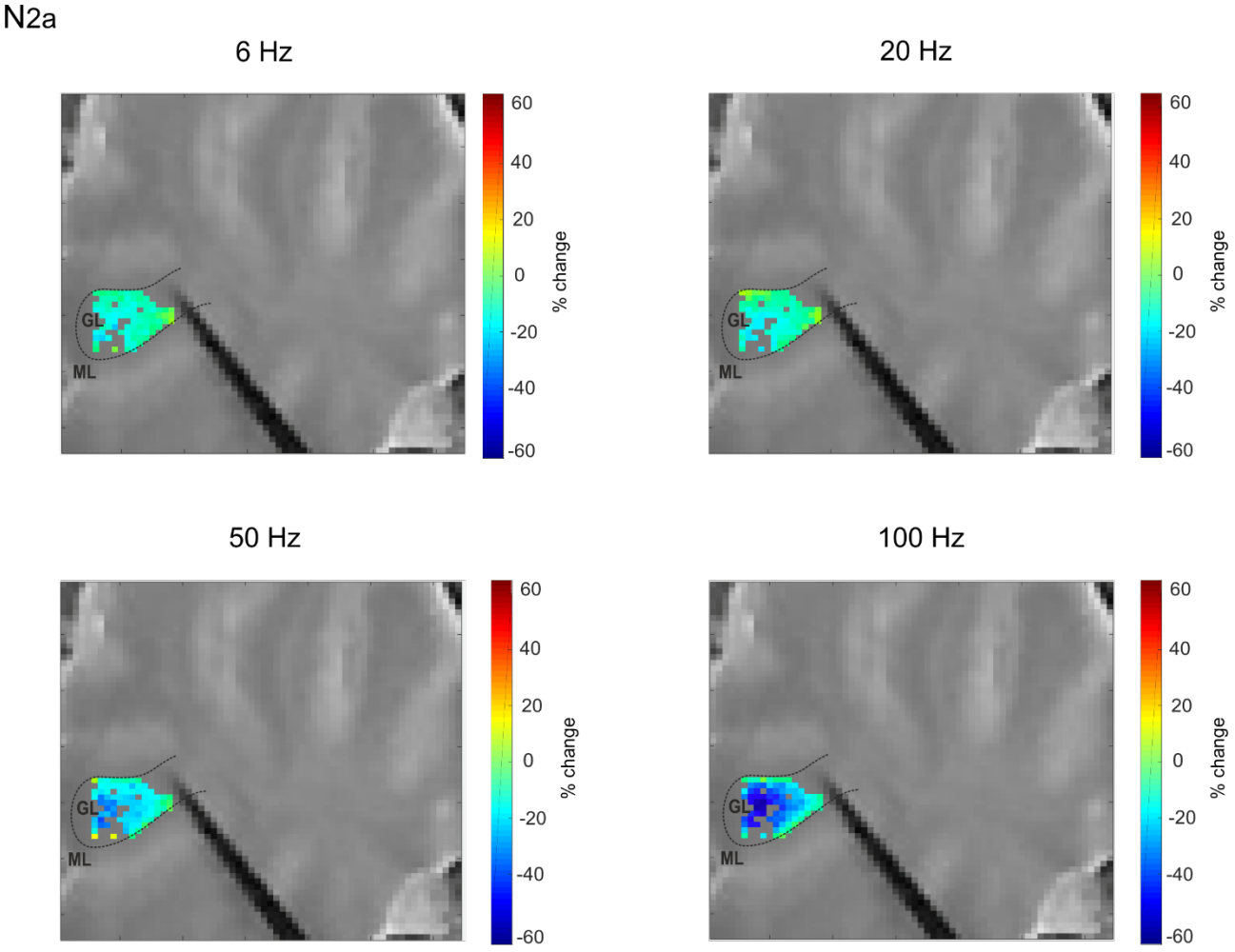

Fig. 3| The spatial organization of STP in a sagittal slice (N_{2a} peak). Colormaps were reconstructed for each stimulation pattern with the percent change of N_{2a} peak amplitude within the 5 pulses stimulation. Here, one sagittal slice (gray area on background) is reported as an example. As it can be observed, short-term depression prevailed (colorscale on the right) and was more pronounced in the middle of the granular layer increasing the input frequency.

An average colormap of all the recordings was reconstructed aligning the slices along the mossy fibers axis (Box 1; Fig. 4). This phenomenon could be simply due to the distribution of activated mossy fibers, more likely to activate granule cells synapses along the longitudinal axis of the stimulated lobule.

Box 1: Averaging Procedure

A

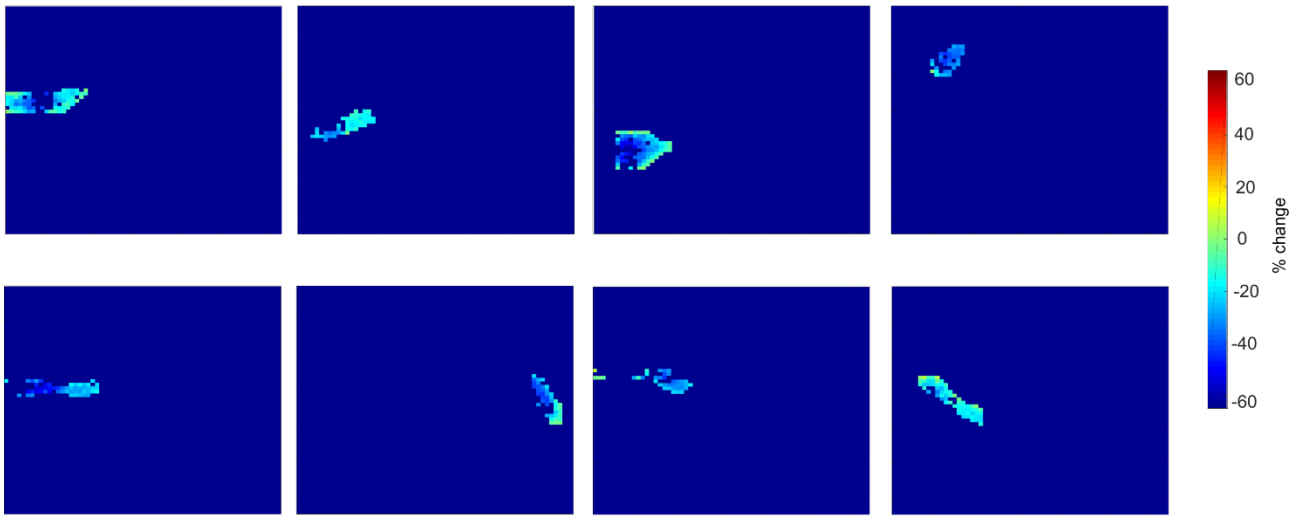

B

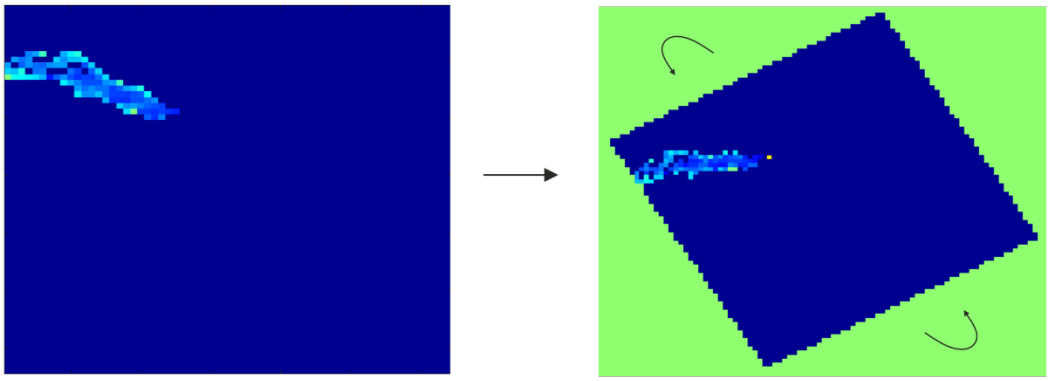

C

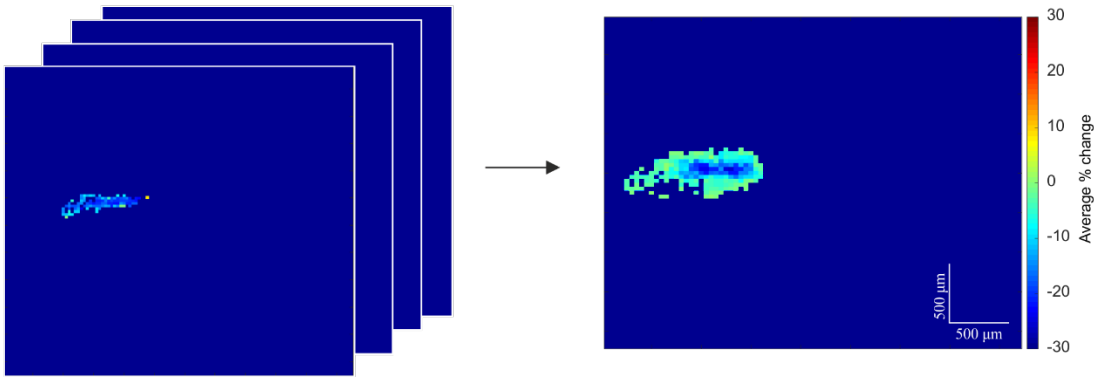

In order to better understand the spatial organization of STP in the granular layer an average colormap of all the recordings was reconstructed aligning the slices along the mossy fibers axis according to the following procedure: **A)** for each slice the percent change of N_{2a} (or N_{2b}) peak was used to generate colormaps, showing the position of the channels in the cerebellar lobule originating the response. Each slice presented a different number of channels recording an LFP signal and a different position of the activated lobule **B)** each colormap was reoriented positioning the stimulation site on the right (yellow dot in the figure) and aligned along the mossy fibers axis **C)** the average colormap was obtained centering all the colormaps on the stimulation site and then computing the average percent change for each channel.

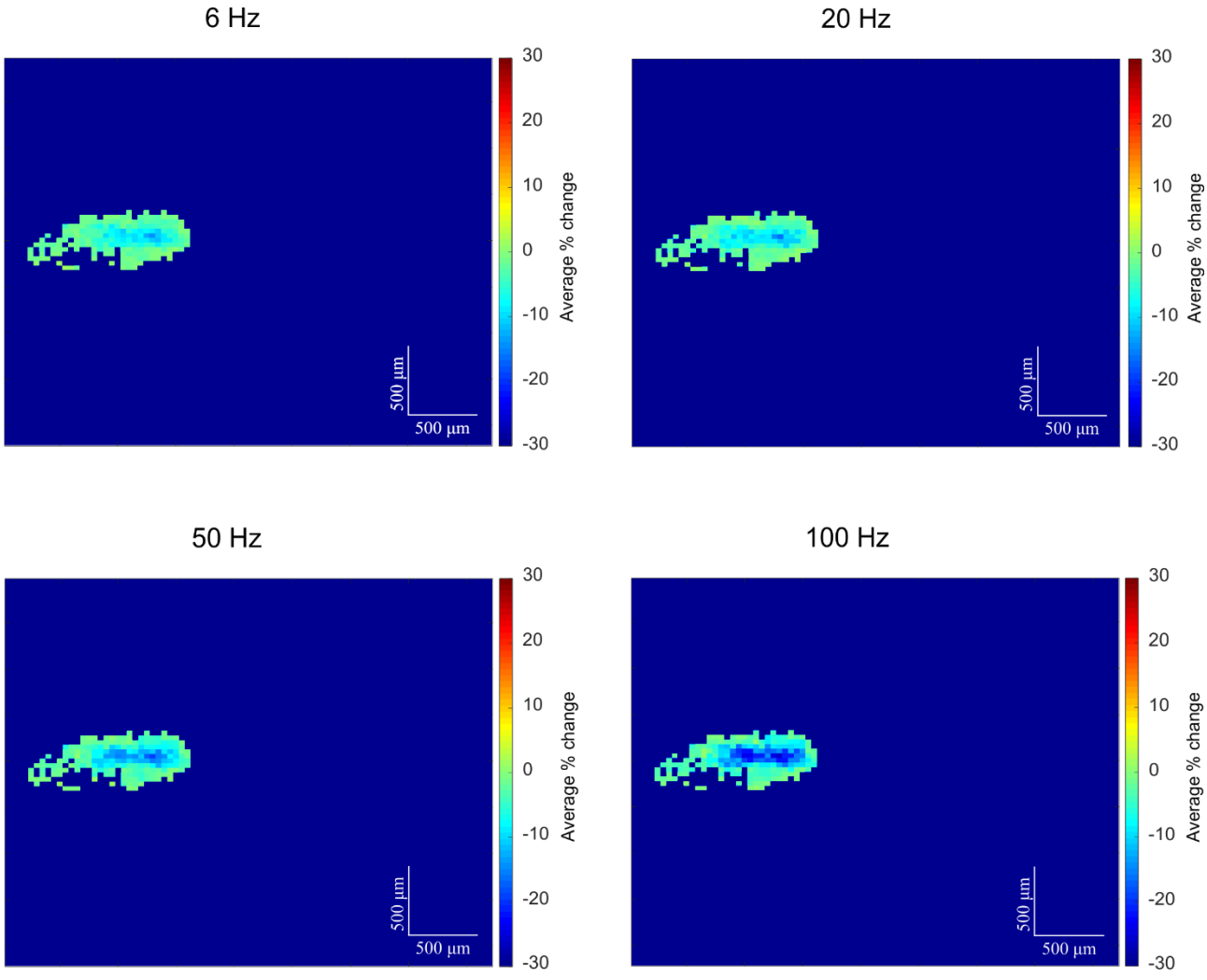

Fig. 4| The spatial organization of STP in the granular layer (N_{2a} peak). The average colormaps obtained aligning all the slices along the mossy fibers axis confirmed the spatial organization of STP in the granular layer. A more pronounced short-term depression phenomenon can be seen in the center of the activated granular layer. The increase of the input frequency enhanced this spatial organization (colorscale on the right).

The spatial organization of N_{2b} percent changes in the granular layer appeared to be different than the one presented by N_{2a} peak. In fact, as evident in the colormaps obtained for the single experiment shown in Fig. 5, the trend to increase of N_{2b} peak appeared more accentuated in the center of the granular layer, and this phenomenon was more evident increasing the input frequency. However, the reconstruction of the average colormap (BOX 1; Fig. 6) led to the observation of a more accentuated trend to increase of N_{2b} peak in different positions of the activated area. Given the role of inhibition in shaping the N_{2b} peak, it is possible that the spatial organization of inhibition in the granular layer, mainly due to the Golgi cell axonal plane, might have a role in this phenomenon.

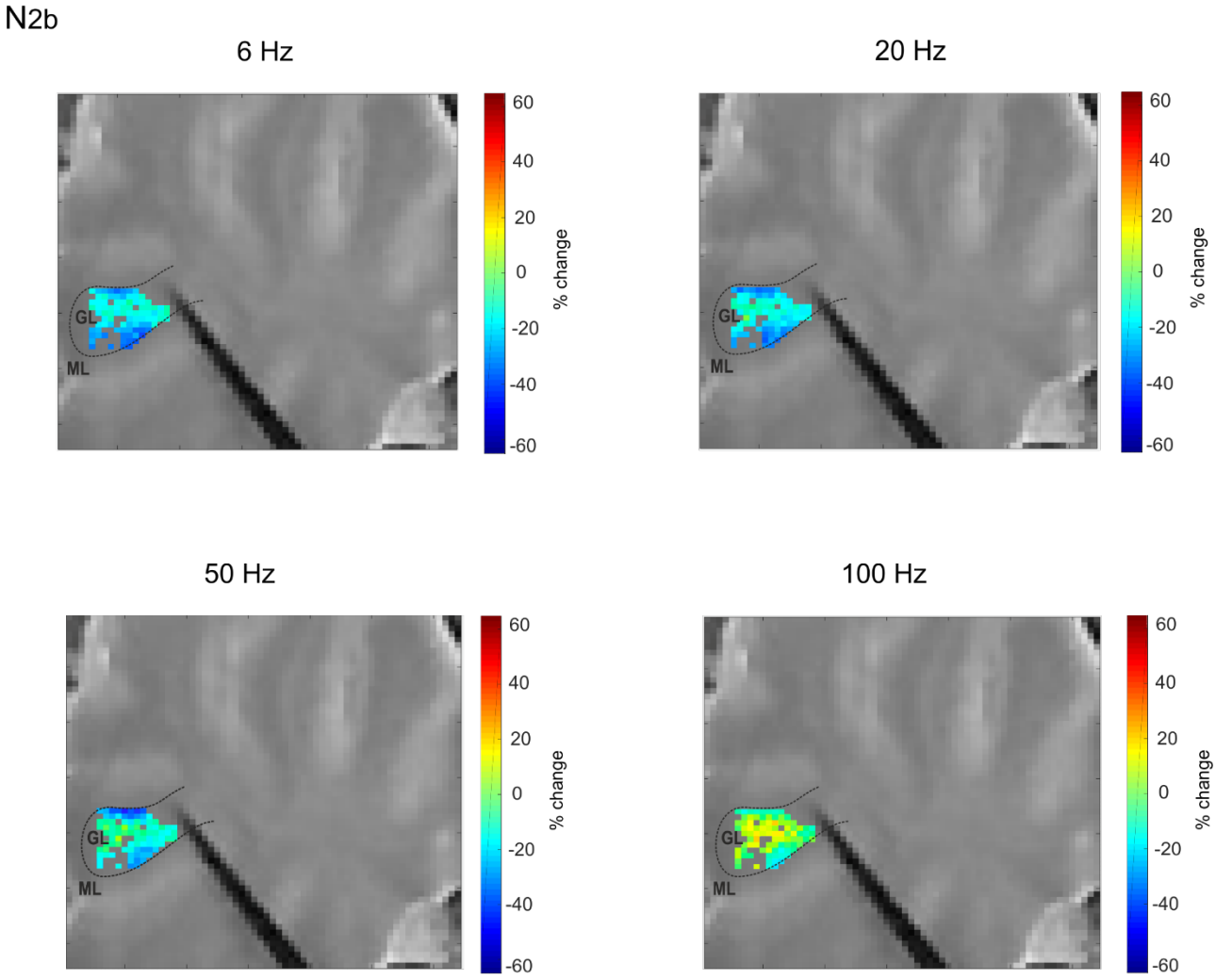

Fig. 5| The spatial organization of STP in a sagittal slice (N_{2b} peak). Colormaps were reconstructed for each stimulation pattern with the percent change of N_{2b} peak amplitude within the 5 pulses stimulation. Here, one sagittal slice is reported as an example (gray area on background). As it can be observed, the trend to increase of N_{2b} peak appeared more accentuated in the center of the granular layer (colorscale on the right), and this phenomenon became more evident increasing the input frequency.

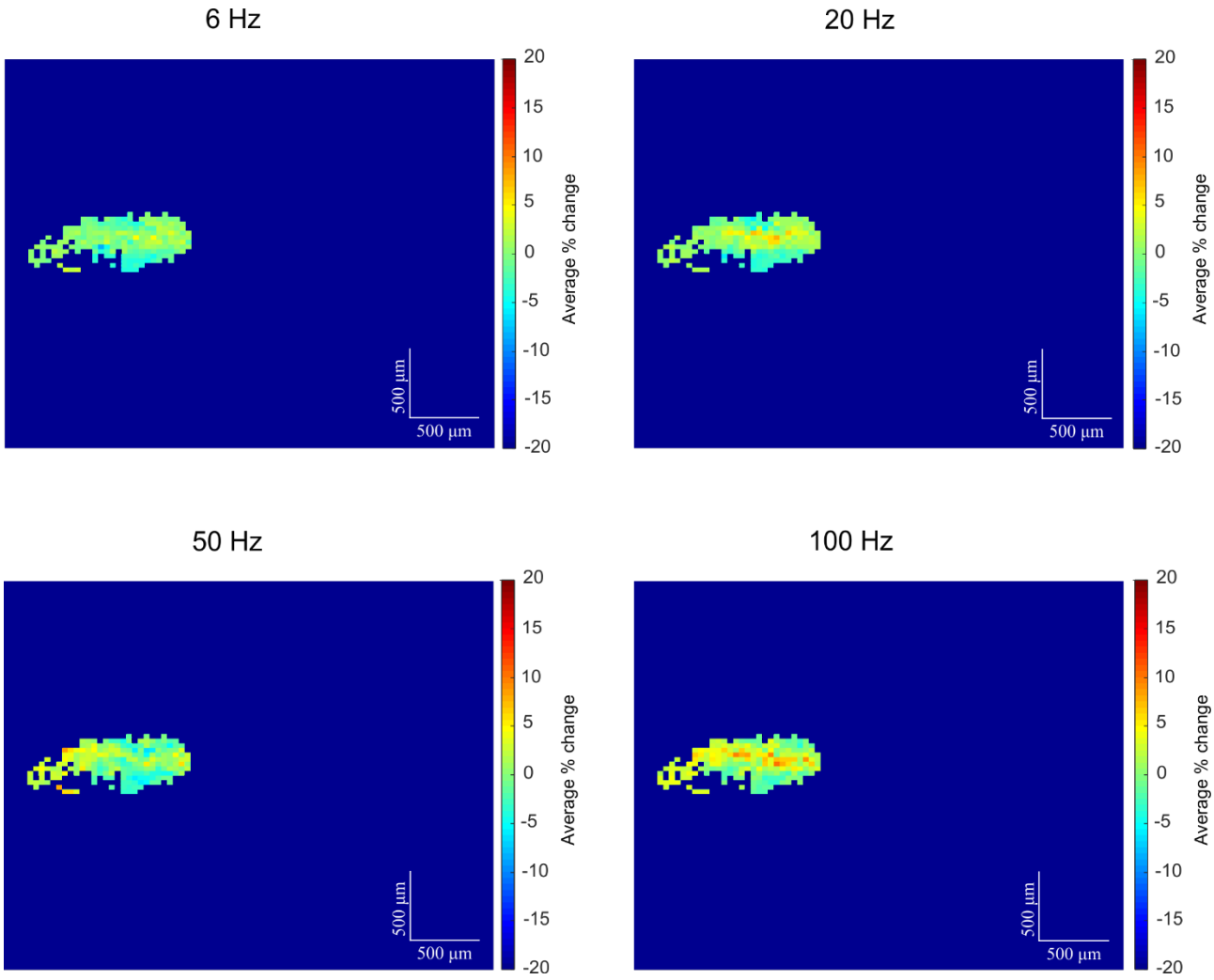

Fig. 6| The spatial organization of STP in the granular layer (N_{2b} peak). The average colormaps obtained aligning all the slices along the mossy fibers axis led to the observation of a complex spatial organization of N_{2b} STP in the granular layer. The trend to increase of N_{2b} peak (colorscale on the right) was more accentuated in different positions of the activated granular layer with respect to the stimulation site (positioned on the right in all the images) and this phenomenon appeared to be influenced by input frequencies variation.

4.4.3 Purkinje cells responses at different input frequencies.

4.4.3.1 The spatial organization of Purkinje cells with different Mean Firing Rates.

Following spike detection and spike sorting analysis (using Brainwave 4, see Methods for details) it was possible to assign a single unit for each channel recording a spontaneous spiking activity of Purkinje cells. For all the units detected, the MFR was calculated taking into account Purkinje cells firing in the 500ms before the stimulation. For each experiment the distribution of the MFR in the Purkinje cells population was evaluated, and Purkinje cells appeared to present different MFR ranging from 20Hz to more than 100Hz. Taking advantage of the high-resolution of the HD-MEA, it was

possible to reconstruct a colormap representing the spatial organization of Purkinje cells with different MFR (Fig. 7). Purkinje cells presenting low MFR values appeared to be alternated with the ones presenting higher MFR, but their organization in bands of activity was not evident.

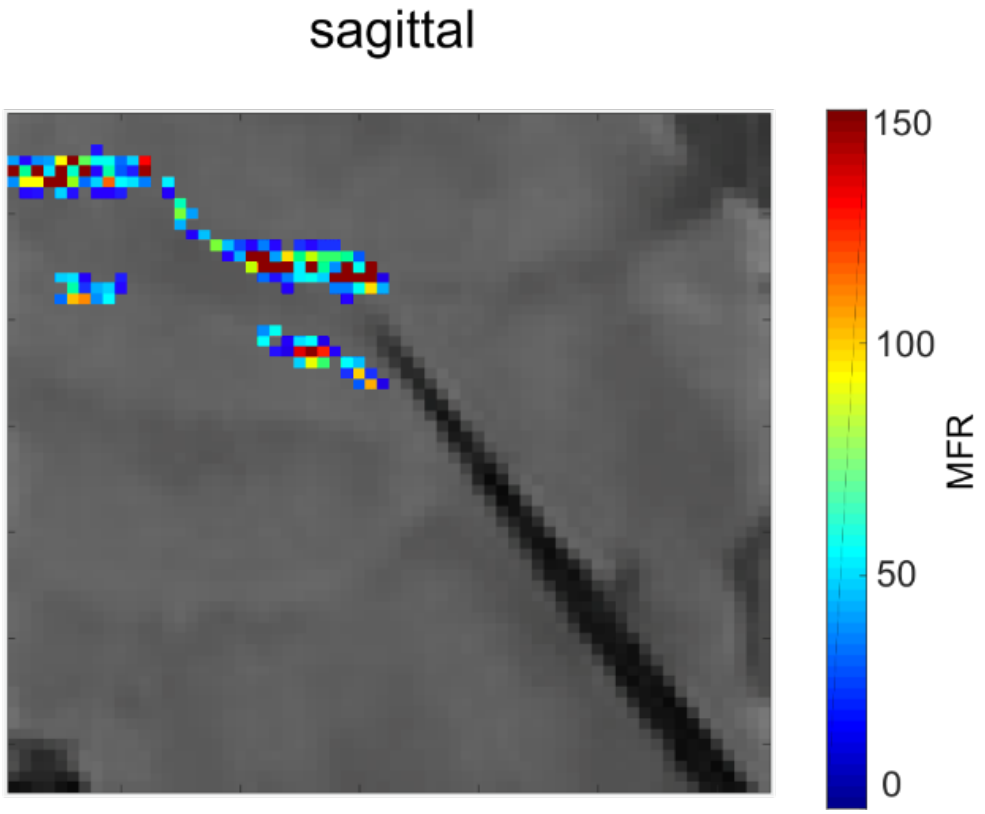

Fig. 7| The spatial organization of Purkinje cells with a different MFR in a sagittal slice. The reconstruction of the spatial location in one cerebellar lobule of the Purkinje cells presenting a different baseline MFR (coloscale on the right) did not show any clear organization in bands of activity, though Purkinje cells with a lower MFR alternated with Purkinje cells presenting higher MFR.

4.4.3.2 The effect of mossy fibers stimulation on Purkinje cells.

To visualize and analyze the results, raster plots and PSTHs were reconstructed for each stimulation frequency used (single stimulus, 6Hz, 20Hz, 50Hz, 100Hz). Over a total of 858 units, two different types of responses to stimulation were identified: the increase of Purkinje cells firing in a small time window after stimulation (20ms, peaks); the decrease of Purkinje cells firing after the stimulation (40ms, pauses). These responses, when present, generated a combination of peaks and pauses in the PSTHs (Fig. 8). Their significance was assessed through a one tailed Permutation Test with FDR correction (alpha 0.01) as explained in the Methods section.

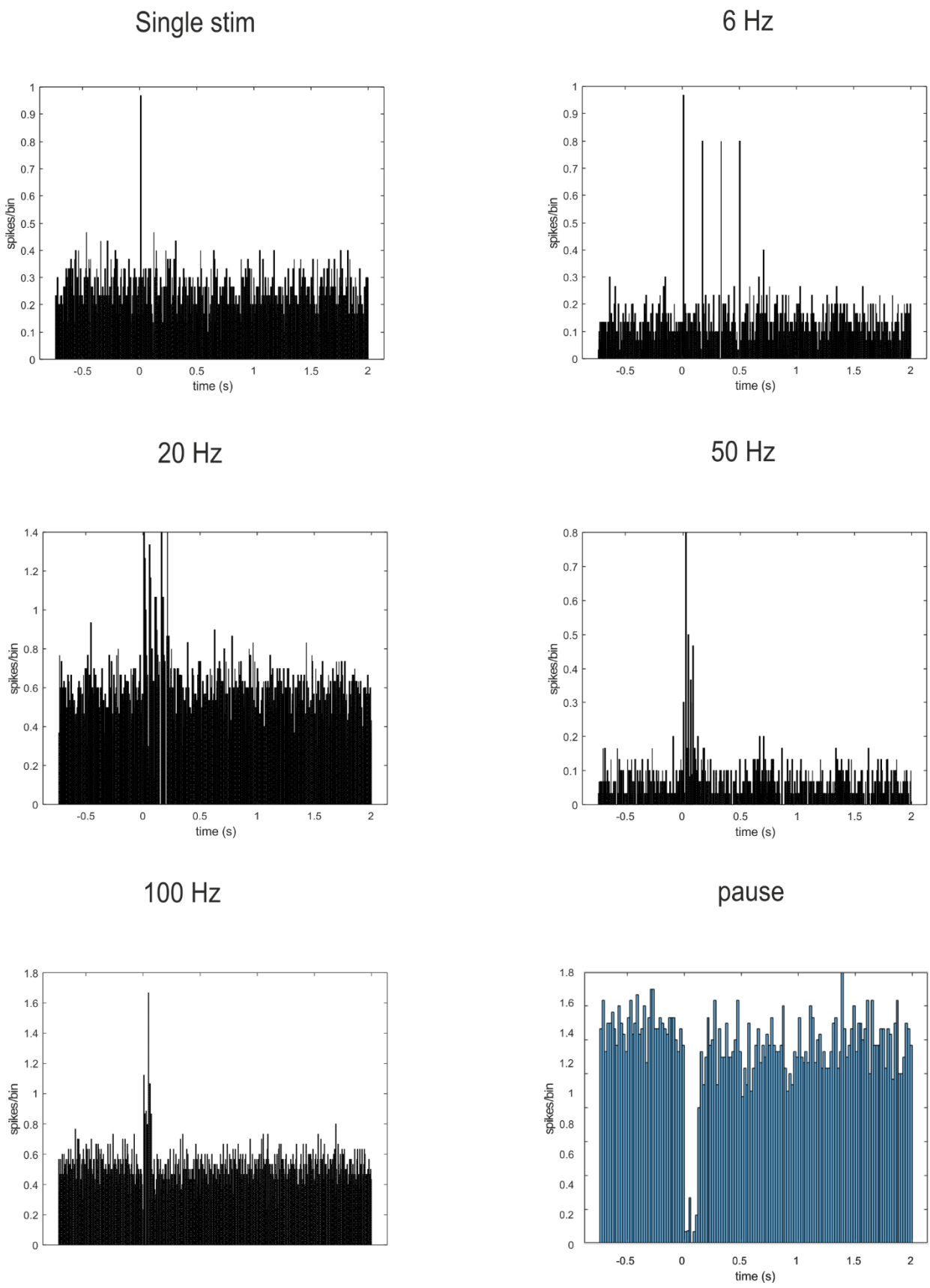

Fig. 8| Examples of peaks and pauses in the PSTHs (each one from a different unit) at different input frequencies. The reconstruction of PSTHs for each stimulation frequency led to the identification of two different types of Purkinje cells responses: the increase of Purkinje cells firing after each stimulation pulse (20ms, peaks) or the decrease of Purkinje cells firing after the stimulation (40ms, pauses).

Purkinje cells responses were evaluated at all the input frequencies, within and after the trains. Unfortunately, the short time interval between pulses at 100Hz hampered the reconstruction of Purkinje cells responses within the train at high frequencies of stimulation. The percentage of units presenting the same response was calculated. As it can be observed in Fig. 9, Purkinje cells in sagittal slices most commonly increase their basal discharge after each pulse of the stimulation at all the frequencies examined. The pause response appeared to be less common.

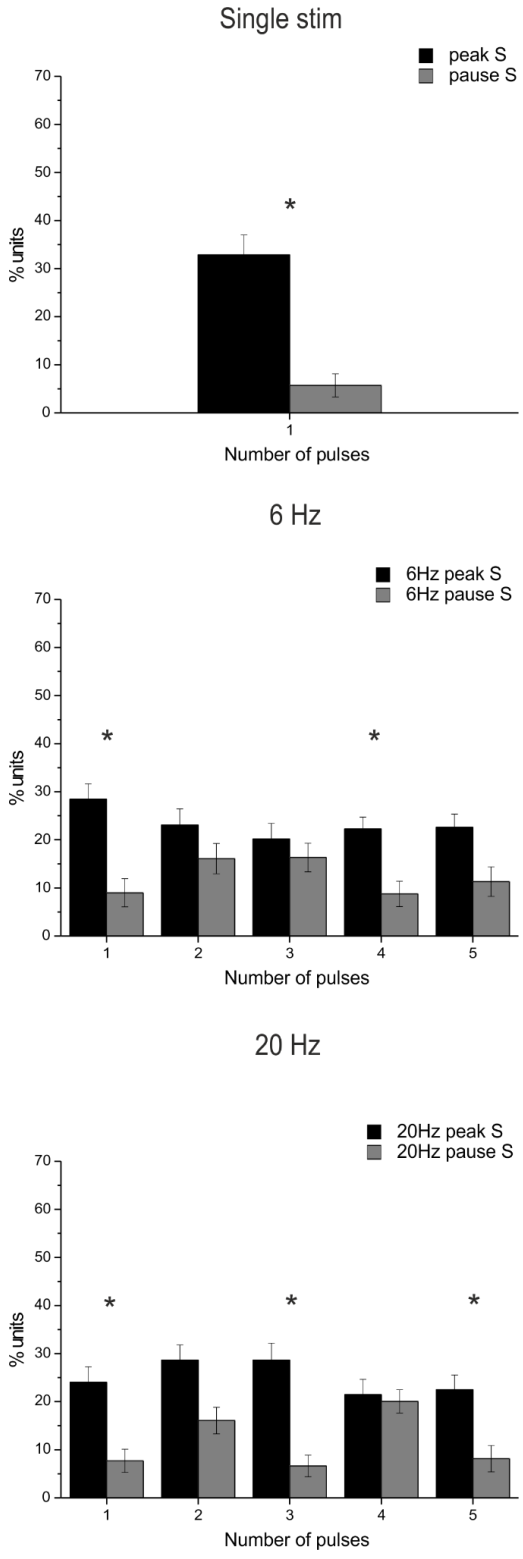

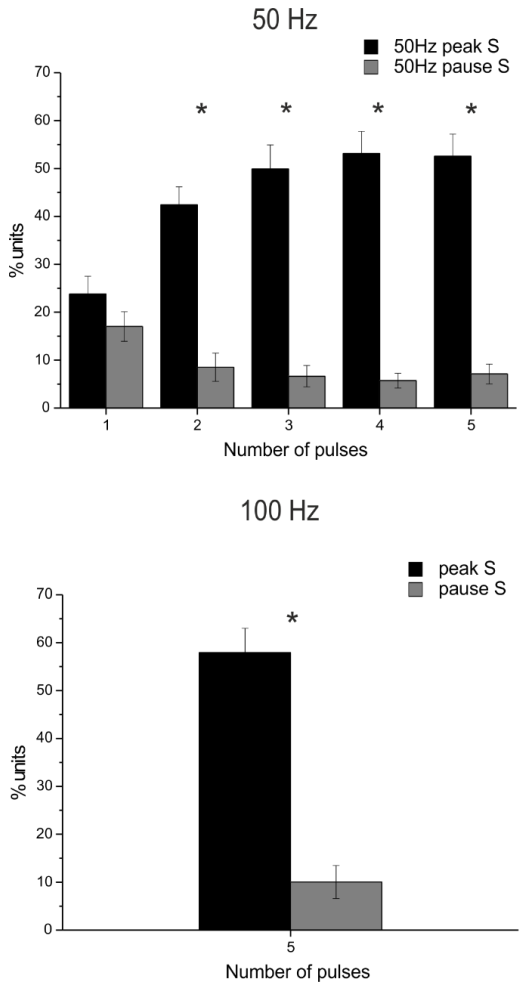

Fig. 9| Characterization of Purkinje cells units responses in the PSTHs. The percentage of units presenting the same response pattern was calculated at all the input frequencies within and after the train. Both peaks and pauses were found for Purkinje cells in sagittal slices (peak S and pause S). However, the percentage of units presenting an increase in their basal discharge was always higher (paired Student's t test, $p<0.05$) than the percentage of units presenting a decrease of the firing after each pulse of the stimulation at all the frequencies examined.

Finally, the percent change of the MFR was calculated within each stimulation pattern (6Hz, 20Hz, 50Hz) excluding the 100Hz stimulation in which the information within the train was lost. Colormaps were generated using this percent change together with the percent change of STP in the granular layer of each experiment (Fig. 10).

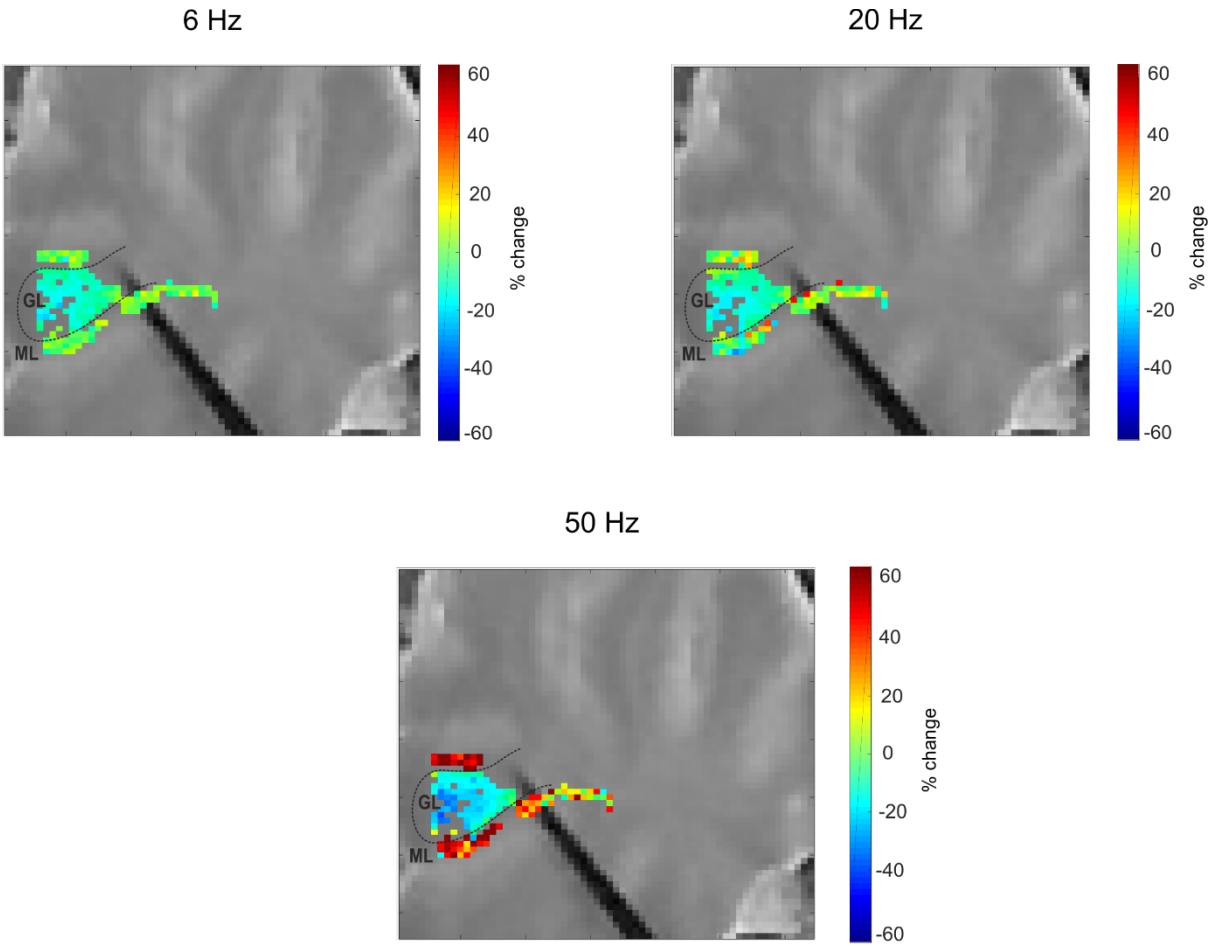

Fig. 10| Whole network activation in a sagittal slice. The percent change of the MFR of Purkinje cells in the excited cerebellar lobule was combined with the percent change of STP in the granular layer reconstructing the whole network activation at each input frequency. As it can be observed, while short-term depression characterized granular layer activity, the MFR of Purkinje cells increased increasing the input frequency.

4.4.4 Correlation of granular layer activity and Purkinje cells responses.

The computation of the Pearson correlation coefficient (see the Methods section for details) showed a frequency-dependence of the correlation of granular layer activity and Purkinje cells responses. Both a positive and a negative correlation were detected in sagittal slices. After a single pulse stimulation, a low percentage of Purkinje cells presented a significant positive or negative correlation with the activity of granule cells (about 9%). Mossy fibers stimulation at different input frequencies, led to an increase in the percentage of Purkinje cells presenting a correlation with granular layer activity (from 10% at 6Hz to 30% at 50Hz both for positive and negative correlations). Moreover, the level of positive and negative correlation increased increasing the input frequency, passing from 0.54 ± 0.006 at 6Hz to 0.61 ± 0.01 at 50Hz and from -0.56 ± 0.01 at 6Hz to -0.62 ± 0.008 at 50Hz.

Coronal slices

4.4.5 Granular layer responses at different input frequencies.

4.4.5.1 N_{2a} and N_{2b} amplitude changes at different input frequencies.

The same analysis performed on sagittal slices was repeated on 9 coronal slices. The percent change of N_{2a} and N_{2b} peaks was calculated at different input frequencies together with the percentage of channels presenting a statistically significant change of N_{2a} and N_{2b} peak amplitudes in the granular layer. Again, the decrease of N_{2a} peaks amplitude prevailed during the stimulation trains, becoming more evident increasing the stimulation frequency. N_{2b} presented both an increase or a decrease of its amplitude (Table 3A). Moreover, the percentage of channels showing a significant change of N_{2a} peak amplitude was more than 50% of channels showing a response, while the percentage of channels presenting a significant change of N_{2b} peak was more than 40% only at higher input frequencies (50Hz and 100Hz) (Table 3B). The percentage of channels presenting a significant increase of N_{2b} peak was always significantly larger than the percentage of channels presenting a decrease of N_{2b} peak amplitude.

A

	6Hz	20Hz	50Hz	100Hz
N_{2a}	-13.44±0.84	-14.92±1.26	-17,56±0.89	-23.93±1.46
N_{2b} +	14.80±1.44	14.26±1.65	18.23±1.69	17.62±1.41
N_{2b} -	-10.63±1.71	-11.55±2.19	-6.53±2.12	-10.28±2.3

B

	6Hz	20Hz	50Hz	100Hz
%ch N_{2a}	53.96±7.18	55.47±6.85	61.59±6.73	78.94±5.37
%ch N_{2b} +	18.01±6.02	19.77±4.94	41.60±4.43	39.41±6.78
%ch N_{2b} -	4.75±1.6	2.23±0.79	0.74±0.29	2.6±1.12

Table 3| N_{2a} and N_{2b} peak changes at different input frequencies. A) The table shows the percent change of the last response peak compared to the first one within each stimulation pattern. **B)** The table shows the percentage of channels in the granular layer recording a significant N_{2a} or N_{2b} peak amplitude change.
In both these tables N_{2b} + stands for N_{2b} amplitude increase during the stimulation trains while N_{2b} – refers to N_{2b} amplitude decrease during the stimulation trains.

N_{2a} and N_{2b} peak amplitude changes were then reconstructed for each stimulus in the trains (Fig. 11), showing different degrees of N_{2a} peak amplitude changes inside the trains with a predominance of short-term depression and a weak increase of N_{2b} peak amplitude. STP was identified for each channel every time that N_{2a} peak amplitude showed a statistically significant change (unpaired Student's *t* test, $p<0.05$) at the end of the 5 pulses stimulation compared to the first response in the train.

6Hz

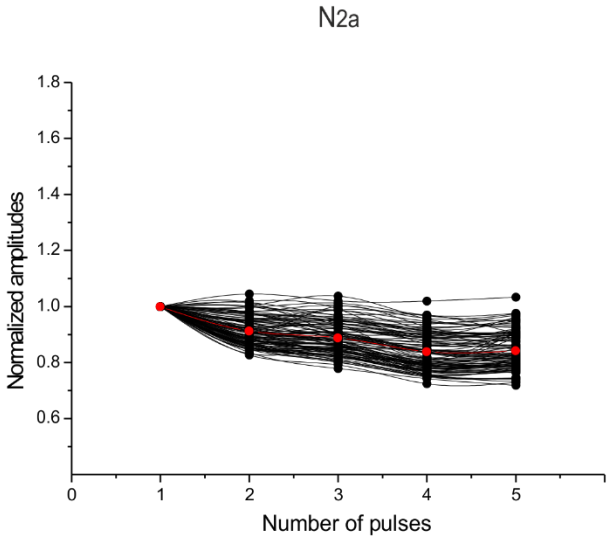
N2a
Normalized amplitudes
Number of pulses

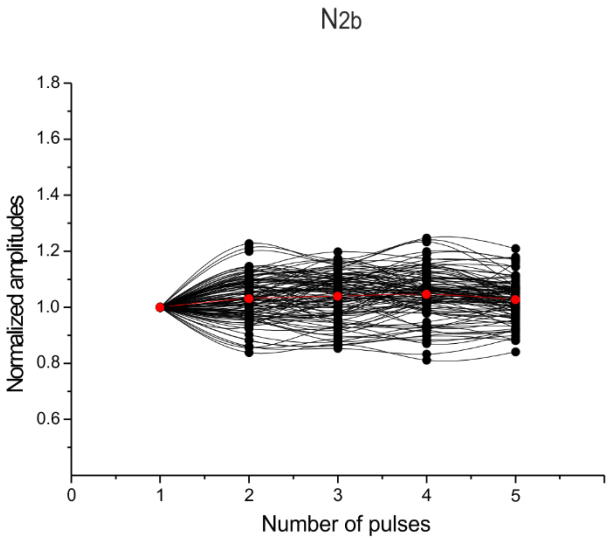
N2b
Normalized amplitudes
Number of pulses

20Hz

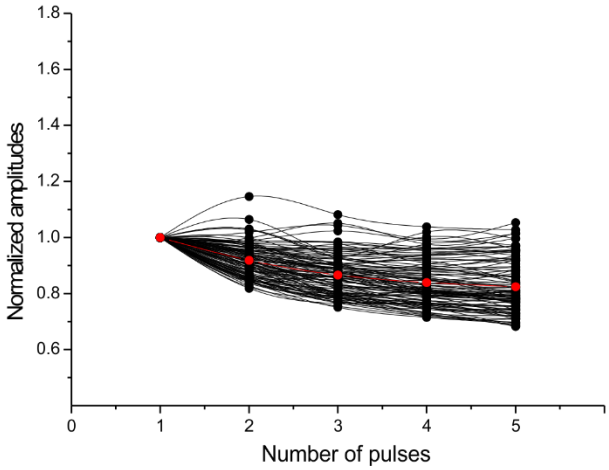
N2a
Normalized amplitudes
Number of pulses

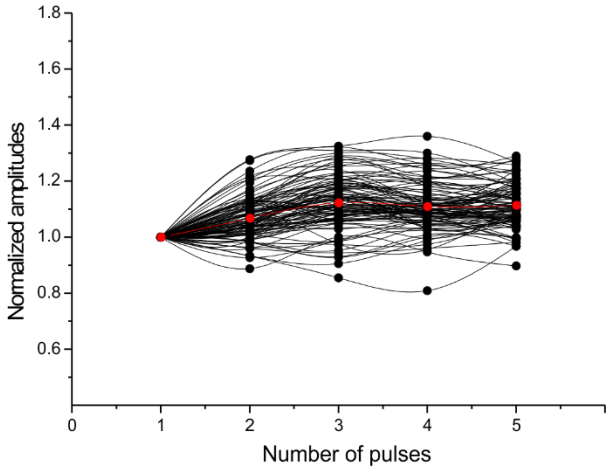
N2b
Normalized amplitudes
Number of pulses

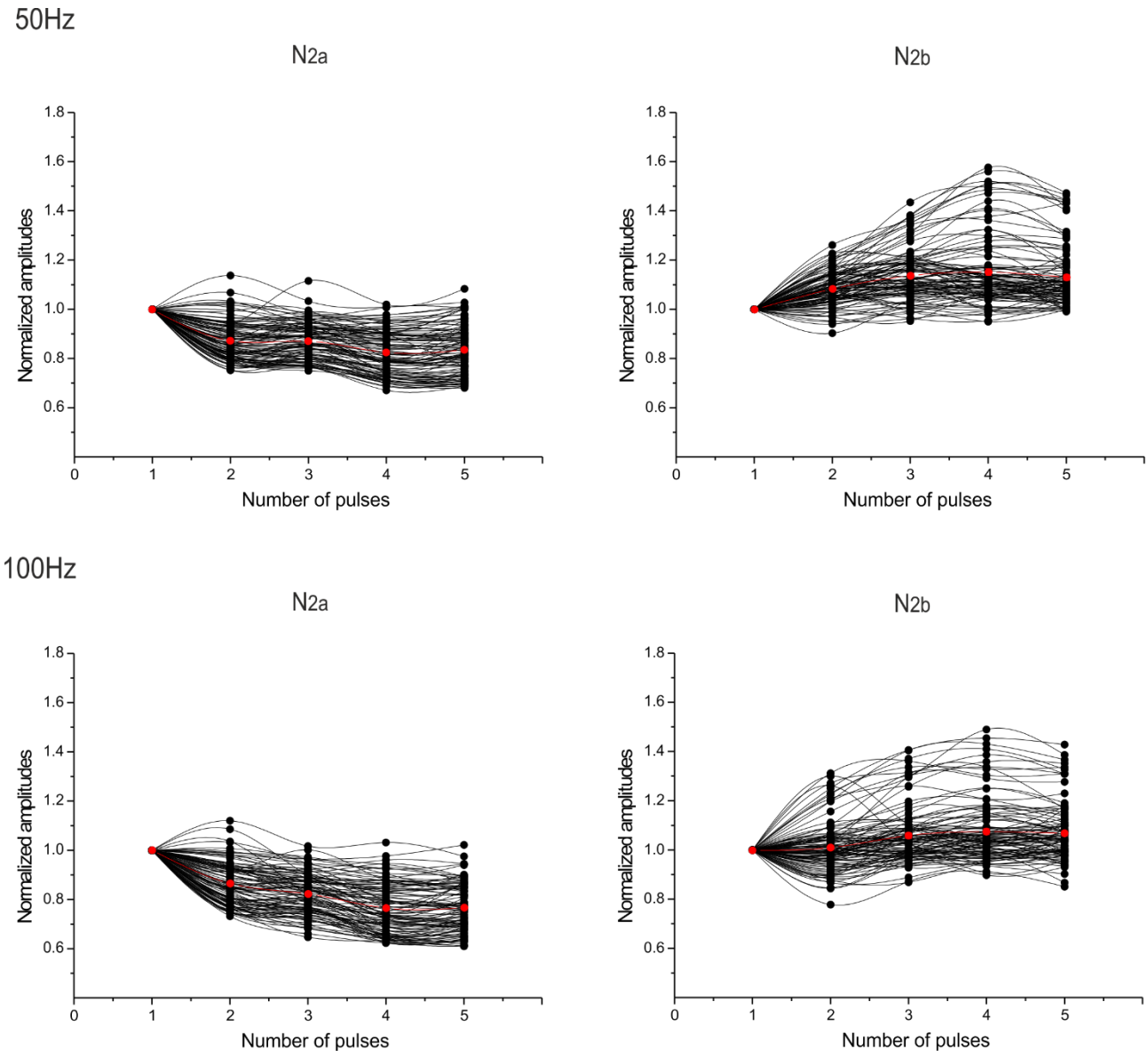

Fig. 11| Normalized N_{2a} and N_{2b} peak amplitudes during the stimulus train at different frequencies. N_{2a} and N_{2b} peak amplitudes were reconstructed in response to each of the five stimulation in the train and normalized to the first response. Each line in the plot represents a channel considered for the analysis. .The red line represents the average trend (a decrease of N_{2a} peak and an increase of N_{2b} peak).

4.4.5.2 The spatial organization of Short-Term Plasticity in the granular layer.

Colormaps were constructed using the percent change of N_{2a} and N_{2b} peaks calculated above in order to observe the spatial organization of STP in the granular layer. Short-term depression appeared to be more pronounced in the center of the granular layer, and the increase of the input frequency enhanced this kind of spatial organization suggesting its frequency-dependence (Fig. 12).

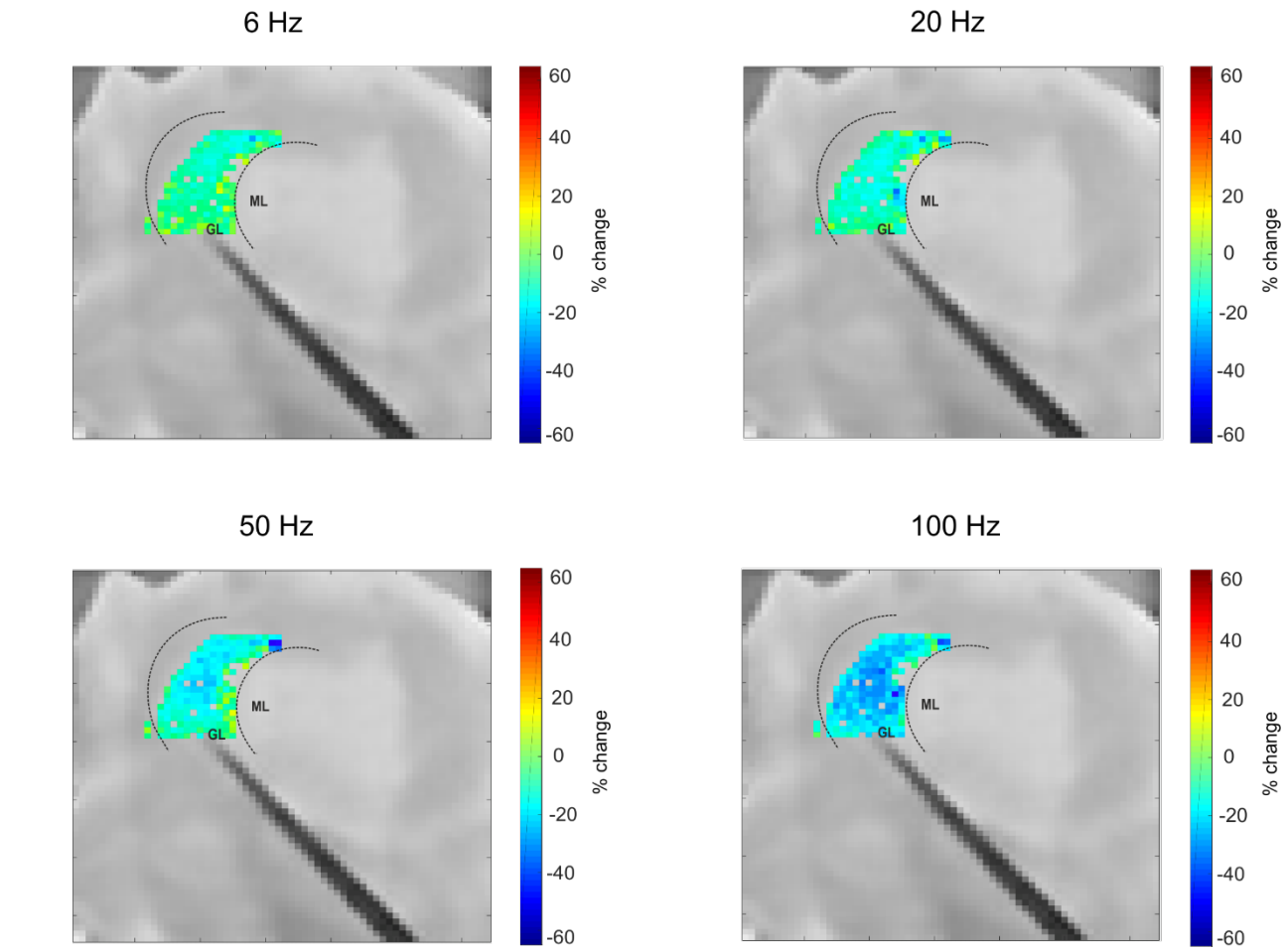

Fig. 12| The spatial organization of STP in one coronal slice (N_{2a} peak). Colormaps were reconstructed for each stimulation pattern with the percent change of N_{2a} peak amplitude within the 5 pulses stimulation. Here, one coronal slice is reported as an example (gray area on background). As it can be observed, short-term depression (colorscale on the right) was more pronounced in the middle of the granular layer and this spatial organization increased with the input frequency.

The average colormap reconstructed with the alignment of all the recordings along mossy fibers axis confirmed the results observed for each single experiment (Box 1; Fig. 13).

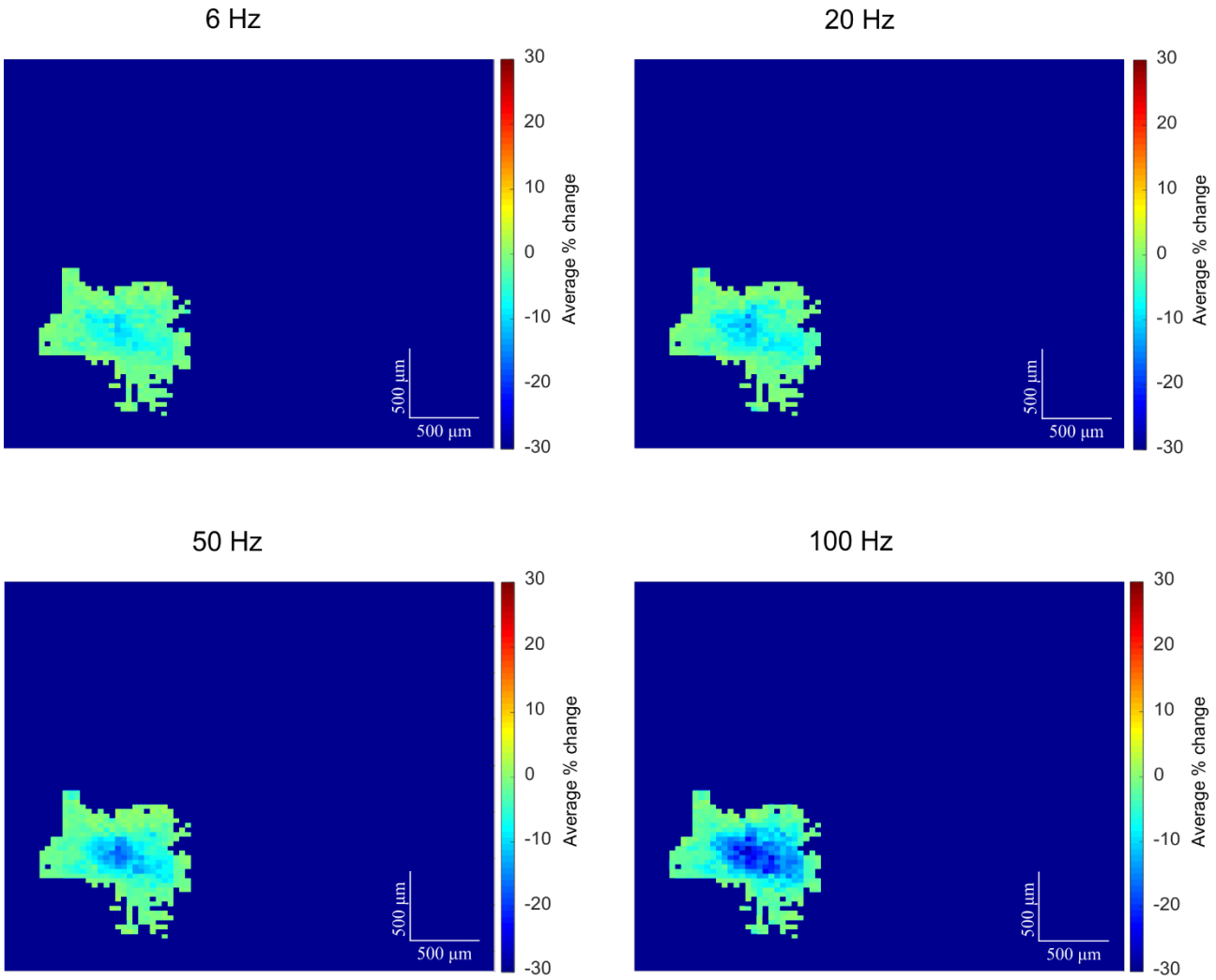

Fig. 13| The spatial organization of STP in the granular layer (N_{2a} peak). The average colormaps obtained aligning all the slices along the mossy fibers axis confirmed the spatial organization of STP in the granular layer. A more pronounced short-term depression phenomenon can be seen in the center of the activated granular layer. The increase of the input frequency enhanced this spatial organization (colorscale on the right).

Colormaps reconstructed with the percent change of N_{2b} peak amplitude showed a more complex spatial organization of N_{2b} changes in the granular layer compared to the one presented by N_{2a} peak amplitude (Fig. 14). N_{2b} peak increase appeared more to prevail in different regions of the activated area at different frequencies.

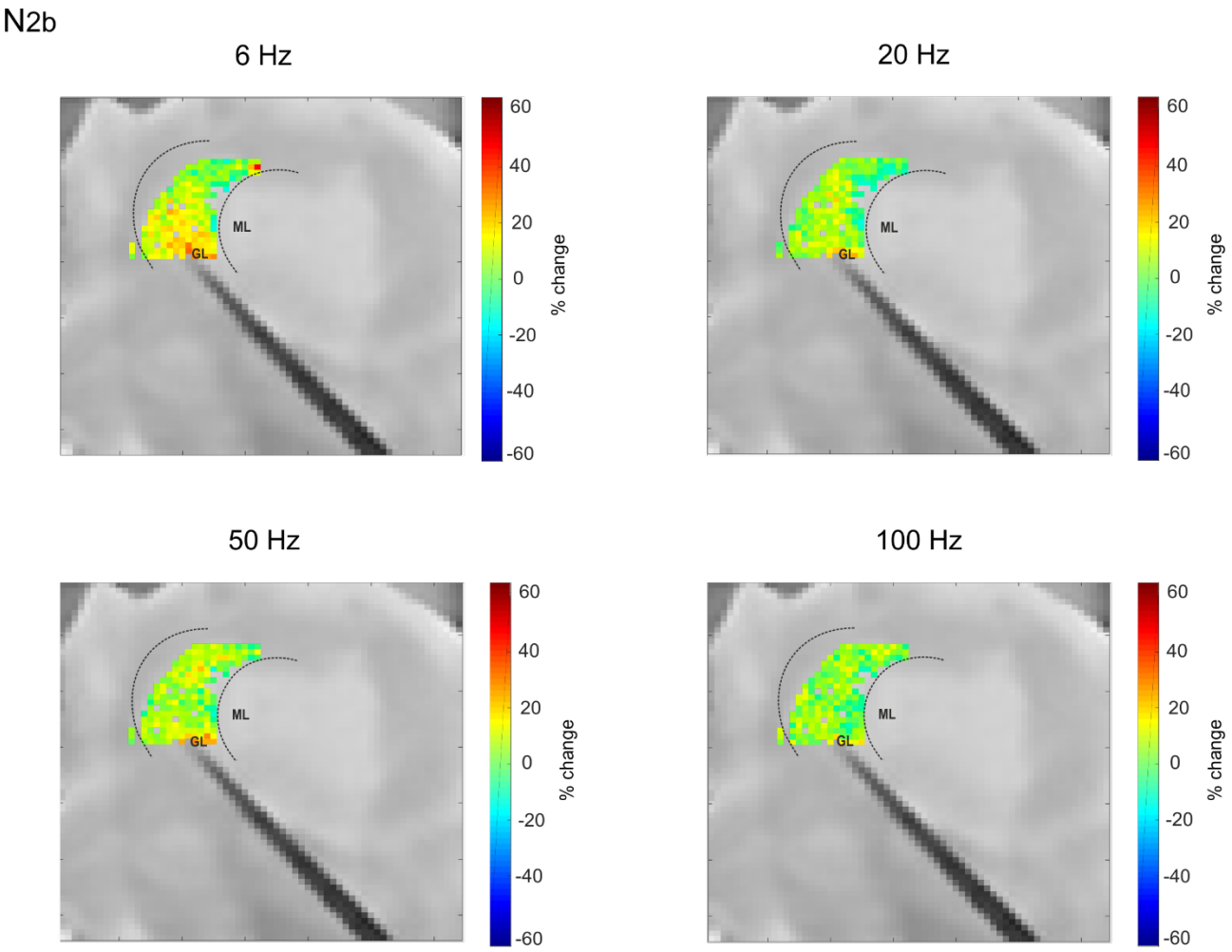

Fig. 14| The spatial organization of STP in one coronal slice (N_{2b} peak). Colormaps were reconstructed for each stimulation pattern with the percent change of N_{2b} peak amplitude within the 5 pulses stimulation. Here, one coronal slice is reported as an example (gray area on background). As it can be observed, the trend to increase of N_{2b} peak appeared more accentuated (colorscale on the right) in different regions of the activated area with respect to the position of the stimulus at different frequencies.

In the average colormap, the spatial and frequency dependence of N_{2b} trend appeared clearer, showing a more pronounced increase of N_{2b} peak in the middle of the granular layer and close to the stimulation site (Box 1; Fig. 15). This increase became more evident increasing the stimulation frequency.

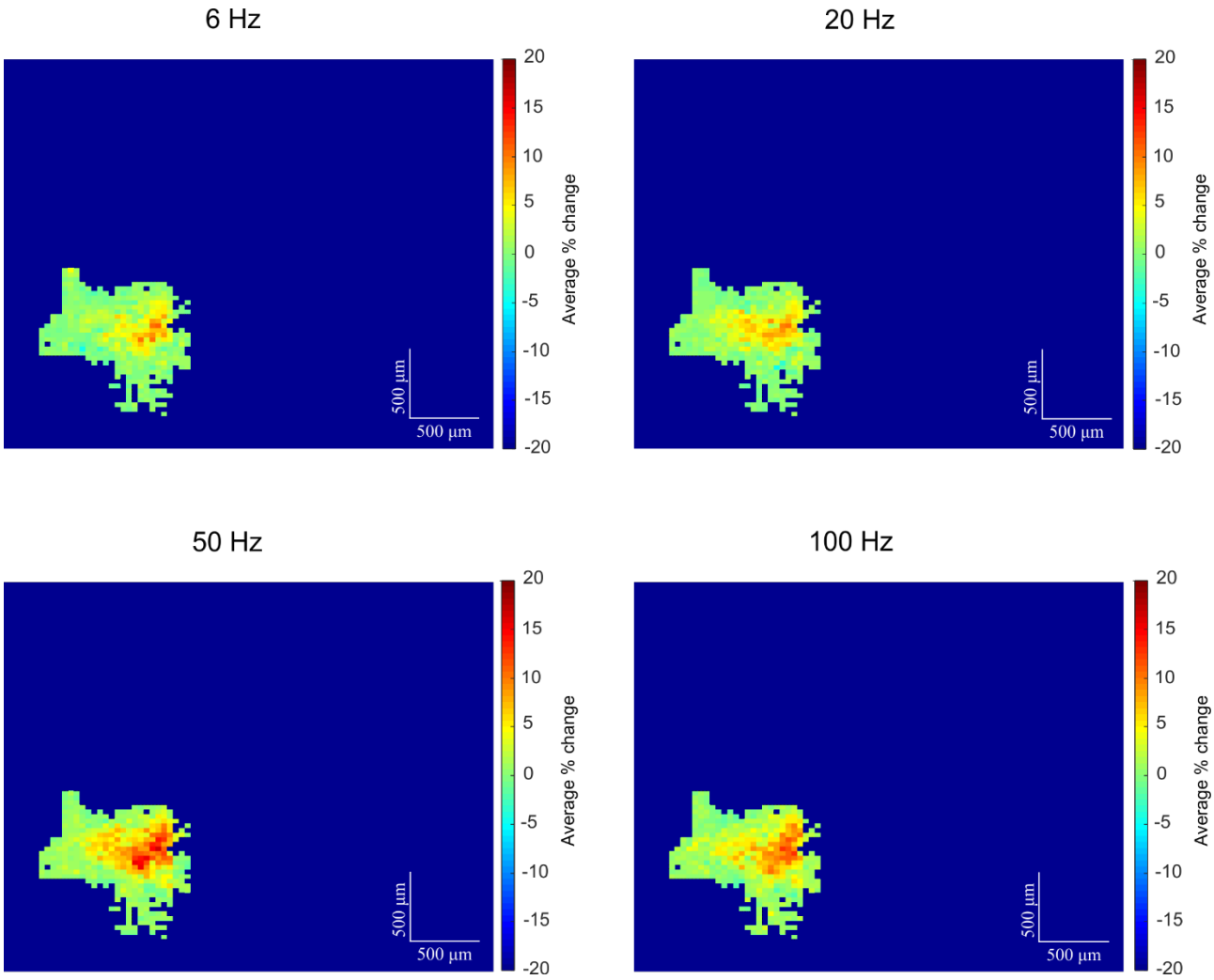

Fig. 15| The spatial organization of STP in the granular layer (N_{2b} peak). The average colormaps obtained aligning all the slices along the mossy fibers axis led to the observation of a clear spatial organization of N_{2b} STP in the granular layer. The trend to increase of N_{2b} peak (colorscale on the right) was more accentuated in the middle of the granular layer and close to the stimulation site (on the right in the maps). This phenomenon became more evident increasing the input frequency.

4.4.6 Purkinje cells responses at different input frequencies.

4.4.6.1 The spatial organization of Purkinje cells basal activity.

Purkinje cells firing rates ranged from 20Hz to more than 100Hz. Interestingly, the units with lower and higher MFR were located in alternated bands, evident in the reconstruction of PCs activity in the colormap in Fig. 16. This kind of organization strongly resembles zebrin-like distribution patterns characterizing Purkinje cells in the coronal plane, according to literature. A significant amount of studies in fact sustain a prominent regional variation in the expression of several molecular markers in Purkinje cells, leading to the identification of several bands or stripes in the cerebellar cortex (Cerminara et al. 2015). Among these markers, zebrin II appears to be the best characterized in Purkinje cells and in several areas of the cerebellar cortex groups of Purkinje cells expressing zebrin

II (zebrin II positive, Z+) alternate with Purkinje cells without zebrin II expression (zebrin II negative, Z-) (Hawkes 2014). Importantly the firing frequency of Z+ Purkinje cells appeared to be significantly lower than the firing rate of Z- cells (Zhou et al. 2014). Thus, the spatial organization of Purkinje cells with different MFR observed in the coronal plane most likely reflects the zebrin-like distribution pattern.

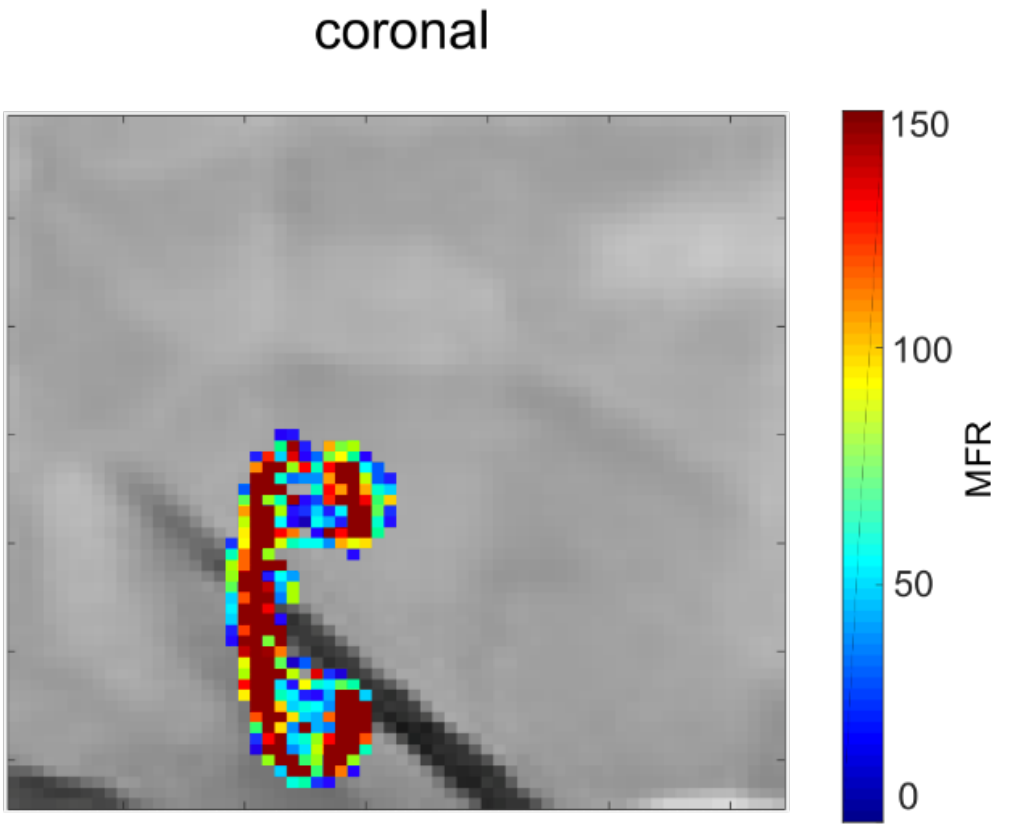

Fig. 16| The spatial organization of Purkinje cells with a different MFR in a coronal slice. The reconstruction of the spatial location in one cerebellar lobule of the Purkinje cells presenting a different baseline MFR (colorscale on the right) led to the observation of alternated bands of activity strongly resembling zebrin-like distribution patterns characterizing Purkinje cells in the coronal plane (Hawkes 2014).

4.4.6.2 The effect of mossy fibers stimulation on Purkinje cells.

Raster plots and PSTHs reconstructed for each stimulation frequency showed a combination of peaks and pauses over a total of 1059 units. As evident in Fig. 17, Purkinje cells in coronal slices most commonly decrease their basal discharge after a single pulse stimulation. This evidence might be due to the inhibition conveyed by molecular layer interneurons on Purkinje cells activity. Parallel fibers activate basket cells and stellate cells in the molecular layer, consequently inhibiting respectively Purkinje cells soma and dendrites (D'Angelo 2018). During stimulation at different frequencies, Purkinje cells responses were characterized by showed pauses prevailing at the beginning and peaks prevailing at the end of the 5 pulses train (Fig. 17). This evidence might depend on the frequency-dependent behavior of molecular layer interneurons activity (Rizza et al, unpublished observations).

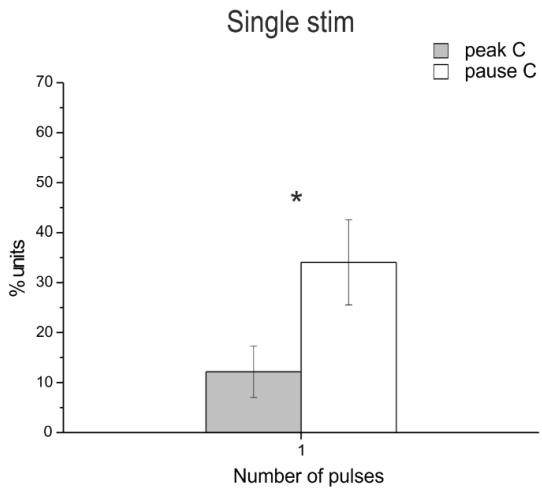
Single stim
peak C
pause C
% units
Number of pulses
*

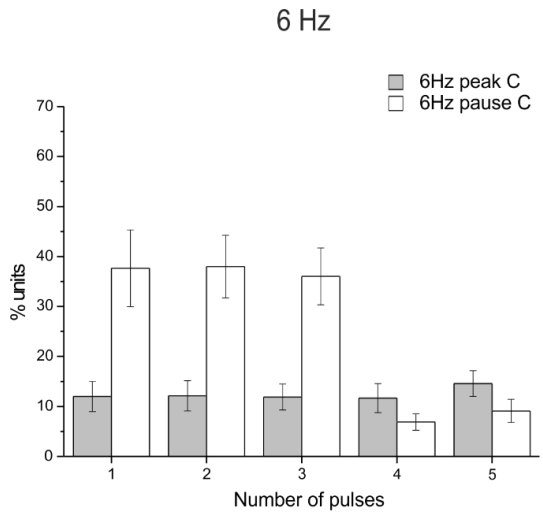
6 Hz
6Hz peak C
6Hz pause C
% units
Number of pulses

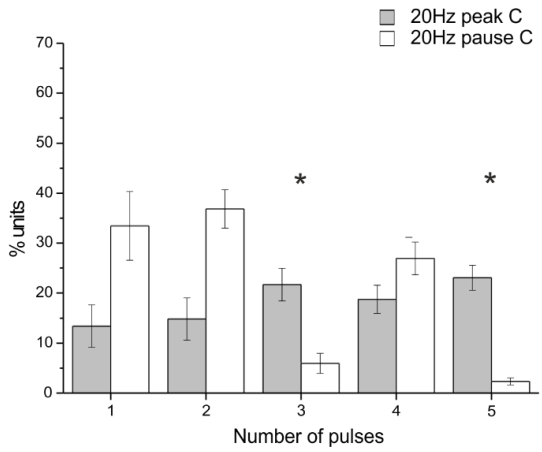
20 Hz
20Hz peak C
20Hz pause C
% units
Number of pulses
*
*

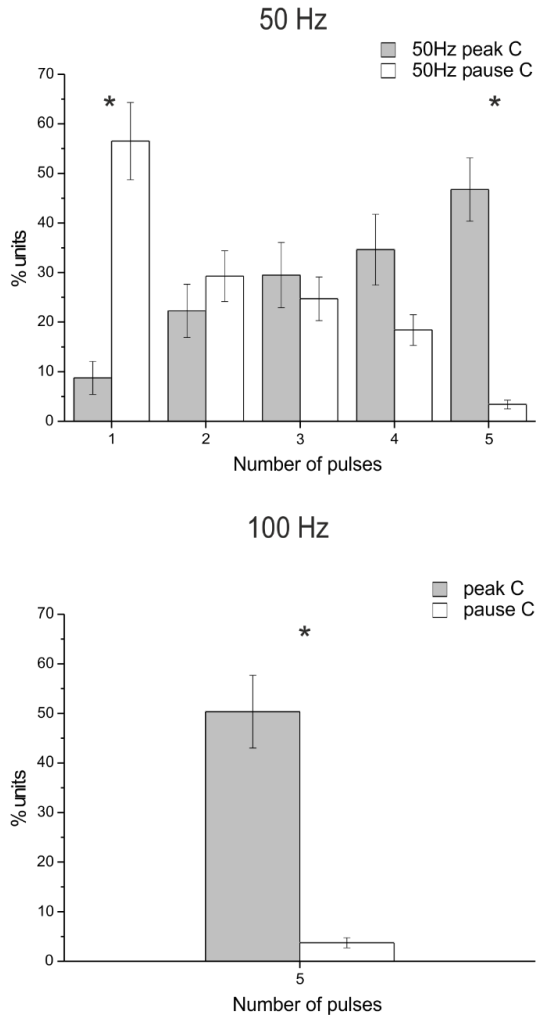

Fig. 17| Characterization of Purkinje cells units responses in the PSTHs. The percentage of units presenting the same response pattern was calculated at all the input frequencies within and after the stimulation train. Both peaks and pauses were found for Purkinje cells in coronal slices (peak C and pause C). After a single pulse stimulation a larger number of units presented a decrease in their basal discharge. During stimulation at different frequencies the percentage of units presenting a pause was higher (paired Student's t test, $p<0.05$) at the beginning of the 5 pulses train and the percentage of units presenting a peak was higher at the end of the 5 pulses train (paired Student's t test, $p<0.05$).

Finally, the percent change of the MFR was calculated within each stimulation pattern (6Hz, 20Hz, 50Hz), excluding the 100Hz stimulation in which the information within the train was lost. Colormaps were generated using this percent change together with the percent change of STP in the granular layer of each experiment (Fig. 18).

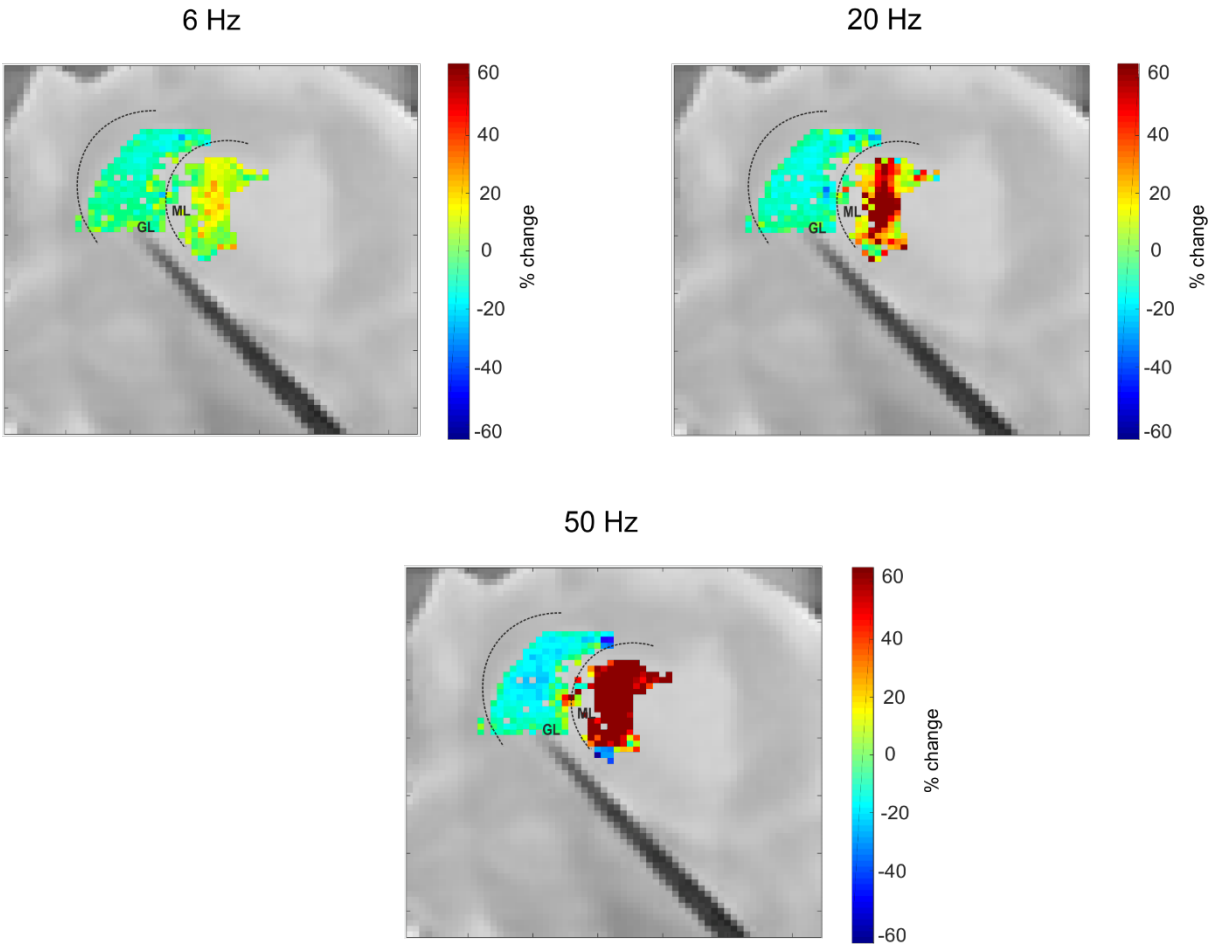

Fig. 18| Whole network activation in a coronal slice. The percent change of the MFR of Purkinje cells in the excited cerebellar lobule was combined with the percent change of STP in the granular layer reconstructing the whole network activation at each input frequency. As it can be observed, while short-term depression characterized granular layer activity the MFR of Purkinje cells increased increasing the input frequency.

4.4.7 Correlation of granular layer activity and Purkinje cells responses.

The computation of Pearson correlation coefficients led to the observation of a frequency-dependent correlation between granular layer activity and Purkinje cells responses. Both positive and negative correlation values were found in coronal slices. After a single pulse stimulation, the percentage of Purkinje cells correlating with granular layer activity was small (9% with a positive correlation and 15% with a negative correlation). Then the stimulation of mossy fibers at different input frequency led to an increase of the percentage of units presenting a positive or a negative correlation with granule cells (from 20% at 6Hz to 50% at 50Hz both for positive and negative correlations). The increase of the input frequency determined a consequent increase in the level of positive and negative correlations, which passed from 0.55 ± 0.004 at 6Hz to 0.64 ± 0.01 at 50Hz and from -0.57 ± 0.005 at 6Hz to -0.65 ± 0.01 at 50Hz.

4.4.8 Comparison of cerebellar network responses in the sagittal and coronal planes.

Mossy fibers stimulation evoked an LFP response propagating through the granular layer. The activated granular layer area appeared to be more extended in coronal slices than in sagittal ones. After a single pulse stimulation, N_{2a} and N_{2b} peak characterizing granule cells responses did not show a statistically significant difference, between the two planes of section. However, the N_{2b} peak amplitude changes appeared to be different varying the input frequency. While N_{2a} in fact mainly showed short-term depression in both sagittal and coronal slices, at higher input frequencies the percentage of channels showing a significant increase of N_{2b} peak amplitude was higher in coronal slices compared to sagittal ones (Fig. 19). Thus, N_{2b} increase appeared to be more evident in coronal slices.

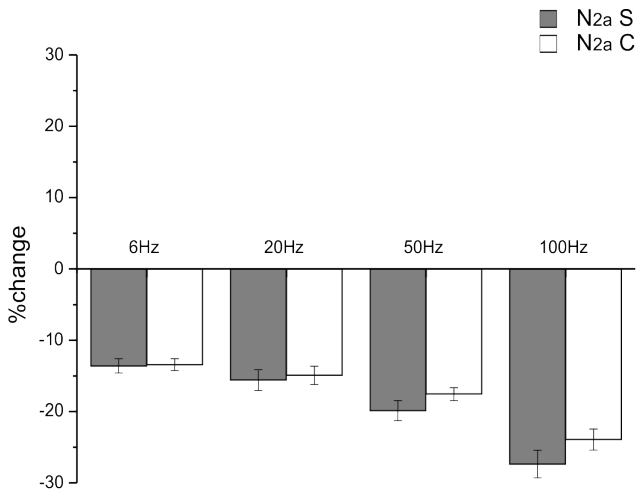

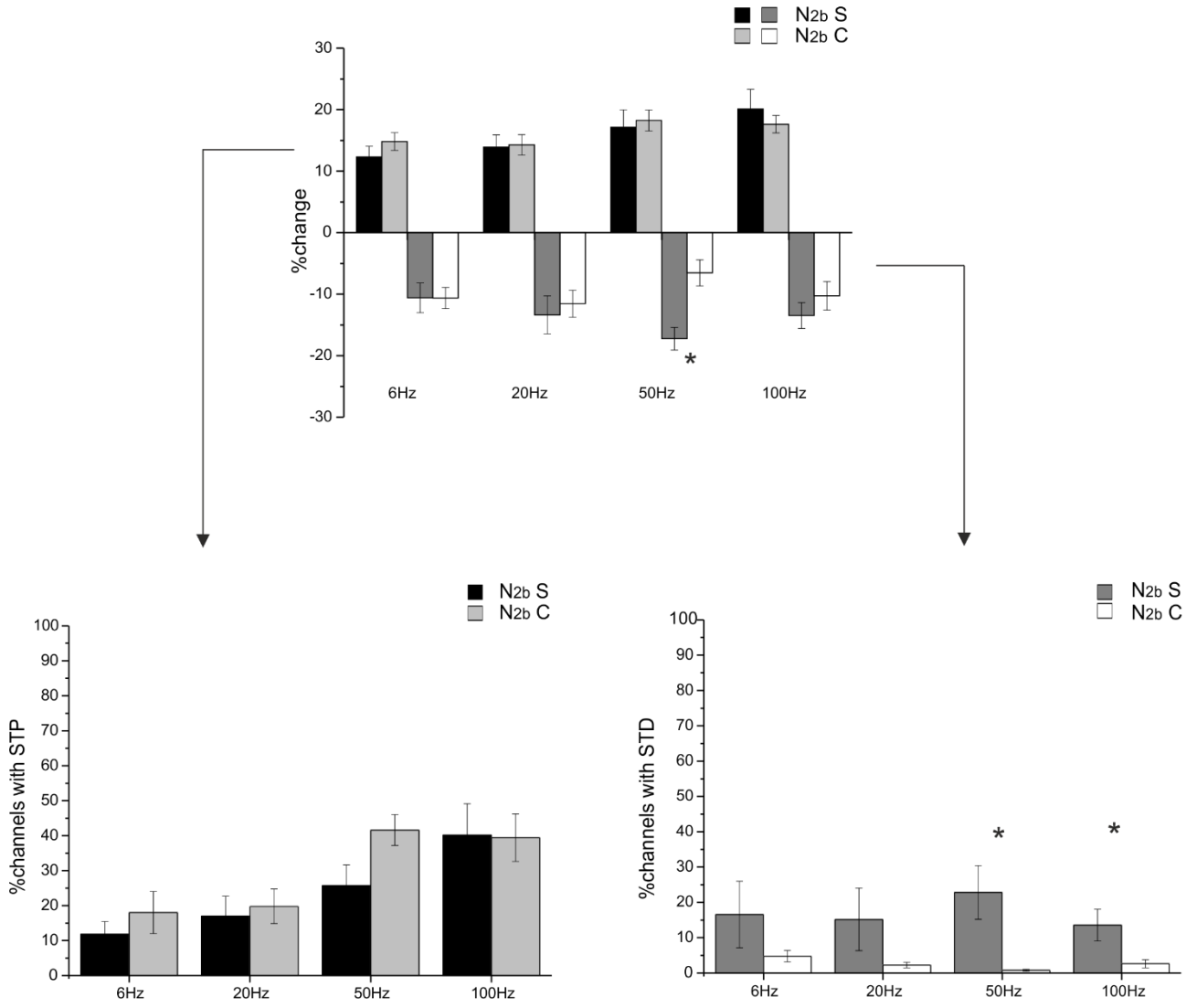

Fig. 19| Comparison of granular layer responses in the sagittal and coronal planes. N_{2a} peak amplitude commonly presented short-term depression in both sagittal and coronal slices (figure on top) while N_{2b} peak amplitude changes differed varying the input frequency. N_{2b} peak amplitude in fact presented both an increase and a decrease of its amplitude (second figure), but the percentage of channels showing a significant change of N_{2b} peak amplitude (indicated by the arrows) appeared to be different between sagittal and coronal slices.

Concerning Purkinje cells activity, the average MFR of these cells appeared to be significantly higher in coronal slices than in sagittal ones. This kind of difference can be explained taking into account the evidence of zebrin-like distribution patterns in coronal slices. Zebrin negative Purkinje cells in fact present an average MFR around 80Hz while the MFR of Zebrin positive cells is around 50Hz (Zhou et al. 2014). HD-MEA experiments led to the observation of zebrin-like distribution patterns only in coronal slices. The consequent recording of an higher number of Zebrin negative cells in coronal slices compared to sagittal ones probably determined the statistically significant difference observed between Purkinje cells MFR.

Examining Purkinje cells responses to mossy fibers stimulation, the inhibition exerted by molecular layer interneurons activity on Purkinje cells determined the prevalence of pauses in coronal slices after a single pulse stimulation. On the other hand, in sagittal slices the increase of Purkinje cells basal discharge was more common, consistently with a prevalent activation of granule cells ascending axon synapses. Within the trains, after each pulse of the stimulation Purkinje cells presented always a peak in sagittal slices, while in coronal ones pauses prevailed at the beginning of the trains and peaks were significantly more common at the end. The computation of the MFR percent change within each stimulation pattern led to the observation of both an increase and a decrease of the Purkinje cells MFR in sagittal and coronal slices (paired Student's t-test, $p<0.05$). However, the percentage of channels presenting an increased MFR of Purkinje cells was significantly larger than the percentage of channels with a decreased MFR (Fig. 20), perfectly in line with the observation of peaks and pauses in the PSTHs.

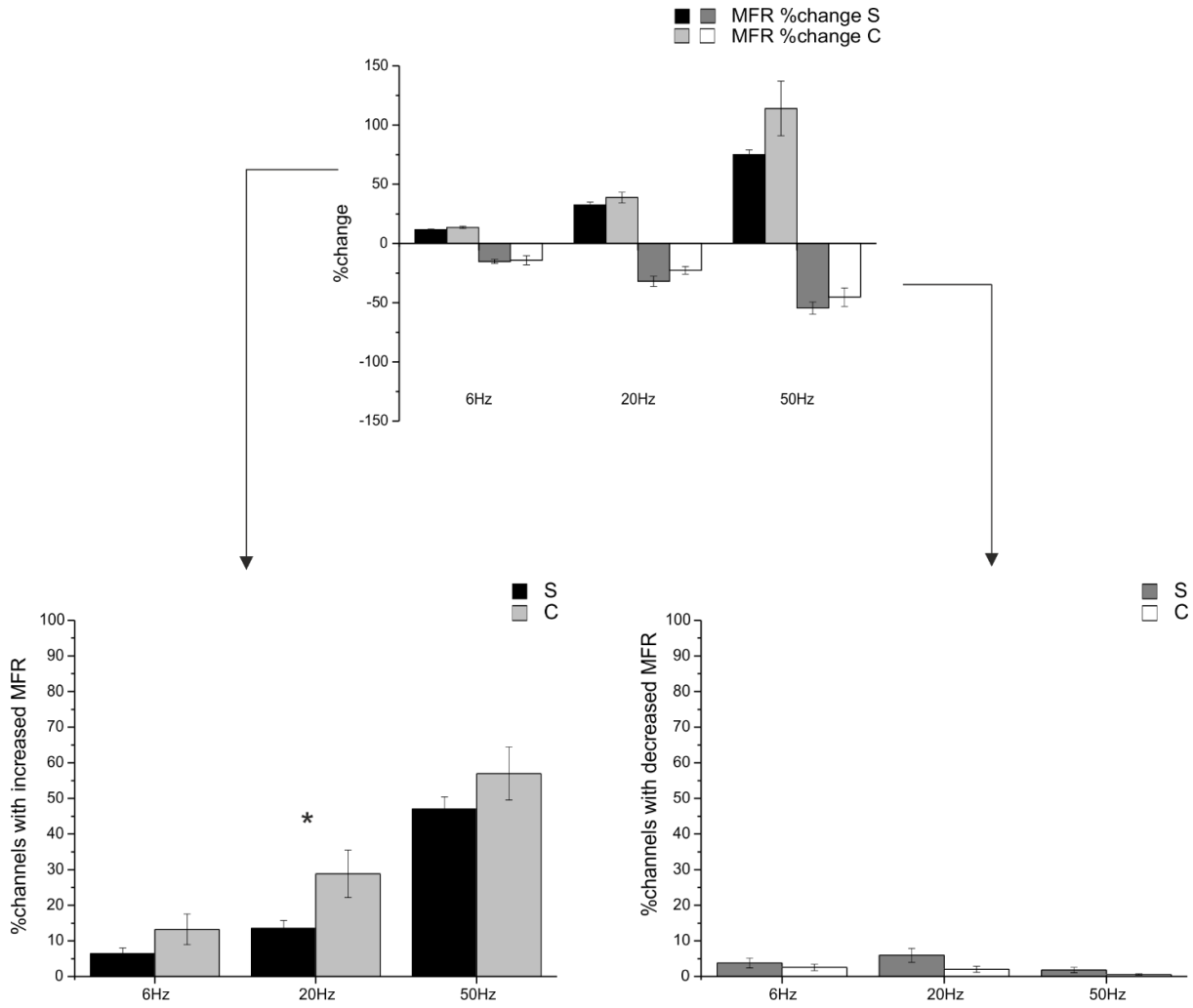

Fig. 20| Comparison of Purkinje cells MFR changes in the sagittal and coronal planes. Purkinje cells in sagittal and coronal slices showed both an increase and a decrease of the MFR (graph on top). The percentage of channels presenting an increased MFR (indicated by the arrow) was larger than the percentage of channels with a decreased MFR.

The computation of the Pearson correlation coefficient at different input frequencies enabled the comparison of the correlation present between Purkinje cells and granule cells activities in sagittal and coronal slices. Both sagittal and coronal slices presented different levels of positive and negative correlations. These correlations appeared to be frequency dependent: the increase of the input frequency determined an increase in the level of correlation and in the percentage of Purkinje cells correlating with granule cells activity. However, in coronal slices the percentage of Purkinje cells showing a correlation was significantly higher compared to the one detected in sagittal slices (unpaired Student's t test, $p<0.05$). This evidence was confirmed at all the input frequencies both for positive and negative correlations.

4.5 DISCUSSION

4.5.1 Frequency-dependent responses of the granular layer in sagittal and coronal slices.

During the evaluation of granular layer responses in sagittal and coronal slices the attention was focused on N_{2a} and N_{2b} peaks amplitudes as a measure of postsynaptic granule cells activation. According to literature, N_{2a} peak amplitude is proportional to the synaptic current derived from AMPA receptor activation and N_{2b} wave is regulated by synaptic inhibition and NMDA receptors activation (Mapelli and D'Angelo 2007). The behavior of N_{2a} and N_{2b} peak amplitudes within the trains delivered at different input frequencies can be explained taking into account the correspondence between N_{2a} and N_{2b} peaks amplitudes and granule cells activity. Both in sagittal and coronal slices the reconstruction of N_{2a} peak amplitude changes led to the observation of a predominant short-term depression becoming more evident increasing the input frequency. Moreover, this short-term depression (STD) appeared to be more pronounced in the center of the granular layer. N_{2a} is representative of AMPA receptor (AMPARs) activation, and during repetitive stimulation AMPARs desensitization typically determine the rise of STD (Gao et al. 2012, Wall 2005, DiGregorio et al. 2007). The spatial organization of STD in the granular layer can be justified taking into account the different number of mossy fibers involved in input transmission in different regions of the granular layer. A higher number of fibers stimulated in fact would determine an increased number of active synapses impinging on granule cells and an increased AMPARs desensitization. Nevertheless, in extracellular recordings it is not possible to establish the accurate number of fibers involved.
On the other hand, N_{2b} behavior can be explained taking into account the effect of Golgi cells inhibition on granule cells. Golgi cells shaping of granule cells activity is a composite process and several phenomena might take a part in the observed N_{2b} changes. The different percentage of channels detecting a significant increase of N_{2b} in coronal slices compared to sagittal ones could be due to the spatial ramification of Golgi cells axons (Tabuchi et al. 2019). The different geometry characterizing Golgi cells axons could determine a decreased inhibition exerted by Golgi cells onto granule cells in sagittal slices, since Golgi cells axonal plexus is oriented in the sagittal plane (D'Angelo 2008, Tabuchi et al. 2019). Moreover, during repetitive stimulation Golgi cells-granule cells synapses undergo short-term depression (Mapelli et al. 2009), and this kind of short-term plasticity would probably contribute to determine the significant increase of the percentage of channels detecting N_{2b} increase at higher input frequencies. The complex spatial organization of N_{2b} percent changes observed remains difficult to interpret. The detected N_{2b} peak increase in different regions of the granular layer suggests a possible different distribution of inhibition efficacy in different regions, probably accompanied by non-linear frequency-dependence, at least to certain

extent. However, pharmacological and computational approaches would be needed to dissect this type of mechanisms.

4.5.2 Different Purkinje cells activity in sagittal and coronal slices.

The evidence of a zebrin-like distribution pattern of Purkinje cells in coronal slices emphasizes the potential of the extremely high spatial resolution of the HD-MEA. Thanks to this state-of-the-art technology it has been possible to observe the activity coming from all the units in sagittal and coronal slices assigning to each cell a precise location inside the cerebellar lobule. Purkinje cells responses elicited by mossy fibers stimulation appeared as peaks and pauses in the PSTHs, representing transient increases and decreases of Purkinje cells firing. In sagittal slices the most common Purkinje cells responses were peaks. Since in sagittal slices parallel fibers are mostly cut, it is conceivable to expect an important role played by granule cells ascending axons inputs in determining this increased firing frequency. The functional equivalence of ascending axons and parallel fibers inputs has been indeed demonstrated (Walter et al. 2009). In coronal slices, molecular layer interneurons activity is most probably responsible for pauses. However, within 5 pulses stimulation trains Purkinje cells in coronal slices presented a more complex pattern of activity, mainly characterized by pauses at the beginning of the bursts and peaks at the end. This result might rely on a frequency-dependent inhibition exerted on Purkinje cells by molecular layer interneurons. In literature, two different forms of short-term dynamics shaping molecular layer interneurons activities have been described: short-term facilitation has been observed at parallel-fibers stellate cells relay and short term depression characterized parallel fibers-basket cells synapses (Carter and Regehr 2000, Bao et al. 2010). In addition, it has been demonstrated that parallel fibers-molecular layer interneurons synapses can be characterized by heterogeneous profiles of STP, determining differences in the firing frequencies and delays of molecular layer interneurons responses at different input frequencies (Dorgans et al. 2019). Moreover, a possible involvement of climbing fibers activity should be taken into account. A pure spillover connection in fact has been confirmed between climbing fibers and basket/stellate cells, but the effect of these fibers stimulation is still controversial being able to determine both the potentiation and the suppression of Purkinje cells inhibition mediated by interneurons activity (Szapiro and Barbour 2007, Satake et al. 2004). Importantly, the extent of climbing fibers activation in slices is not clear but should be negligible. Nevertheless, the phenomenon observed in coronal slices is most likely compound in its origin and it probably involves different mechanisms acting in concert, determining the shift from pauses to peaks responses observed for Purkinje cells.

4.5.3 The correlation of granular and Purkinje cells layers activity at different input frequencies.

Both in sagittal and coronal slices positive and negative significant levels of correlation were found between granular and Purkinje cells layers activity. The presence of either types of correlation can be due to the different activation of the system. Purkinje cells responses in fact can be determined by the activation of ascending fibers or by the parallel-fibers pathway. The direct activation of Purkinje cells through ascending axons can lead to an high level of correlation with granule cells activity, while parallel fibers involvement can explain the presence of a negative correlation due to the activation of molecular layer interneurons inhibiting Purkinje cells responses. The levels of correlation and the percentage of units presenting a correlation, appeared to be frequency dependent both in sagittal and coronal slices. This evidence can be explained taking into account the description of the granular layer as an high-pass filter able to enhance transmission of higher frequencies compared to lower ones (Mapelli et al. 2010b). Unfortunately, in this study it was not possible to reconstruct the level of

correlation at 100Hz of stimulation due to technical limitations, but the low levels of correlation found at 6Hz and 20Hz support the ability of the granular layer to cut-off signals below 50Hz. Interestingly, the number of Purkinje cells significantly correlating with granule cells activity was always larger in coronal slices compared to sagittal ones. The high number of units presenting a positive correlation with granular layer activity can be explained taking into account the "Beam Theory" (Eccles et al. 1967). Parallel fibers travel transversally and contact several Purkinje cells determining the activation of beams of Purkinje cells (D'Angelo 2011). In coronal slices parallel fibers are mostly preserved and the activation of parallel fibers through mossy fibers stimulation would determine an higher number of Purkinje cells correlating with granule cells. On the other hand, the presence of the entire network in coronal slices can cause the activation of molecular layer interneurons. The consequent inhibition exerted on Purkinje cells by molecular layer interneurons activity would determine the number of units presenting a negative correlation with granule cells. The cut of parallel fibers characterizing sagittal slices might be a plausible explanation for the smaller number of Purkinje cells with positive and negative correlations. Obviously, in order to confirm this kind of hypothesis a spatial reconstruction of the levels of correlations detected is needed.

4.6 CONCLUSION.

In this work it has been possible to provide a detailed description of cerebellar circuit activation at different frequency ranges. Notably, this is the first comprehensive study of the frequency-dependence of cerebellar processing. The recording of spontaneous and evoked activity of granule cells and Purkinje cells in sagittal and coronal slices increased our knowledge of two different pathways in the cerebellar cortex: the ascending pathway of mossy fibers-granule cells-ascending axons-Purkinje cells synapses and the one of mossy fibers-granule cells-parallel fibers-molecular layer interneurons-Purkinje cells synapses. The activity of both these pathways appeared to be strictly frequency-dependent. Short-Term-Plasticity in the granular layer presented a specific spatial organization and the differences observed in sagittal and coronal slices supported a possible frequency-dependence of inhibitory mechanisms, involving Golgi cells and the different distribution of their axonal plexus in the sagittal and coronal planes. On the other hand, Purkinje cells showed a wide range of basal discharge, with a zebrin-like distribution pattern evident only in the coronal plane. The comparison of Purkinje cells responses in sagittal and coronal slices unraveled compelling differences, suggesting an additional frequency-dependence of inhibitory mechanisms in the molecular layer (molecular layers interneurons activity). Moreover, frequency variation affected the levels of correlation between Purkinje cells and granule cells activities, while the number of units presenting a correlation appeared to be different in sagittal and coronal planes. Taken together, this considerable amount of data with its high level of complexity prompts new research on the frequency-dependence of cerebellar network activity. The combination of pharmacological tools and computational models could extend the investigation of the computational power of the cerebellar cortex. This opens a new perspective for the evaluation of cerebellar cortex involvement in higher cognitive functions, additionally taking into account its possible role in complex brain states related processes never considered for the cerebellum before, such as consciousness.

5.

Neuronal correlates of neurovascular coupling in the cerebellum: providing a neurophysiological substrate to region and frequency dependence of vascular responses in the granular layer.

Monteverdi A.[1], Casali S. [1], Gagliano G. [1], Mapelli L[1]. and D'Angelo E.[1*]*

[1] Dept of Brain and Behavioral Sciences, University of Pavia, 27100 Pavia, Italy

AUTHOR CONTRIBUTIONS: L.M. and E.D. designed research; A.M. performed HD-MEA recordings and data analysis; G.G. performed capillaries dilations recordings; S.C. performed the computational reconstruction of granular layer activity; A.M., L.M., and E.D. wrote the paper.

* Lisa Mapelli and Egidio D'Angelo are co-senior authors

In preparation

5.1 ABSTRACT

According to latest neuroimaging studies cerebellar vermis and hemisphere present different linear and non-linear BOLD responses during the execution of the same motor task (Alahmadi et al. 2017). In order to determine whether different cerebellar regions are able to differentiate the neurovascular response, a recent investigation has been conducted on capillaries motility in cerebellar slices at different input frequencies (Gagliano et al. *in preparation*). The granular layer vascular motility following mossy fibers stimulation interestingly showed a region and frequency dependence. To date, differences between neuronal activity in cerebellar vermis and hemisphere has never been investigated *ex-vivo*. The main aim of this work is to provide a first description of the neuronal correlates of neurovascular coupling responses in the cerebellum taking into account their region and frequency dependence. Thanks to the unprecedented spatial and temporal resolution of an HD-MEA (4096 electrodes simultaneously recording), granule cells activity in the granular layer of cerebellar vermis and hemisphere was investigated at different input frequencies. Granular layer neuronal responses to stimulation were observed as Local Field Potentials (LFP) and showed a region and frequency dependence when evaluating the two main LFP components informative of granule cells synaptic activation (N_{2a} and N_{2b} peaks). In particular, the N_{2b} peak appeared as the ideal candidate to explain vessel caliber changes recorded *ex-vivo.* Indeed, this peak is known to be influenced by NMDA receptors (NMDAR) activation (Mapelli and D'Angelo 2007), and NMDARs-NO pathway plays a pivotal role in the regulation of neurovascular coupling in the granular layer (Mapelli et al. 2017). Thanks to a biophysically realistic computational model, granular layer activity has been simulated at different input frequencies, validated against the experimental data, and used to extract NMDA currents values. These data suggested that the NMDAR-NO pathway is sufficient to explain

the time-course of vessel dilations in response to stimulation, while the non-linearity in the frequency-dependence of this phenomenon most likely involves additional mechanisms. The results achieved in this work prompt a new way to address the study of the neuronal mechanisms underlying the origin of the neurovascular coupling and ultimately of the BOLD signals.

5.2 INTRODUCTION

Cerebral blood flow (CBF) requires an extremely fine regulation in order to provide the proper levels of nutrients and oxygen to the brain. This regulation involves neuronal activity, and the complex process leading to the activation of several signal pathways cooperating for the tuning of vessel constriction and dilation is called neurovascular coupling (NVC). To date, a complete understanding of the processes underlying NVC is still missing, and the relationship between neuronal activation and vessels diameter changes still deserves a thorough investigation. This relationship is of particular interest, especially considering that the dynamic changes of CBF operated by NVC can be directly exploited by neuroimaging techniques like functional magnetic resonance imaging (fMRI). This technique measures the blood-oxygen-level-dependent (BOLD) signal, which is strongly influenced by CBF adaptations and is considered as a reference to map brain activity changes. However, the understanding of BOLD signals neuronal origin is not straightforward and is still under debate. For all these reasons, it is compelling to investigate *ex-vivo* the relationship between neuronal activity and vascular changes. The cerebellar cortex appears to be very suitable to perform this kind of investigation, due to its functional and structural properties. Previous investigations were conducted on the cerebellar molecular layer and focused on Purkinje cells and molecular layer interneurons activity (Lauritzen et al. 2012) (Box 1). However, granule cells are the most abundant and energy consuming elements in the cerebellum (Howarth, Peppiatt-Wildman and Attwell 2010), and can be regarded as a consistent determinant of cerebellar NVC. Actually, a recent study has been conducted on the granular layer of cerebellar slices, shading a new light on the mechanisms underlying NVC in the cerebellum (Mapelli et al. 2017). It has been demonstrated that granule cells activation in response to mossy fibers stimulation induces capillary vasodilation through a nitric oxide (NO)/NMDA receptors system (Box 1). This evidence supports the pivotal role played by the granular layer in determining the cerebellar NVC, leading to the CBF changes influencing the fMRI signals detected in the cerebellum.

The latest neuroimaging studies conducted in humans, revealed a new puzzling evidence. The activation of two different regions in the cerebellum, the vermis and hemisphere, appeared to significantly differ during the execution of the same motor task (Alahmadi et al. 2017). In particular, cerebellar vermis lobule V showed a BOLD signal increasing linearly with the grip force, while hemisphere lobule VI presented a non-linear BOLD activation. Interestingly, cerebellar vermis and hemisphere present different connections with other brain areas. The cerebellar vermis receives extensive somatosensory information (Roostaei et al. 2014) and is primarily involved in motor control, while connections with non-motor areas characterize the cerebellar hemisphere (Stoodley and Schmahmann 2010) and support its role in higher cognitive functions. In order to discern how the vermis and hemisphere contribute to cerebellar NVC during different ranges of activity, an investigation focusing on capillaries motility in the mouse granular layer of the cerebellar vermis and hemisphere in slices has been recently conducted in our laboratory (Gagliano et al. *in preparation*) (Box 2). Since it is known that the motor cortex codes the grip force by increasing the firing rate (Cramer et al. 2002), mossy fibers were stimulated using patterns varying in frequency (6Hz, 20Hz, 50Hz and 100Hz). The analysis of the consequent degree of capillary dilation in the granular layer led to the observation of a different frequency dependence characterizing vascular responses of

cerebellar vermis and hemisphere (Box 2). The investigation of the neuronal activity correlates of this difference is the main aim of the present work. In literature, the relationship between vascular motility and neuronal activity has been frequently inspected using local field potentials (LFPs). In particular, a strong correlation has been found between the sum of LFP and CBF changes (Mathiesen et al. 1998, Mathiesen, Caesar and Lauritzen 2000). The sum of the evoked field potentials during the stimulation period is considered more reliable than a single LFP because this electrophysiological response is usually fast (occurring in the ms time range) while CBF responses last for seconds. Therefore, the accumulated neuronal activity needs to be taken into account when comparing synaptic activity and hemodynamic changes. Herein, the differences between cerebellar vermis and hemisphere neuronal activity are described for the first time *ex-vivo*, taking advantage of the extremely high spatial and temporal resolution of an high-density multi-electrode array (HD-MEA, with 4096 electrodes simultaneously recording neuronal activity). LFPs responses in cerebellar vermis and hemisphere were recorded in the same stimulating conditions used for determining capillary motility (Box 2), leading to the reconstruction of the region and frequency dependence of neuronal activity. The correlation between neuronal activity and vessel diameter changes previously observed was achieved using the biophysical realistic reconstruction of network activity performed through computational models. Taken together, these results help to deepen our knowledge of the neurophysiological basis of different cerebellar fMRI responses and represent an innovative way to study the neuronal correlates of neurovascular coupling. In the near future, these data will be fundamental to develop mathematical bottom-up models of NVC and to gain a deeper insight into the neuronal activity underlying the origin of BOLD signals.

Box 1| Neuronal pathways for NVC in the cerebellum.

For years the molecular layer has been regarded as the main determinant of the NVC in the cerebellum. Several investigations have been conducted focusing the attention on Purkinje cells (PC) and molecular layer interneurons (MLI) activity and their influence on cerebellar hemodynamic changes. The nitric oxide (NO) appeared in these studies as the main vasoactive agent involved in NVC processes (Lauritzen et al. 2012). In particular, the main contribute to CBF changes came from MLIs (Mathiesen et al. 1998). Parallel fibers stimulation determines PCs inhibition through the GABAergic activity of MLIs and the authors suggested that for this reason PCs firing weakly correlates with CBF increase after cerebellar cortical activation. Indeed, parallel fibers stimulation determines glutamate release and the consequent activation of postsynaptic NMDA receptors (NMDARs). NMDARs activation triggers a calcium dependent pathway leading to the activation of the neuronal isoform of nitric oxide synthase (nNOS) and consequently to NO production. NO acts as a strong vasoactive agent and determines vasodilation activating the soluble guanylyl cyclase (sGC) and elevating the cyclic guanosine monophosphate (cGMP) intracellular concentration in the vessel endothelium or in the pericytes (which control capillary motility). Importantly, the functional isoform of NOS appeared to be expressed in MLI but not in PCs (which also lack NMDARs at the synapses with parallel fibers) (Mathiesen et al. 1998). Recently the pivotal role of the molecular layer in determining the cerebellar NVC has been questioned looking at NVC mechanisms in the granular layer. Granule cells in fact are the most abundant neurons in the cerebellum and present an high expression of NMDARs (Monaghan et al. 1991) and nNOS (Southam, Morris and Garthwaite 1992). Moreover, it has been demonstrated that mossy fibers stimulation can induce NO release (Maffei et al. 2003). Therefore, an investigation of capillaries motility has been conducted in the granular layer, unravelling the pathways determining vasodilation or constriction. This study highlighted the central

role of granule cells in producing NO through NMDARs activation after mossy fibers stimulation. The vasodilation induced through this NMDARs/NO system appeared to overcome the vasoconstrictor action of another active agent called 20-HETE and derived from metabotropic glutamate receptors (mGluRs) activation (probably involving glial cells) (Attwell et al. 2010) (Fig.1). Therefore, the granular layer emerged as fundamental to trigger cerebellar NVC and most likely to shape the BOLD signals detected in the cerebellum.

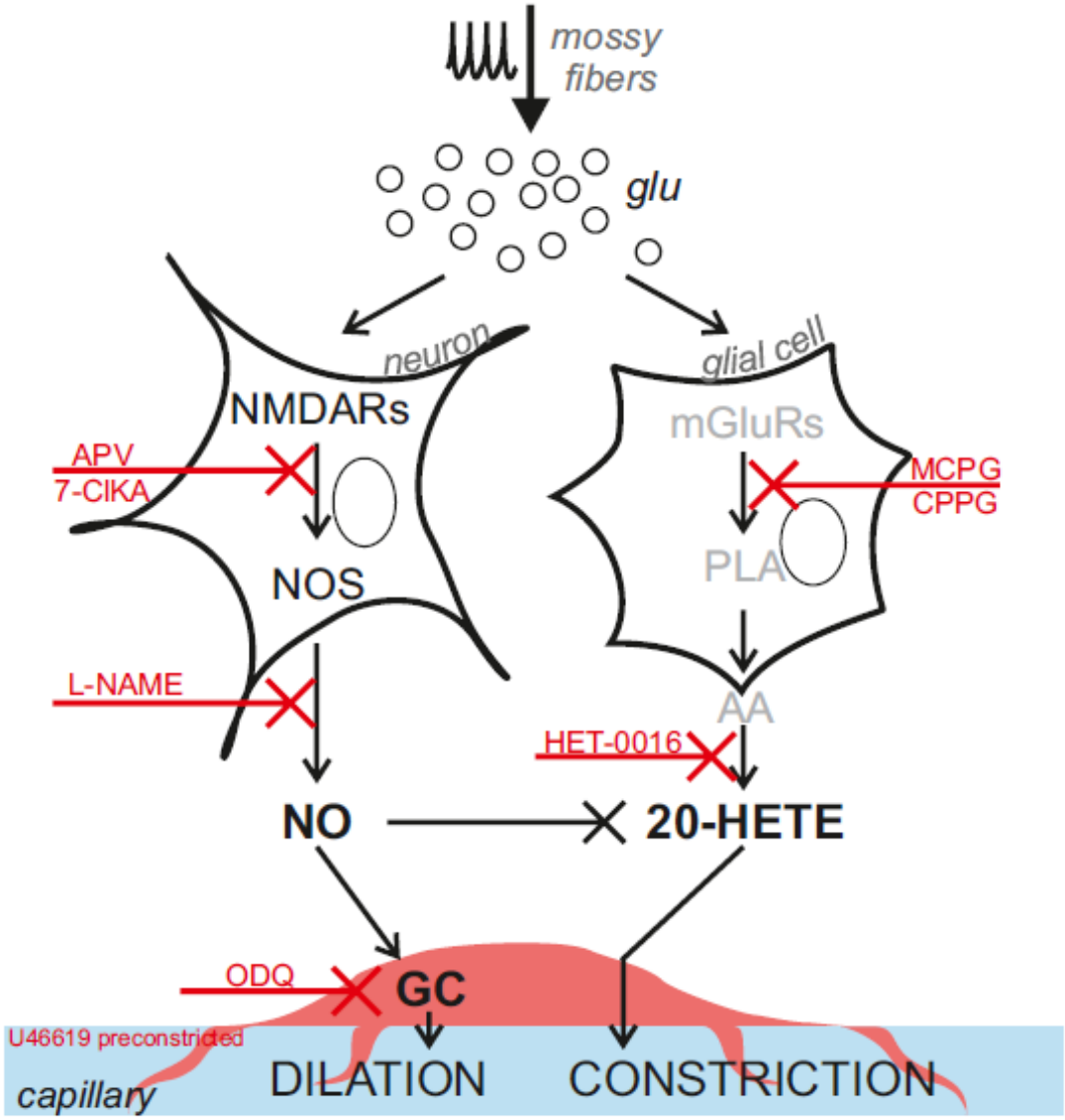

Fig.1| Neuronal pathways for NVC in the granular layer of cerebellum. Mossy fibers stimulation leads to glutamate release determining both NMDARs and mGluRs activation. NMDARs activity causes NOS activation with a consequent increase of the concentration of NO. NO is a strong vasodilator agent, and acts on adjacent pericytes increasing the activity of the soluble guanylyl cyclase (GC) and determining capillary dilation. On the other hand, the activation of mGluRs, presumably located on astrocytes, determines the activation of phospholipase A2 (PLA) and the consequent production of arachidonic acid (AA). This triggers the synthesis of 20-HETE, determining vasoconstriction. In the granular layer of the cerebellum, the balance between these two pathways plays a pivotal role in neurovascular mechanisms. The pharmacological assessment of these pathways is indicated in red, and refers to the investigation reported in Mapelli et al., 2017.

Box 2| The region and frequency dependence of neurovascular responses in the cerebellum.

Recent fMRI studies in humans have shown that the activation of cerebellar vermis and hemisphere can be different during the execution of the same motor task (Alahmadi et al. 2017). A possible explanation comes from the different connections of cerebellar vermis and hemispheres with other brain areas (Stoodley and Schmahmann 2009), taking into account their different role in motor control and higher cognitive functions. Since making detailed neurophysiological inferences from fMRI signals is not feasible, an *ex-vivo* investigation has been conducted on cerebellar slices of vermis lobule V and hemisphere lobule VI to better understand the origin of the different BOLD signals detected. Vascular activity was evaluated in the granular layer stimulating mossy fibers with several input frequencies, in order to mimic different ranges of activity. The stimulation frequencies chosen were 6Hz, 20Hz, 50Hz, 100Hz, and 300Hz due to their relevance for cerebellar activity: theta band (6Hz) activity has been observed during resting state *in vivo* recordings (Courtemanche et al. 2013) and the granular layer appears to be well equipped for the development and maintenance of this low-frequency rhythm (D'Angelo and De Zeeuw 2009); beta band (20Hz) has been recorded *in vivo* as a "background activity" within the granular layer (Pellerin and Lamarre 1997) and its relevance for sensorimotor processing (Courtemanche et al. 2009) and vestibulo-ocular reflex performances (Rössert et al. 2014) is well known; gamma (50Hz) and fast (100Hz) band were chosen considering the cerebellar synchronization with primary sensory and motor cortices during sensorimotor integration (Popa et al. 2013) and the improved signal transmission operated by the granular layer towards the molecular layer at high frequencies (Mapelli et al. 2010b); finally, ultra-fast bands (300Hz) were taken into account due to their *in vivo* observation (de Solages et al. 2008), though their specific role in concert with low-frequency oscillations remains unknown (De Zeeuw et al. 2008). Mossy fibers were stimulated for 35 seconds and capillaries changes were observed at three different time points: 2 seconds, 20 seconds, and 35 seconds. As shown in Fig. 2 (Gagliano et al., *unpublished observations*) significant capillaries dilations were recorded both in vermis and hemisphere cerebellar slices in response to the different frequencies of mossy fibers activation. Interestingly, the NVC response did not increase linearly with the input frequency, showing different non-linear responses in the vermis compared to the hemisphere. In particular, capillaries dilation appeared to be different between cerebellar vermis and hemisphere especially at high frequencies of stimulation. These results support that cerebellar NVC might be region and frequency dependent. Further investigations are needed to unravel a possible region and frequency dependence of granule cells responses determining this difference in the vascular events recorded.

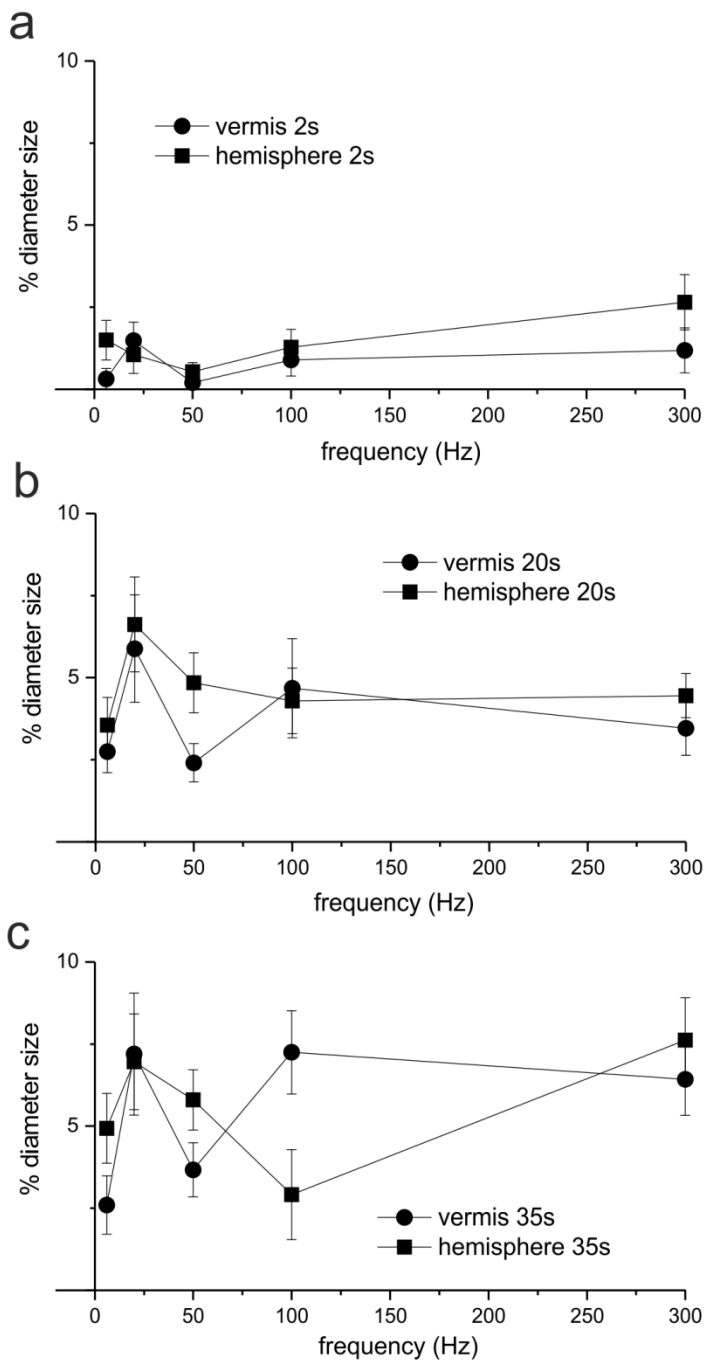

Fig.2| Vascular responses to different input patterns in cerebellar vermis and hemisphere. Reconstruction of the average time course of capillaries percentage of dilation in cerebellar vermis and hemisphere at different input frequencies (6Hz, 20Hz, 50Hz, 100Hz) during mossy fibers stimulation at 2 seconds (a), 20 seconds (b) and 35 seconds (c). Importantly, the NVC response did not show a linear trend increasing the input frequency. Moreover, capillaries dilation differed in cerebellar vermis and hemisphere. Taken together these evidences support the region and frequency dependence of NVC phenomenon in the cerebellum.

5.3 MATERIALS AND METHODS

5.3.1 Cerebellar slices preparation.

Acute parasagittal slices (220 µm thick) were obtained from cerebellar vermis and hemisphere of 18 to 23-days-old C57BL/6 mice. Animals were anesthetized with halothane (Sigma Aldrich) and killed by decapitation. The cerebellum was gently removed and slices from cerebellar vermis and hemisphere were cut with a vibroslicer (VT1200S, Leica Microsystems). During the whole procedure, the tissue was maintained in cold and oxygenated Krebs solution which contained (in mM): 120 NaCl, 2 KCl, 1.2 $MgSO_4$, 26 $NaHCO_3$, 1.2 KH_2PO_4, 2 $CaCl_2$, 11 glucose, pH 7.4 equilibrated with 95% O_2–5% CO_2. Before recording, slices were recovered for 1 hour in the same solution and then incubated for 1 hour with 75 nM of the thromboxane agonist U46619 (Abcam), at room temperature. This treatment is used to restore the vascular tone in slices, as previously described (Mapelli et al. 2017). For the recording, cerebellar slices were gently positioned on the HD-MEA chip and fixed with a nylon mesh attached to a platinum wire, to improve tissue coupling with the electrode array. Krebs solution was continuously perfused (2-3 ml/min) in the glass reservoir during the whole recording session and maintained at 37 ºC with a Peltier feedback temperature controller (TC-324B; Warner Instrument Corporation).

5.3.2 HD-MEA recordings.

Extracellular electrophysiological recordings of neuronal activity in the slices were performed using a complementary metal-oxide-semiconductor (CMOS) based high-density multielectrode array (HD-MEA; Biocam X, 3Brain AG). This state-of-the-art technology enables the extracellular signals detection in cerebellar slices with an unprecedented spatial resolution, being characterized by 4096 electrodes recording simultaneously. The electrodes are arranged in a 64x64 matrix on a small and compact area (2.67mm x 2.67mm). The electrode size is 21µm x 21µm with a pitch of 42 µm (Biochip Arena). HD-MEA signals were sampled at 18kHz/electrode with a high pass filter at 100Hz. Electrical stimulation was obtained using a bipolar tungsten electrode placed on the mossy fibers bundle and delivering current pulses of 50µA (pulses duration 200 µs). Taking into account the pivotal role played by the granular layer in triggering neurovascular events in the cerebellum (Mapelli et al. 2017), an investigation of capillaries motility was recently conducted using *ex-vivo* cerebellar slices (Gagliano et al, *unpublished observations*) and led to the observation of different vascular activities between vermis and hemisphere (Box 2). Thus, in order to better understand the neuronal basis of this difference, the same experimental protocol was chosen for HD-MEA recordings. Slices were stimulated at 6Hz, 20Hz, 50Hz, and 100Hz for 35 seconds. The neuronal activity was recorded as Local Field Potential (LFP) in the granular layer of vermis lobule V and hemisphere lobule VI.

5.3.3 Data analysis.

5.3.3.1 Local field potentials analysis.

Data were acquired on-line and stored using the BrainWave X Software (3Brain AG). Data analysis was performed using *ad-hoc* routines written in MATLAB (Mathworks). Mossy fibers stimulation activated granule cells in cohorts, determining the propagation of large-amplitude Local Field Potentials (LFP) along the granular layer. In agreement with previous studies (Mapelli and D'Angelo, 2007, (Diwakar et al. 2011), The LFP showed a typical N_1-N_{2a}-N_{2b}-P_2 complex: N_1 corresponded to

presynaptic volley activation, N_{2a}- N_{2b} were informative of granule cells postsynaptic activation and P_2 represented the currents returning from the molecular layer. In order to characterize granule cells responses to stimulation, the analysis was focused on N_{2a} and N_{2b} peaks amplitude. For each recording, N_{2a} and N_{2b} negative peaks were measured in an appropriate time window (1.9ms ± 1.1ms and 4.5ms ± 1.2ms from the stimulus artifact, for N_{2a} and N_{2b}, respectively) and subtracted from the baseline (measured as the average of the 300ms preceding the stimulus). Presumed LFP signals were considered for the analysis only when peaks amplitudes exceeded 2.75 times (for N_{2a}) and 2 times (for N_{2b}) the standard deviation calculated over the baseline period. Mossy fibers activation reliably resulted in granule cells activation originating LFP signals that spread along the granular layer for tens of micrometers. Herein, the attention was focused only on LFP signals detected from channels about 200μm distant from the stimulating electrode, in order to measure neuronal activity at a distance from the stimulating electrode similar to that used for assessing capillaries motility (Gagliano et al., *unpublished observations*). A visual inspection of the LFPs was performed for all the channels selected (n=159 channels; total number of recordings checked=636) and a correction of the baseline of LFP signals were needed at certain frequencies (in this case, signals were sampled every second, until 10 seconds of stimulation, and then every 5 seconds until 35 seconds of stimulation, in order to perform a peak-to-baseline correction with Clampfit software). This sampling operation was not necessary for N_{2b} peaks. Finally, the cumulative integral of LFP peaks was calculated over the 35 seconds of stimulation both for vermis and hemisphere, as a measure of total neuronal activity. Statistical significance was assessed using unpaired Student's *t* test. Data are reported as mean ± SEM (standard error of the mean).

5.3.3.2 Computational simulation of granular layer activity.

A detailed and biophysically realistic model of the granular layer (Casali et al. 2020) was chosen to deepen the mechanisms underlying LFP responses at different input frequencies. About 50 contiguous glomeruli in the simulation were stimulated reproducing the experimental setting (35 seconds of stimulation at 6Hz, 20Hz, 50Hz, and 100Hz). Then, AMPA currents, the number of spikes of granule cells, and NMDA currents were selected as variables of interest and extracted after the simulation. First, AMPA currents and granule cells spiking activity were chosen to test the overlap between simulated and experimental data. A 200ms bin width was chosen to analyze AMPA currents and granule cells spiking activity reconstructing their changes within 35 s of stimulation. Data obtained were normalized between 0 and 1 and then fitted using a logarithmic function and setting the first value and the last as constraints. According to literature, N_{2a} peak in the LFP recorded in the granular layer corresponds to granule cells spiking activity and AMPA receptors activation (Mapelli and D'Angelo 2007). Thus, the curves obtained from the simulated data were linearly summed and a Pearson correlation was computed between the resulting trends and experimental data. The comparison of NMDA currents extracted from the model and experimental data on capillaries dilation previously obtained (Gagliano et al., *unpublished observations*) was performed to investigate the role of neuronal activity in the neurovascular coupling mechanisms of the cerebellar granular layer.

5.4 RESULTS

5.4.1 HD-MEA recordings of cerebellar activity.

HD-MEA recordings in cerebellar slices showed spontaneous activity revealing the presence of autorhythmic firing in Purkinje cells, Golgi cells and molecular layer interneurons, as expected (Fig. 3). Evoked neuronal activity was recorded as LFPs in the granular layer of either vermis lobule V or hemisphere lobule VI slices, in response to mossy fibers stimulation at the different frequencies (6Hz, 20Hz, 50Hz, and 100Hz) for 35s (Fig. 3). The typical LFP complex (Fig. 3) was characterized by N_1, N_{2a}, N_{2b}, and P_2 waves in agreement with previous observations (Mapelli and D'Angelo 2007).

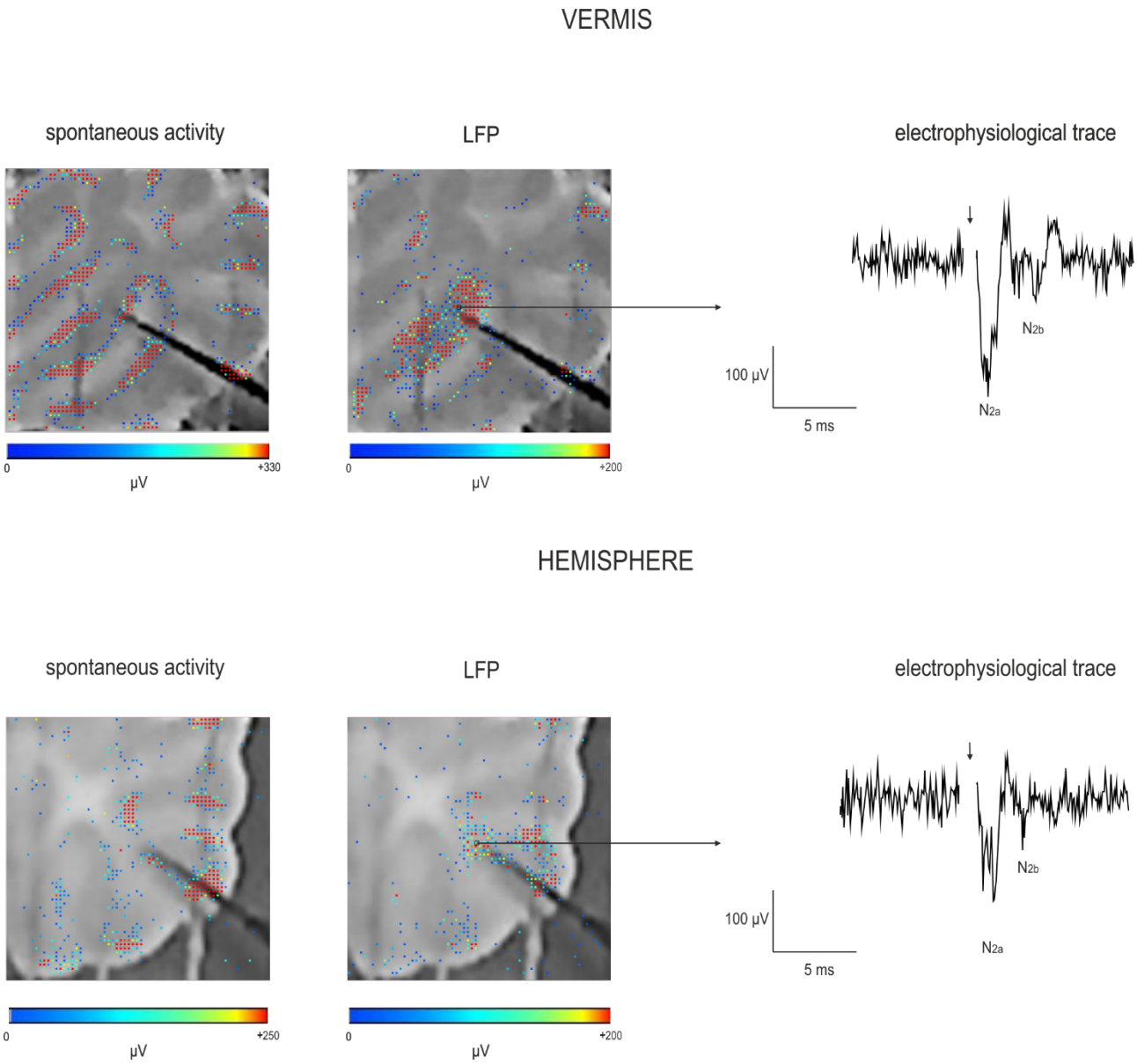

Fig.3| HD-MEA recordings of cerebellar activity. Both in cerebellar vermis and hemisphere the coupling with the HD-MEA chip led to the recording of Purkinje cells, Golgi cells and molecular layer interneurons spontaneous activity (on the left in red). The stimulation of mossy fibers with an external electrode evoked a Local Field Potential (LFP) propagating through the granular layer (in the middle). The electrophysiological trace corresponding to the channel indicated by the arrow is shown at right, where the LFP response, characterized by the typical N_1-N_{2a}-N_{2b}-P_2 complex, is reported.

5.4.2 Granular layer responses in cerebellar vermis and hemisphere.

The characterization of granular layer responses in cerebellar vermis and hemisphere was performed recording 10 slices from vermis lobule V and 10 slices from hemisphere lobule VI. The analysis of granular layer LFPs was focused on N_{2a} and N_{2b} peak amplitudes, as measures of postsynaptic granule cells synaptic activation. At first, the attention was focused on the responses after a single pulse stimulation of mossy fibers. LFP signals appeared to be different in terms of peak amplitude between the vermis and the hemisphere. In the vermis (n=10 slices; n=81 electrodes), N_{2a} peaked at 1.59 ± 0.03 ms and N_{2b} at 4.36 ± 0.1 ms, with a value of respectively -158.74 ± 5.53 μV and -67.93 ± 3.04 μV (Fig. 4). In the hemisphere (n=10 slices; n=76 electrodes), the average time-to-peak of these waves was 2.05 ± 0.06 ms for N_{2a} and 3.79 ± 0.09 ms for N_{2b}, and the corresponding amplitudes were -137.39 ± 4.66 μV for N_{2a} and -78.88 ± 2.9 μV for N_{2b} (Fig. 4). The latency of the first peak was significantly shorter ($p=6.85*10^{-10}$) in the vermis compared to the hemisphere, while the latency of the second peak was shorter in the hemisphere compared to the vermis ($p=1.23*10^{-4}$). N_{2a} peak amplitude was larger in the vermis compared to the hemisphere (p=0.003), while N_{2b} peak amplitude was smaller in the vermis compared to the hemisphere (p=0.01). The average distance between the stimulating electrode on mossy fibers and the electrodes recording the LFP signals was 133 ± 3.32 μm (n=20 slices; n=159 electrodes). This distance was not statistically different (unpaired Student's *t* test, p=0.99) compared to the one associated to capillaries vasodilation investigation as in BOX 2 (133±3.83 μm, n=99). These results suggest that cerebellar vermis and hemisphere granular layer respond differently to mossy fiber stimulation.

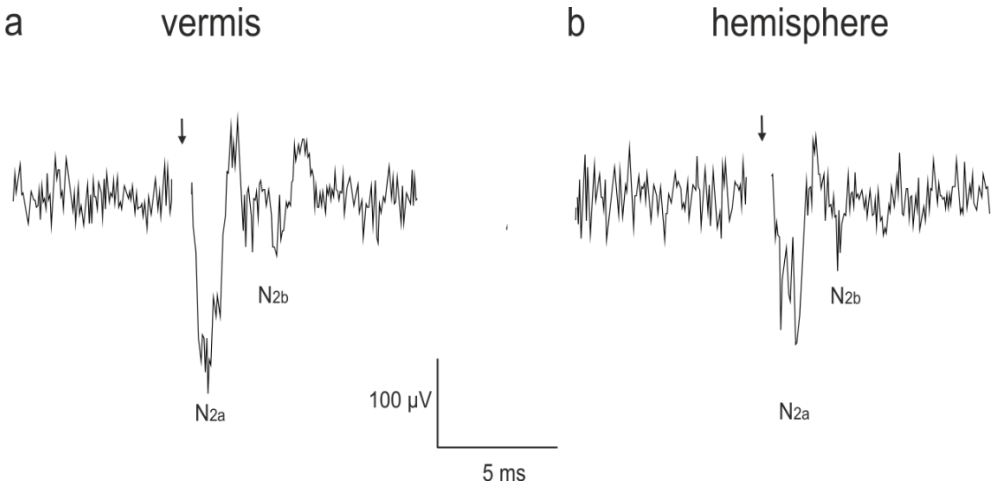

Fig. 4| Different granular layer responses in cerebellar vermis and hemisphere. Local field potentials recorded after a single pulse stimulation in cerebellar vermis (a) appeared to be significantly different from signals recorded in cerebellar hemisphere (b). In particular N_{2a} peak presented a larger amplitude in the vermis compared to the hemisphere, while N_{2b} peak was smaller in the vermis compared to the hemisphere.

5.4.3 Granular layer responses to long lasting trains of stimulation at different frequencies.

Granular layer responses to stimulus trains of 35 seconds at different frequencies (6, 20, 50, and 100Hz) were then assessed. In order to determine the changes in granule cells responsiveness to during the stimulation, LFP N_{2a} and N_{2b} peak amplitudes were taken into account. (Fig. 5 and 6). Both in cerebellar vermis and hemisphere, N_{2a} and N_{2b} peak amplitudes showed a different trend: while N_{2a} amplitude significantly decreased during the stimulation (becoming more evident increasing stimulation frequency) (Fig. 5), the trend observed in N_{2b} peak amplitude was less marked, though revealing some decrease during the stimulation (again, becoming more evident increasing the stimulation frequency) (Fig. 6).

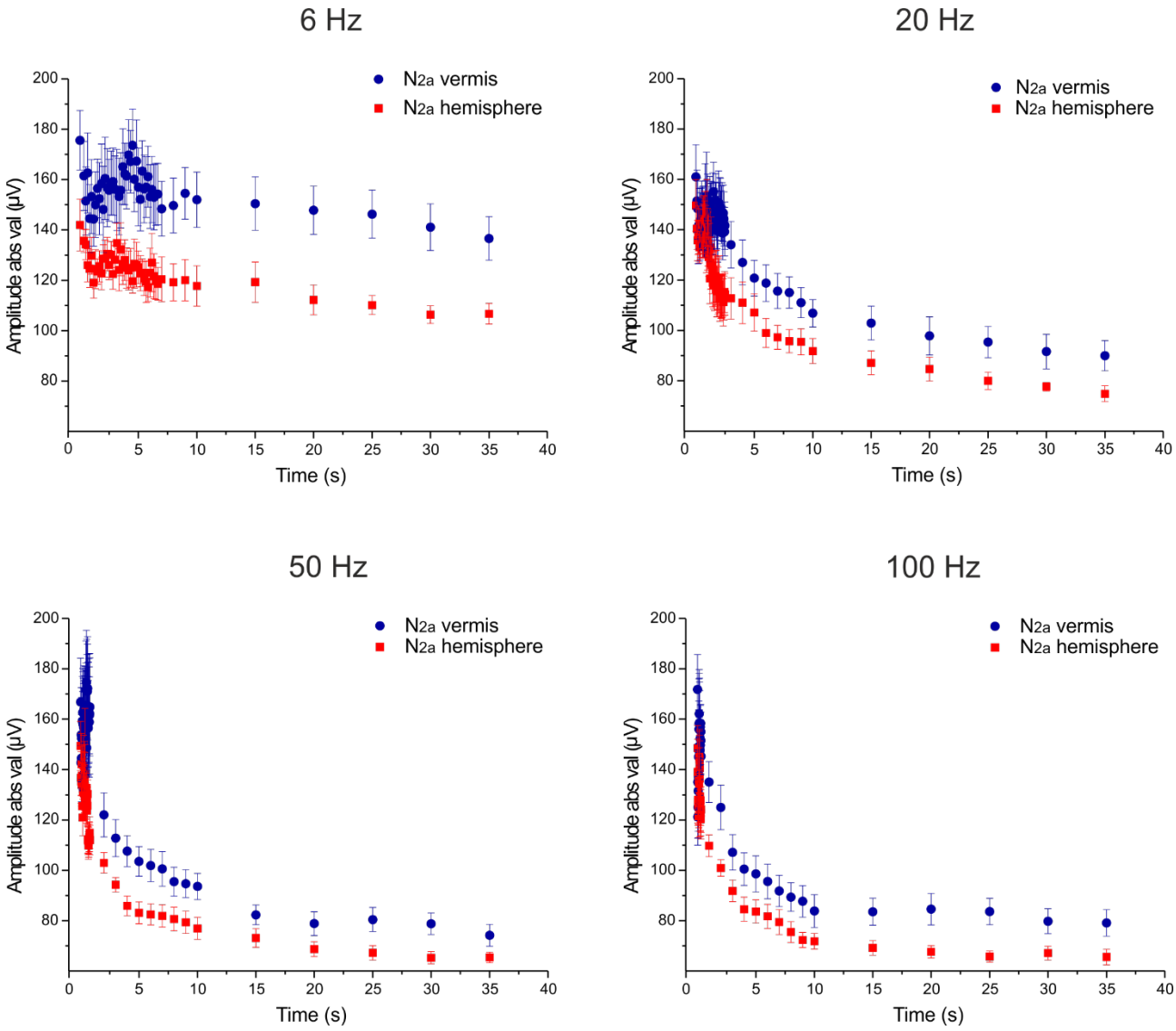

Fig. 5| N_{2a} amplitude trend within long-lasting trains of stimulation. Both in cerebellar vermis (blue dots) and hemisphere (red dots) N_{2a} peak of the LFP showed a more pronounced trend to decrease within the 35 seconds of stimulation increasing the input frequency.

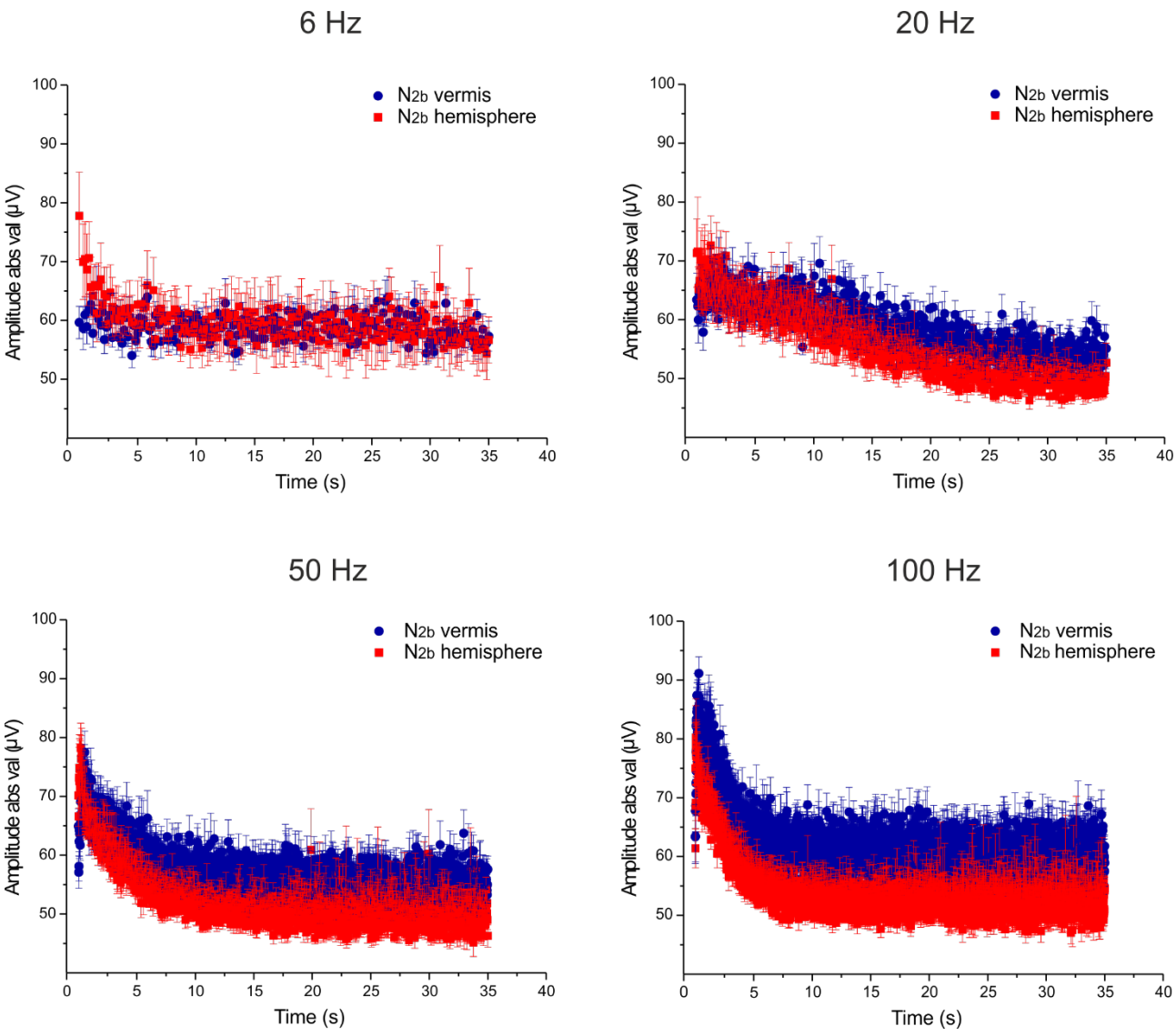

Fig. 6| N_{2b} amplitude trend within long-lasting trains of stimulation. Both in cerebellar vermis (blue dots) and hemisphere (red dots) N_{2b} peak of the LFP presented a slower and weaker trend within the 35 seconds of stimulation compared to the N_{2a} one (Fig.5).

The % change of peak amplitudes in response to the last stimulus compared to the first one in the trains within each stimulation pattern is shown in Table 1.

	6Hz	20Hz	50Hz	100Hz
VERMIS N_{2a}	-20.26±4.34	-41.73±4.39	-52.36±3.89	-52.19±3.37
VERMIS N_{2b}	-2.99±4.26	-12.31±4.5	-7.22±5.56	-2.79±6.31
HEMISPH N_{2a}	-22.08±4.45	-47.91±3.9	-54.98±2.53	-54.66±2.82
HEMISPH N_{2b}	-23.06±6.37	-22.81±6.21	-29.09±5.50	-22.96±5.46

Table 1| N_{2a} and N_{2b} peak amplitudes changes at different frequencies. This table shows the % change of the peak amplitude of the last response compared to the first response in the train, within each stimulation pattern.

Taken together, these results showed that both in cerebellar vermis and hemisphere N_{2a} and N_{2b} peaks show different trends within long lasting trains of stimulations (vermis $p=4.86*10^{-14}$; hemisphere $p=1.91*10^{-6}$).

5.4.4 Differences in granule cells responses to the stimulation frequencies used in cerebellar vermis and hemisphere.

In order to have an estimate of total neuronal activity, the cumulative integral of the LFP peaks during the 35s of stimulation was calculated both for vermis and hemisphere. The sum of granular layer total activity (for N_{2a} and N_{2b}) showed a similar frequency-dependent trend and tended to decrease increasing the stimulation frequency. This total activity was statistically different between vermis and hemisphere at 35s for all the stimulation patterns (unpaired Student's *t* test, $p<0.05$), supporting larger granule cells activation in the vermis compared to the hemisphere (Fig. 7).

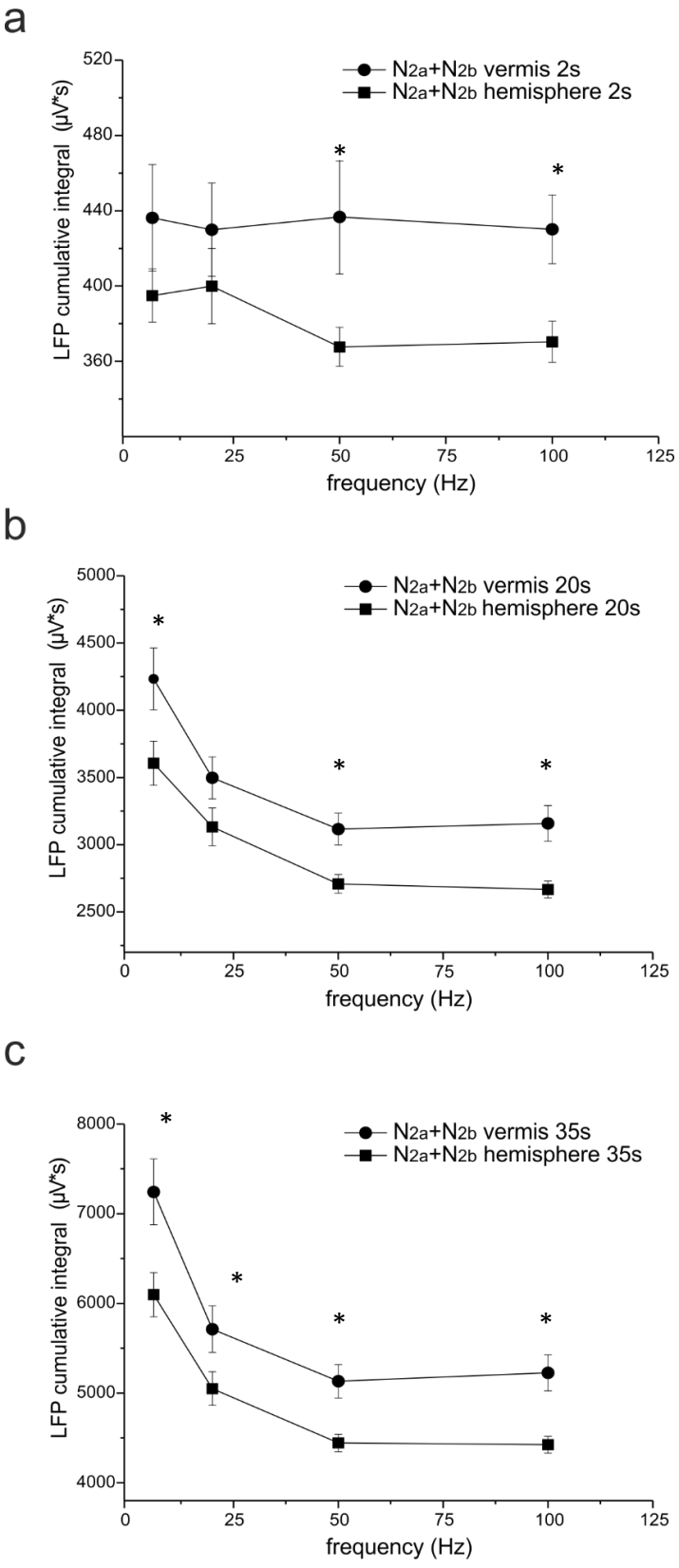

Fig. 7| Granule cells responses to different input patterns in cerebellar vermis and hemisphere. The cumulative integral of LFP responses (N_{2a} and N_{2b}) in the granular layer showed a trend to decrease increasing the input frequencies at 2 seconds (a), 20 seconds (b) and 35 seconds (c) of mossy fibers stimulation. This total granular layer activity was significantly larger in the vermis compared to the hemisphere at 35 seconds of stimulation for all the input patterns.

Interestingly, the cumulative integral of the N_{2a} and N_{2b} peaks showed different trends considering stimulus frequencies (Fig. 8 and 9). While N_{2a} component decreased with the increasing of the stimulation frequency in both cases (Fig. 8), the frequency-dependence of N_{2b} signals was different between cerebellar vermis and hemisphere (Fig. 9). The difference of both N_{2a} and N_{2b} peaks amplitudes in vermis and hemisphere was statistically significant at 20s and 35s of 50Hz and 100Hz patterns (unpaired Student's *t* test, $p<0.05$).

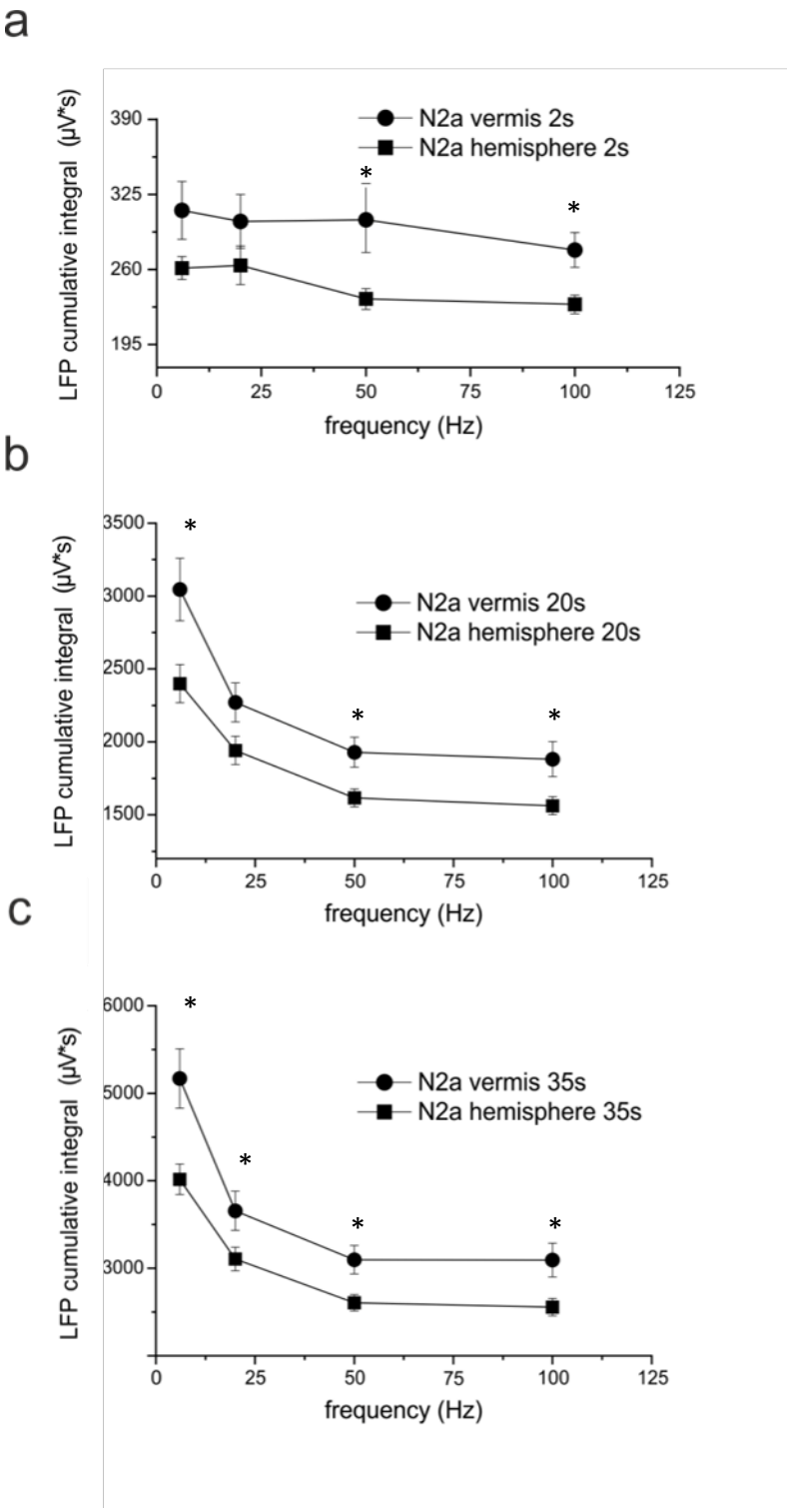

Fig. 8| Granule cells responses to different input patterns in cerebellar vermis and hemisphere (N_{2a} peak). The cumulative integral of N_{2a} peak showed a trend to decrease increasing the input frequencies at 2 seconds (a), 20 seconds (b), and 35 seconds of stimulation (c). Granular layer activity was always significantly larger in the cerebellar vermis compared to the hemisphere at high input frequencies (50Hz and 100Hz).

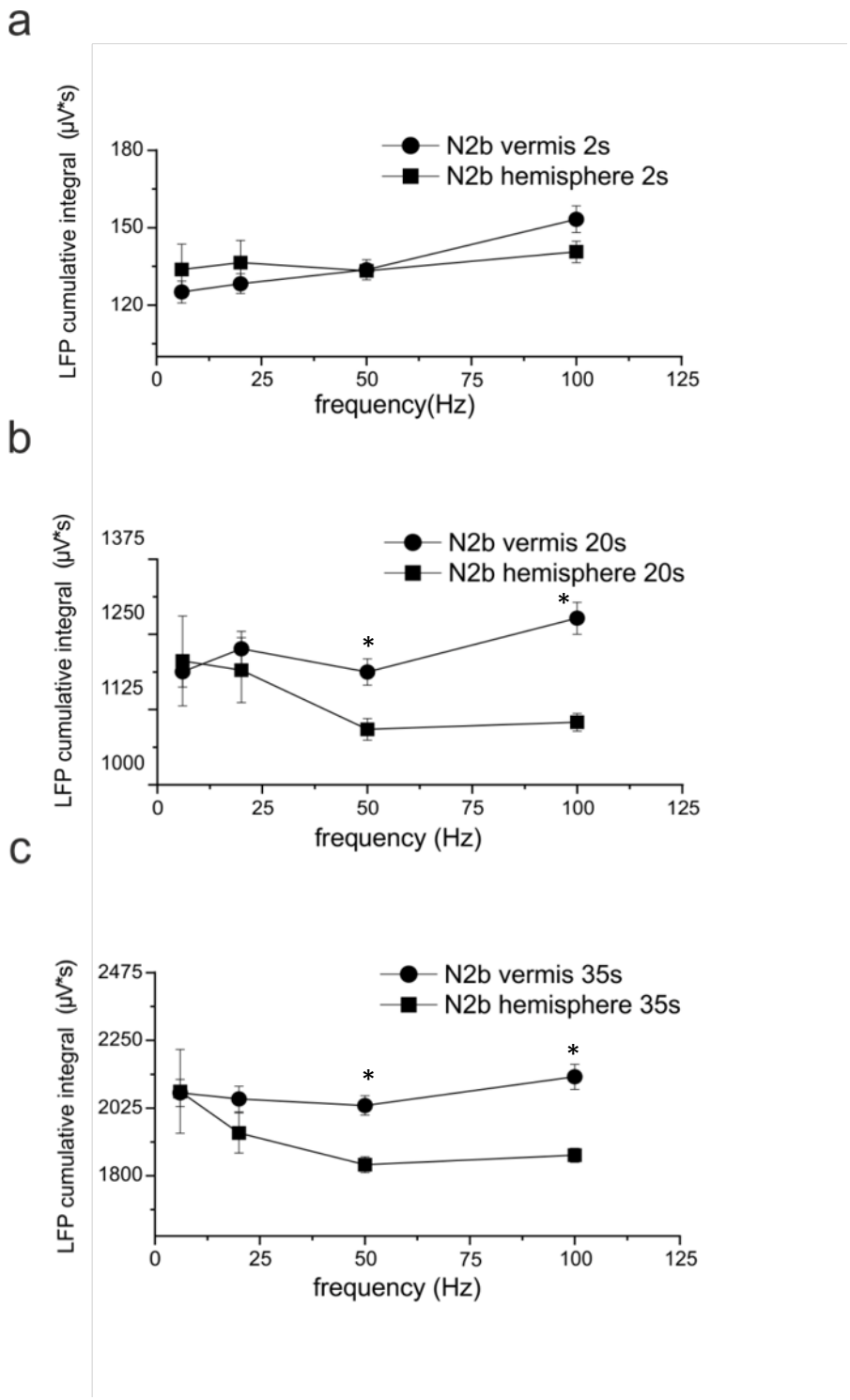

Fig. 9| Granule cells responses to different input patterns in cerebellar vermis and hemisphere (N_{2b} peak). The cumulative integral of N_{2b} peak showed a non-linear trend increasing the input frequencies at 2 seconds (a), 20 seconds (b), and 35 seconds (c) of mossy fibers stimulation. Granular layer activity was significantly larger in the vermis compared to the hemisphere only at higher frequencies (50Hz and 100Hz) after 20 seconds or 35 seconds of stimulation.

5.4.5 Modeling the granular layer response at different input frequencies.

The simulation of granular layer activity at different input frequencies led to the extraction of three main parameters: AMPA currents, granule cells spiking activity, and NMDA currents. Taking into account the relationship between N_{2a}, AMPA receptors activation, and granule cells spiking activity (Mapelli and D'Angelo 2007), AMPA currents and the number of granule cells spike were chosen as variables of interest to preliminary validate the model ability to reproduce the activation of the granular layer at different input frequencies. The trends of AMPA currents and granule cells spiking activity were reconstructed in a 200ms time bin and logarithmic fitted. As a result, AMPA currents showed a trend to decrease while the number of granule cells spikes increased within the 35 seconds of stimulation (Fig. 10). N_{2a} is expected to result from a combined action of both AMPA currents and granule cells firing. Therefore, the curves obtained were linearly summed and the resulting curve showed an exponential decay not different to that observed for N_{2a} experimental data (Fig. 10).

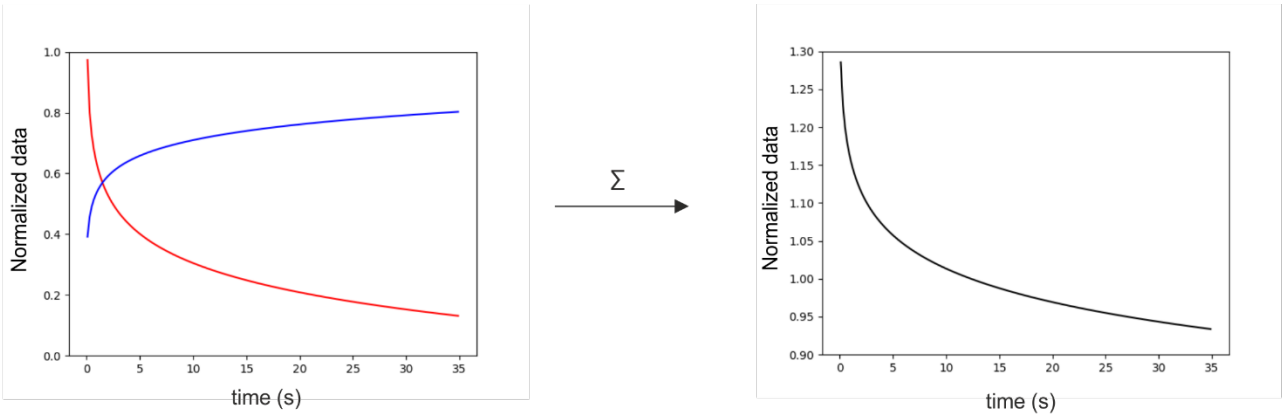

Fig. 10| The combination of AMPA currents and granule cells spiking activity extracted from the computational model. In order to compare modeled and experimental data, a combination of AMPA currents and granule cells spiking activity was performed. N_{2a} peak of the LFP correlates both with AMPA receptor activation and granule cells spiking activity. Therefore, AMPA currents and the number of granule cells spikes were extracted from the model reconstructing their trend within 35 seconds of stimulation (at left). Granule cells firing (blue line) appeared to increase within the long-lasting train while AMPA currents (red line) presented a trend to decrease. The linear sum of these curves led to a trend in which the exponential decay prevailed over the logarithmic one (at right). This result was obtained at all the input frequencies tested (the example reported here refers to the simulation performed stimulating mossy fibers at 50Hz).

This result was confirmed at all the input frequencies, and high correlation values were found between modeled trends and the logarithmic fit of experimental data (r^2>0.9) (Fig. 11).

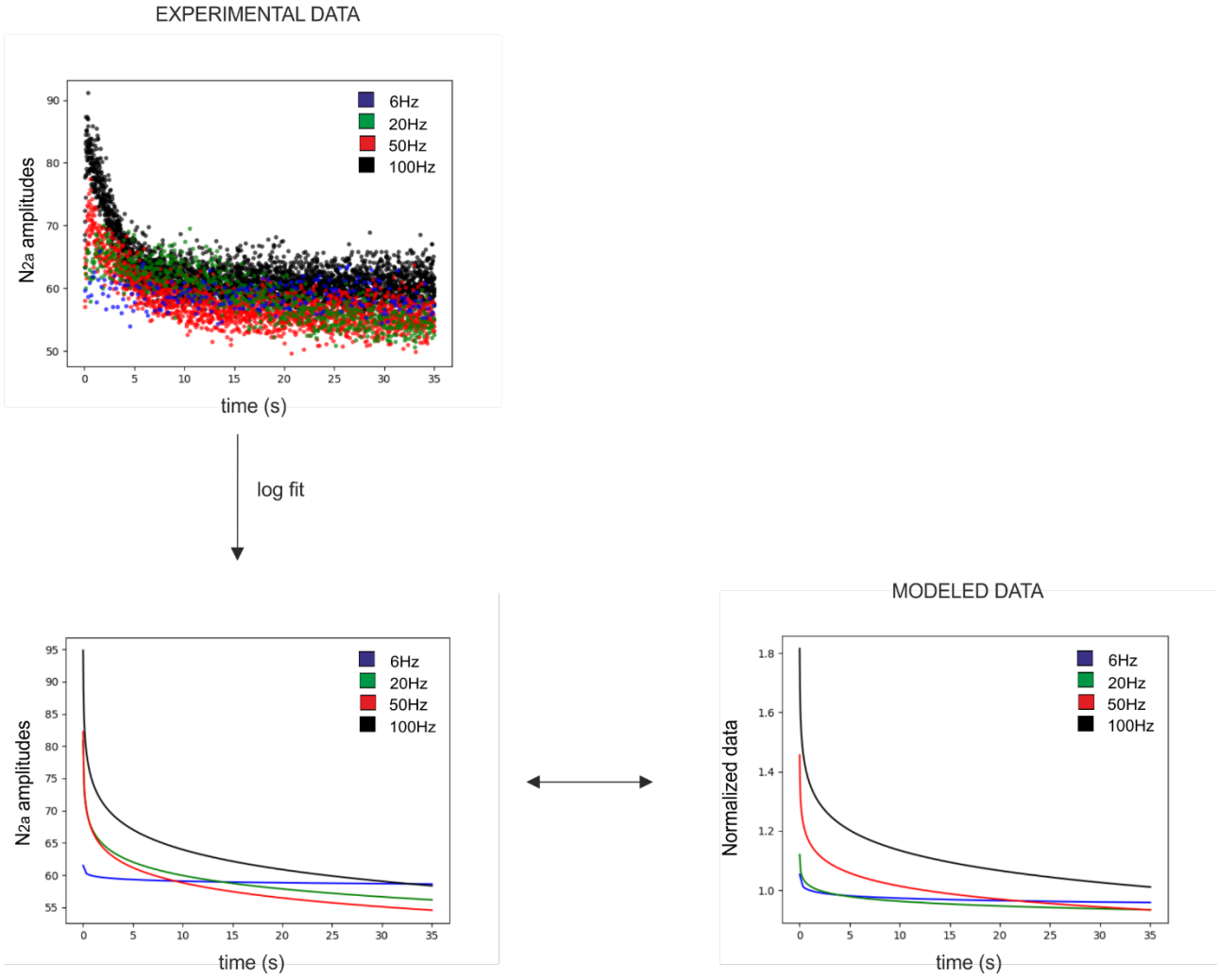

Fig. 11| The comparison between experimental and modeled data. The trend of N_{2a} peaks amplitudes obtained experimentally was logarithmic fitted in order to make a comparison between experimental and modeled data. High correlation values were found between the two trends, supporting the ability of the model to predict granule cells activity within long-lasting trains of stimulations at different input frequencies.

This is a qualitative correlation and for this reason it needs to be considered as preliminary. A detailed computational reconstruction of the LFP in the granular layer is actually under development to further validate these data. At the moment, the presence of this qualitative correlation supports the use of this model to reconstruct granular layer activation at different input frequencies. Consequently, NMDA currents extracted from the model were taken into account to investigate the role of neuronal activity in the neurovascular mechanisms of the granular layer.

5.4.6 The relationship between NMDA component of neuronal activity and vasodilation.

NMDA currents values were extracted at 2 seconds, 20 seconds, and 35 seconds of the stimulus train in order to make a comparison with the % change of capillaries dilations previously recorded (Gagliano et al., *unpublished observations*). In order to compare the trend of accumulation of NMDA

currents and vessel dilation, all values were normalized to the response at 2 seconds and their trends were reconstructed within the 35 seconds of stimulation (Fig. 12).

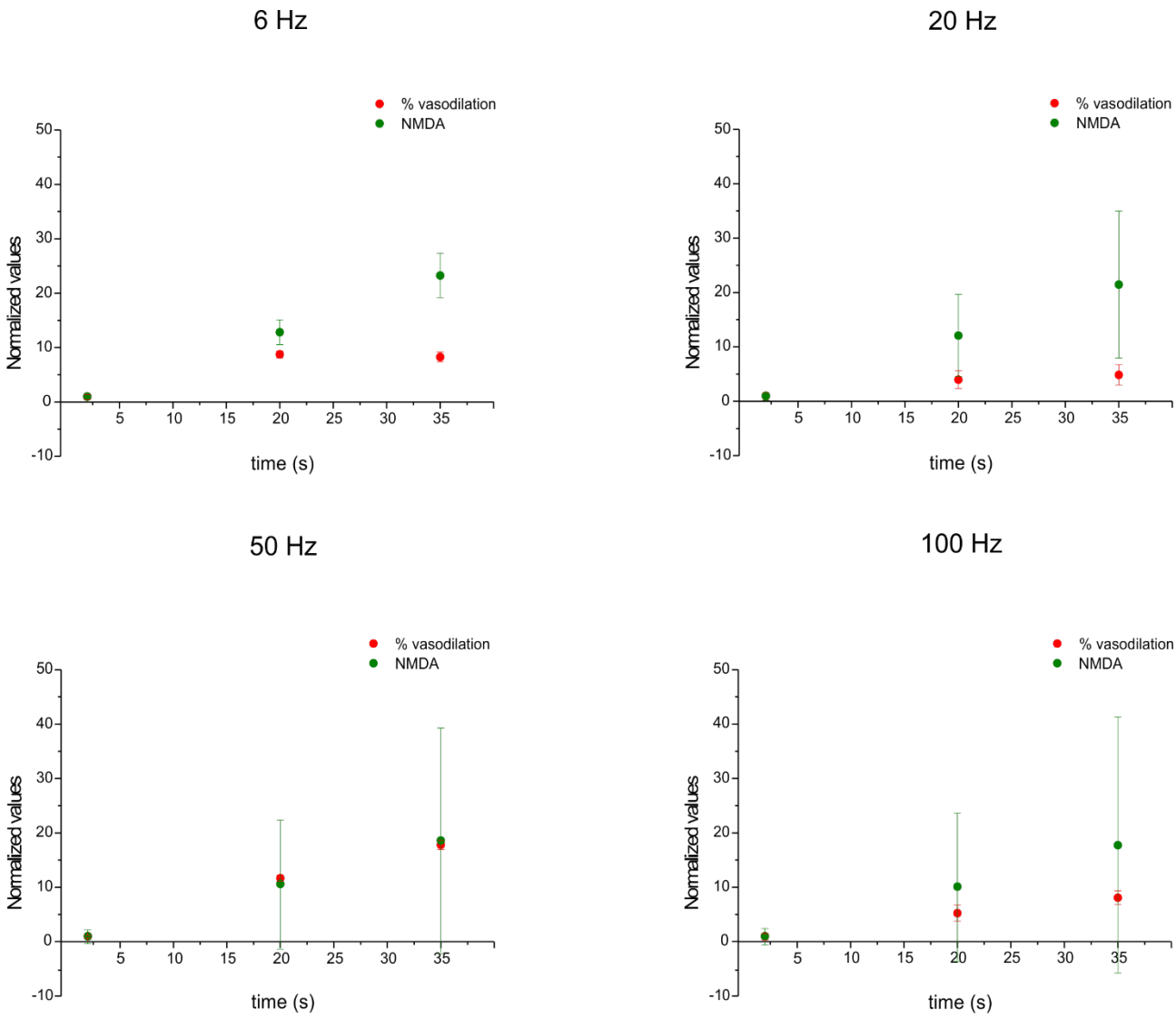

Fig. 12| The comparison between NMDA component of neuronal activity and vasodilation. NMDA currents extracted from the computational model at 2 seconds, 20 seconds, and 35 seconds of stimulation were compared with the values relative to capillaries % of dilation in the granular layer of cerebellar vermis. Though at higher input frequencies a good overlap was already present, an additional correction was applied to take into account the biochemical steps between NMDA receptors activation and vessel dilations mediated by cGMP production.

An additional correction was needed in order to completely explain the data. According to literature, NMDA currents is coupled to NO production through a linear relationship. NO increasing concentrations leads to a linear increase in cGMP production through the activation of the guanylyl cyclase on pericytes. Vasodilation is dependent on cGMP concentration levels. However, long-lasting trains of stimulation determine phosphodiesterase enzyme (PDE) activation, which curtails cGMP increase with an activation constant around 20s (Batchelor et al. 2010). Batchelor and colleagues showed that the reduction of cGMP concentration due to PDE activation is of about 25% at 20 seconds and 50% at 35 seconds of continuous stimulation. Therefore, this correction was applied to the NMDA values obtained from the model, resulting in trends which almost overlapped with capillaries

% changes (Fig. 13; at each frequency, the corrected values fell within the confidence interval of the experimental data on vasodilation). This suggests a relationship between NMDA component and vasodilation, supporting the role of NMDAR-NO pathway in determining vasodilation course over time.

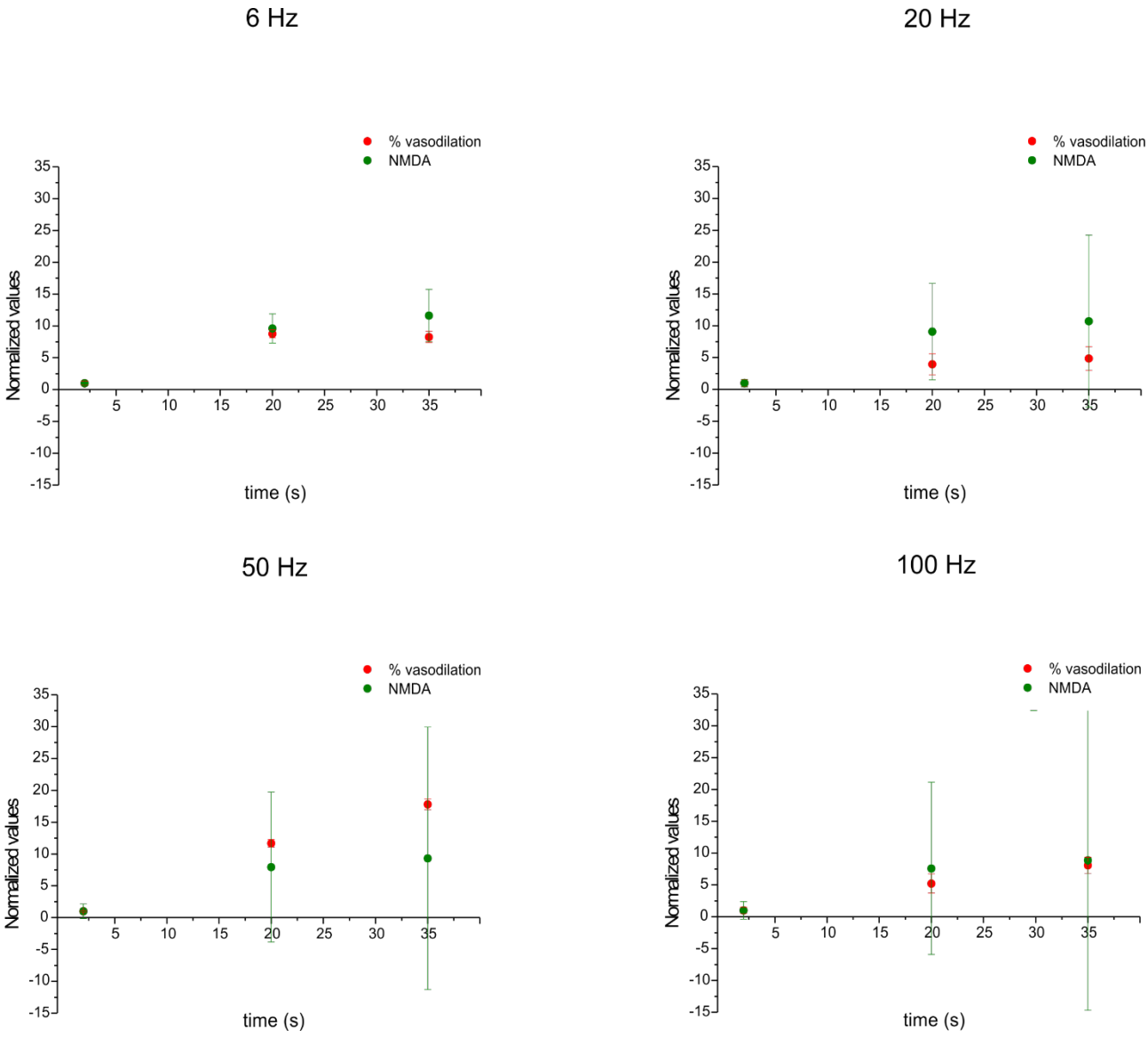

Fig. 13| The role of the NMDA component of neuronal activity in determining the time course of vasodilation. Taking into account phosphodiesterase enzyme activation during long-lasting stimulations, NMDA current values were decreased of the 25% at 20 seconds of stimulation and of 50% at 35 seconds of stimulation. This consequently led to the observation of the overlap between experimental and simulated data, supporting the role of NMDA component of neuronal activity in shaping vasodilation time course within 35 seconds of stimulation at different input frequencies.

Furthermore, a comparison between NMDA current values and capillaries vasodilation was performed at different input frequencies. Interestingly, while capillaries % change showed a non-linear frequency-dependent variation, NMDA currents tended to increase with the input frequency

(Fig. 14). Therefore, in this case the NMDA component is not sufficient to explain the non-linear trend observed for vasodilation at different input frequencies.

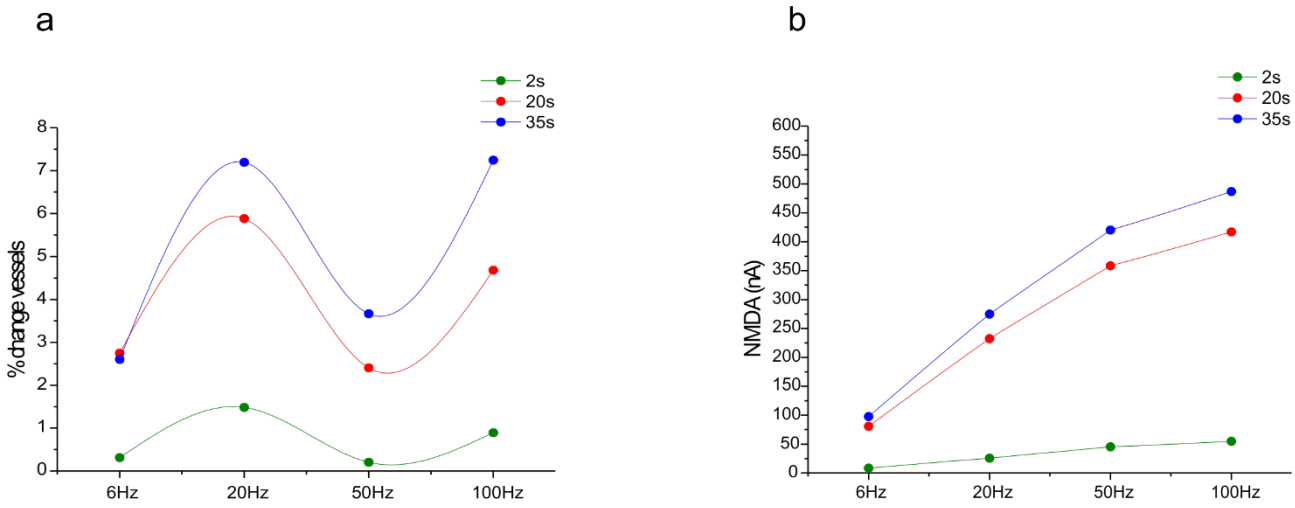

Fig. 14| The NMDA component of neuronal activity does not explain the frequency dependence of neurovascular responses. While vascular responses in the granular layer showed a non-linear trend increasing the input frequencies (a) NMDA currents extracted from the model tended to increase with the input frequencies (b).

5.5 DISCUSSION

5.5.1 Differences between cerebellar vermis and hemisphere neuronal activity.

To date, differences between cerebellar vermis and hemisphere neuronal activity have never been investigated in this detail *ex-vivo*. Recent fMRI studies have shown that the activation of cerebellar vermis and hemisphere differs during the execution of the same motor task (Alahmadi et al. 2017). Thus, in this work the response of vermis and hemisphere in acute cerebellar slices has been evaluated and then compared at different stimulation patterns. The recording of LFP responses to mossy fibers stimulation in the granular layer of vermis lobule V and hemisphere lobule VI with the HD-MEA led to the observation of a different neuronal activation to the same input. Granule cells responses to a single-pulse stimulation of mossy fibers presented different peaks amplitude values for the N_{2a} and N_{2b} components of the LFP, with a larger activation of cerebellar vermis granule cells compared to the hemisphere ones (Fig. 4). The region dependence of granule cells response was maintained also within long lasting trains of stimulation at different input patterns. In fact, the sum of granular layer total postsynaptic activity (N_{2a} and N_{2b}) showed a statistically significant difference between vermis and hemisphere, especially at higher frequencies of stimulation (Fig. 7). Taken together, these observations support that granular layer responses to mossy fibers stimulation differ in cerebellar vermis and hemisphere.

5.5.2 The frequency-dependence of neuronal activity.

Both in vermis and hemisphere N_{2a} and N_{2b} peaks amplitudes showed a different trend within long lasting trains of stimulation: while N_{2a} component tended to decrease with the increasing of stimulation frequency (Fig. 5), the N_{2b} component showed a less evident trend (Fig. 6). This difference might reflect the kinetics characterizing AMPA and NMDA glutamate receptors. Though

several factors may concur in generating the LFP signal, N_{2a} is usually informative of the AMPA component while N_{2b} of the NMDA component of the glutamatergic response (Maffei et al. 2002). The voltage-dependence of NMDA receptor activation and its slow kinetics (D'Angelo et al. 1995) provides the basis to explain the observations on the N_{2b} component. The cumulative integral of the amplitude trends of N_{2a} and N_{2b} components of the LFP in vermis and hemisphere, computed over the 35 seconds of stimulation, confirmed the same trends. While N_{2a} generally showed a trend to decrease with the increasing of the input frequency (Fig. 8), the N_{2b} peak presented different frequency dependent trends between vermis and hemisphere (Fig. 9). Overall these observations support the frequency-dependence and region-dependence of neuronal activity in the cerebellum granular layer.

5.5.3 The relationship between neuronal activity and vascular responses.

In humans, fMRI investigations showed different BOLD responses in cerebellar vermis and hemisphere during the execution of the same motor task (Alahmadi et al. 2017). In particular, the BOLD signal appeared to linearly increase with the grip force in vermis lobule V, while it presented a non-linear profile in hemisphere lobule VI. Detailed neurophysiological inferences from fMRI signals is not feasible at the moment, since the relationship between neuronal activity and blood flow changes has not been clarified yet. An investigation of capillaries motility in cerebellar vermis and hemisphere slices in response to neuronal activation has been recently conducted in our laboratory (Gagliano et al. *in preparation*, Box 2). Considering the pivotal role played by the granular layer in triggering neurovascular events in the cerebellum (Mapelli et al. 2017), the vasodilation study has been performed looking at the granular layer vascular activity in response to several mossy fibers stimulation patterns (6Hz, 20Hz, 50Hz, 100Hz), which mimic different ranges of activity (as increasing grip force) and are common with different brain states. Interestingly, capillaries dilations were statistically different between vermis and hemisphere at 50Hz and 100Hz (Fig. 2, Box 2). These results appear to be in line with the ones related to LFPs responses (Fig. 9), supporting the frequency and region dependence of neurovascular coupling in the cerebellum. According to literature, the correlation between neuronal activity and blood flow can be evaluated *ex-vivo* taking into account the sum of the evoked field potentials during the stimulation period (Mathiesen et al. 1998, Mathiesen et al. 2000). Therefore, in this study the cumulative integral of the LFP peaks during the 35 seconds of stimulation was considered, as a measure of total neuronal activity. Interestingly, N_{2b} peak seems to be the ideal candidate to explain the vessel caliber changes previously observed. N_{2b} signal presented a frequency dependent trend similar to the one observed during vascular activity investigation. This should not be surprising, since the NMDAR-NO pathway is known to regulate the NVC phenomenon in the granular layer (Mapelli et al. 2017, Box 1) and NMDAR-mediated currents are among the main contributors to the N_{2b} peak . A computational simulation of the granular layer activity was essential to clarify the mechanisms underlying the relationship between neuronal activity and vascular responses.

5.5.4 The key role of NMDAR-NO pathway in the regulation of NVC in the granular layer vermis.

The correlation found between simulated values and experimental recordings (Fig.11) enabled the use of NMDA currents extracted from the granular layer model to deepen the investigation of neurovascular mechanisms in the cerebellum. NMDA currents appeared to explain the experimental data relative to the time course of capillaries vasodilation, at all the input frequencies tested. Concerning the biochemical pathway, it is known that NMDA receptors activation leads to the

increase of nNOS activity and the consequent production of NO. NO acts as a strong vasodilator, increasing the levels of cGMP through the activation of sGC. However, long-lasting stimulations determine phosphodiesterase enzyme (PDE) activation, which causes a decrease in cGMP concentrations. Therefore, NMDA current values obtained from the model were corrected in order to account for the non-linearity added to the process by PDE activation. This determined an almost overlap between simulated and experimental data (Fig.13), supporting the key role of NMDAR-NO pathway in regulating NVC during long-lasting trains of stimulation. However, NMDA component of neuronal activity was not sufficient to explain the non-linearity observed in capillaries vasodilation at different input frequencies (Fig.14). This result suggests that additional mechanisms are involved in causing a frequency-dependence of vessel dilation. A plausible explanation could involve the balance between vasodilation and vasoconstriction pathways, already described as active in the cerebellar granular layer (Mapelli et al., 2017). In the cerebellar granular layer, vasoconstriction is mainly mediated by 20-HETE production (Mapelli et al., 2017). 20-HETE most likely derives from mGluRs activation on glial cells and its synthesis is blocked by NO (Attwell et al.2010). It is known that mGluRs needs glutamate build-up at the synapse or spillover from the synaptic cleft to be activated. It is therefore feasible that, at low frequencies of stimulation (6-20Hz), the amount of 20-HETE produced is negligible, compared to NO production through NMDAR activation. At 6 and 20Hz, vessel dilation is probably dependent on the amount of NO production (and therefore on the amount of NMDAR activation). At 50Hz, mGluRs are likely to be activated in a significant way, leading to a certain production of 20-HETE and the consequent competition between vasodilation and vasoconstriction, accounting for the non-linearity experimentally observed (vasodilation at 50Hz is smaller compared to that at 20Hz). Finally, high input frequencies (100Hz) should determine the overcome of NMDARs-NO system over vasoconstriction mechanisms (the amount of NO produced is sufficient to completely block 20-HETE synthesis). Experimental data support a difference between vermis and hemisphere non-linear frequency dependent behavior (Gagliano et al., *unpublished observations*). Therefore, a new set of NMDA currents values need to be extracted from the computational model of the granular layer in order to investigate this difference. The computational model needs to be adjusted on hemisphere neuronal activity and validated with experimental data to repeat the analysis reported here for the cerebellar vermis. These procedures are currently ongoing.

5.6 CONCLUSION

The evaluation of neuronal activity performed with the HD-MEA led to the observation of different neuronal responses in cerebellar vermis and hemisphere. This evidence supports for the first time a region dependence of neuronal activity in the cerebellum. This result is particularly important, considering the different connections shown by cerebellar vermis and hemisphere with other brain areas (Stoodley and Schmahmann 2009). A different neuronal activation observed *ex-vivo* suggests a possible different way to process incoming inputs exerted by neuronal population of cerebellar vermis and hemisphere. Differences detected between N_{2a} and N_{2b} LFP peaks in cerebellar vermis and hemisphere could be determined by a different neuronal density or a different network organization optimized to process inputs coming from motor and non-motor areas. Interestingly, cerebellar vermis and hemisphere additionally showed a frequency dependent activation. The non-linear trend observed for N_{2b} peak guided the extraction of NMDA currents from a computational model of granular layer activity at different input frequencies. The time course of capillaries dilations can be explained by the NMDA-NO pathway, while other mechanisms are most likely involved in determining non-linear capillaries changes at different input frequencies. Taken together, these results show a new way to

investigate NVC mechanisms *ex-vivo*. Computational model adjustments are actually under development in order to investigate the same pathways in the cerebellar hemisphere. At the end, these results will represent a novel detailed description of the NVC mechanisms and their frequency and region dependence in the cerebellum, ultimately providing for the first time a neurophysiological substrate to the non-linearity observed during fMRI recordings in humans.

6. General discussion and conclusions.

Due to its highly ordered organization, the complexity of cerebellar network processing has been underestimated for years. The functional aspects of this well-organized structure have been evaluated almost only in a motor control perspective, highlighting the essential role of cerebellum in motor learning and coordination (D'Angelo et al. 2011). Moreover, a simplified description of circuit dynamics has been accepted, believing that anatomical considerations would be sufficient to understand the underlying network activity. Recently though, an increased amount of studies is suggesting a cerebellar involvement in higher cognitive processes (D'Angelo 2019) and experimental data are demonstrating that the cerebellum operates in a more complex manner than predicted (D'Angelo 2018). Therefore, a thorough investigation of cerebellar network functioning and its level of complexity is actually needed. The main aim of this thesis has been to gain a deeper insight into cerebellar network input processing. A comprehensive study of cerebellar cortex responsiveness at different input frequencies is still missing and deserves experimental assessment. Exploring the neuronal underpinnings of cerebellar frequency dependent processing would finally lead to a better understanding of the cerebellar role in complex brain states related processes.

First, the attention has been focused on the whole network activation at different frequency ranges. Different ranges of activity, likely mimicking different brain states, were obtained by stimulating mossy fibers at different frequencies (5 pulses at 6Hz, 20Hz, 50Hz and 100Hz). Mossy fibers convey information to the cerebellar cortex from other brain areas and these specific frequencies were chosen in order to simulate *ex-vivo* the typical frequency bands associated to cortical activity. Moreover, the whole circuit activation was reconstructed recording data from both sagittal and coronal slices. Granular layer activity was evaluated analyzing N_{2a} and N_{2b} peaks of the LFP evoked by mossy fibers stimulation. Both N_{2a} and N_{2b} peaks showed a frequency-dependent trend, with specific spatial organizations of Short-Term Plasticity in the granular layer. In particular, N_{2a} peak mainly presented short-term depression (STD), particularly marked in the medial granular layer. This spatial organization became more evident increasing the input frequency and was confirmed both in sagittal and coronal slices, though it might simply reflect the degree of activation and distribution of mossy fibers in the activated lobule. N_{2a} peak trend can be explained taking into account its correlation with AMPA receptors activation (Mapelli and D'Angelo 2007) and the desensitization typical for AMPA receptors during repetitive stimulation (Nieus et al. 2006). On the other hand, N_{2b} frequency-dependence appeared more difficult to explain. This component of the LFP response presented a significant short-term potentiation (STP) only at higher frequencies of stimulation, and a different number of recording channels detected a significant STP between sagittal and coronal slices. In coronal slices the percentage of channels detecting a significant response was higher. Moreover, different areas of the granular layer showed a more pronounced STP changing the input frequencies, especially in sagittal slices. All these evidences suggest a possible non-linear frequency dependence of inhibitory mechanisms, involving Golgi cells and the different distribution of their axonal plexus in the sagittal and coronal planes. However, a pharmacological approach would be needed to demonstrate this hypothesis. Beyond granular layer analysis, the attention has been focused on Purkinje cells activity and the frequency dependence of Purkinje cells responses. An extremely large number of units was analyzed both in sagittal and coronal slices (858 and 1059, respectively). Thanks to the unprecedented high spatial resolution of the HD-MEA, it has been possible to study the activity coming from all these units assigning to each cell a precise location inside the cerebellar lobule. Interestingly, in coronal slices a zebrin-like distribution patterns of the basal Mean Firing Rate (MFR) of the units was observed. Mossy fibers stimulation elicited an increase or a decrease of Purkinje cells

MFR, evident as peaks and pauses in the Peri-Stimulus Time-Histograms (PSTHs). In sagittal slices, peaks were mostly observed as Purkinje cells responses at different input frequencies. This was probably due to the cutting of parallel fibers in sagittal slices, leaving the granule cells ascending axons pathway as the main responsible of Purkinje cells activation. On the other hand, in coronal slices pauses characterized the beginning of the stimulation and then a higher number of peaks was detected at the end of the bursts. This observation might be explained taking into account the possible frequency-dependence characterizing molecular layer interneurons activity. These data allowed the reconstruction of a map representing the spatial distribution of granular and Purkinje cells layers activation. This spatio-temporal description of the spread of activity in the cerebellar network at different input frequencies opened a new perspective in the development of computational models able to take into account the frequency dependence of cerebellar activity.

In the second part of the thesis the attention was focused on the neuronal correlates of neurovascular coupling in the cerebellum. A frequency and region dependence has been recently demonstrated for vascular responses in the cerebellar granular layer (Gagliano et al. *in preparation*). In particular, the investigation of capillaries motility in the granular layer of cerebellar vermis lobule V and hemisphere lobule VI was driven by the observation of particular non-linear responses in fMRI studies in humans during the execution of the same motor task (Alahmadi et al. 2017). Since making neurophysiological inferences from fMRI studies is not feasible, the question to be addressed *ex-vivo* was cerebellar ability to generate different non-linear and region dependent vascular responses independently from cortical inputs. The investigations conducted on capillaries motility in cerebellar vermis and hemisphere sagittal slices led to the observation of a frequency and region dependent vascular activity. However, the neuronal basis underlying these differences remained unknown. Therefore, HD-MEA recordings of granular layer activity were performed both in cerebellar vermis and hemisphere slices in the same condition of stimulation used for capillaries motility quantifications (35 seconds of stimulation at 6Hz, 20Hz, 50Hz, 100Hz). The analysis of the main peaks of the LFP response, N_{2a} and N_{2b}, led to the observation of a different neuronal activation to the same input. Granule cells responses to a single-pulse stimulation of mossy fibers presented different peaks amplitude values for the N_{2a} and N_{2b} components of the LFP, with a larger activation of cerebellar vermis granule cells compared to the hemisphere ones. The region dependence of neuronal responses was maintained within long lasting trains of stimulation at different frequencies. N_{2a} and N_{2b} peaks amplitudes showed a different trend within long lasting trains of stimulations, probably reflecting the kinetics characterizing AMPA and NMDA glutamate receptors. While the N_{2a} component tended to decrease with the increasing of stimulation frequency, the N_{2b} component showed a less clear trend. Moreover, the computation of the cumulative integral as a measure of total neuronal activity to be correlated with vascular responses (Mathiesen et al. 1998, Mathiesen et al. 2000), led to the observation of a non-linear frequency dependent trend of N_{2b} component, in some way resembling that observed during vascular activity investigation. Therefore, N_{2b} peak seemed to be the ideal candidate to explain vessel caliber changes, and this evidence was additionally supported by its well-known correlation with NMDA receptors activation (Mapelli and D'Angelo 2007). Taking into account the pivotal role played by NMDAR-NO pathway in triggering neurovascular responses in the granular layer of the cerebellum (Mapelli et al. 2017), a computational reconstruction of granular layer activity in cerebellar vermis was performed (Casali et al. 2020), extracting NMDA currents during long-lasting trains of stimulations at different frequencies. Importantly, a correlation was found between NMDA currents and vasodilation time course, but NMDA currents were not sufficient to explain the frequency dependence of vascular responses. This is likely to be due to a frequency-dependent activity of vasoconstriction pathways counteracting NO activity in the granular layer. In

the near future, the computational model will be modified in order to simulate neuronal activity in the cerebellar hemisphere and perform the same analysis reported above for the vermis. Taken together, the findings of this project provided new clues for the investigation of neurovascular phenomena unraveling a frequency and region dependence.

In conclusion, the investigation of cerebellar cortex input processing with the HD-MEA yielded a huge amount of complex data. Differences were found in the input processing of cerebellar network granular and molecular layers in sagittal and coronal slices: different types of STP presenting a precise frequency-dependent spatial organization characterized granular layer activity, while the involvement of parallel fibers-molecular layer interneurons-Purkinje cells pathways shaped Purkinje cells responses. On the other hand, a region and frequency-dependence of neuronal activity was confirmed comparing granule cells responses during long-lasting trains of stimulations in cerebellar vermis and hemisphere. Therefore, these data point out an extremely high level of complexity characterizing cerebellar network functioning, opening a new perspective in the study of its frequency dependence, and supporting its role beyond a simple motor controller.

7. Future perspective.

The considerable amount of data provided by this work can be suitable to be used to calculate the Perturbational Complexity Index (PCI) for cerebellar cortical processing (Appendix A). This type of index has been recently introduced in clinical practice aiming to evaluate different levels of consciousness in patients. Practically, the PCI algorithm measures the complexity of the electroencephalographic (EEG) response following a cortical perturbation delivered using transcranical magnetic stimulation (TMS). The resulting value provides a tool to discriminate consciousness levels in healthy humans as well as in brain-injured patients (Storm et al. 2017). In order to study the neuronal bases of consciousness levels, an in vitro adapted version of the PCI called slice PCI (sPCI) has been recently developed and applied to cortical slices (D'Andola et al. 2018). Interestingly, this adapted version of the PCI showed to be sensitive to different activity states in slices. In this work performed on cerebellar slices the perturbation has been provided through the electrical stimulation of mossy fibers. Therefore, sPCI could be used to explore the cerebellar level of complexity and its modulation during different ranges of activity. Hopefully, this analysis in future would be able to shed new light on the role of the cerebellum in cognitive functions, providing the first clues to speculate on its possible involvement in consciousness.

Appendix A

The Perturbational Complexity Index (PCI) as a measure of network complexity.

Consciousness is a composite and multi-faced phenomenon that everyone experiences but no one is completely able to explain. For years, consciousness investigations have been conducted through philosophical speculations, and understanding consciousness has been assumed to be out of the reach of science. However, actually several invasive and noninvasive techniques, from electrophysiology to brain imaging, have been devoted to disentangle consciousness mechanisms, and aroused a great

interest in the so called “scientific study of consciousness”. This type of study is forced to face the “hard problem “of consciousness: explaining how a matter such the human brain can give rise to a conscious experience (Miller 2007, Tononi and Koch 2015). Nevertheless, all the investigations trying to infer the neurological underpinnings of conscious experience starting from the observation of brain activity, found this problem not only hard, but almost impossible to solve. Thus, consciousness understanding has been addressed in a new way. An “easy problem” has been outlined: the search of the neuronal correlates of consciousness (NCC). NCC are the *minimal neuronal mechanisms sufficient for any one specific conscious percept* (Tononi and Koch 2008). The assessment of NCC is conducted examining the correlation of brain activity changes with different consciousness conditions, and is actually the most efficient tool available for neuroscience to deepen activity patterns underlying consciousness. NCC appear to be located in the cortico-thalamic system, while other brain areas do not seem to contribute to conscious experience (Tononi 2005, Tononi and Koch 2008). A complete understanding of the neuronal substrate of consciousness is still missing, and a new way to approach this need has been proposed over the last years by the Integrated Information Theory (IIT) (Tononi and Edelman 1998, Tononi et al. 2016). The IIT establishes some essential properties, or axioms, of conscious experience rather than starting from a group of neurons and arguing how they could contribute to consciousness. This kind of strategy emphasizes two main properties of consciousness: conscious experience is integrated, because it cannot be subdivided into a subset of disjoint components, and at the same time is highly differentiated, because a significant number of different conscious states can be experienced within a short time (Tononi et al. 2016). Thus, neuronal processes both integrated and differentiated contribute to conscious experience. A measure of the level of information integration (called Φ) could be used to establish whether a physical system takes part in the generation of consciousness. In a system, different groups of elements called complexes can be identified, each one with a corresponding value of Φ. Higher Φ values are associated to an higher ability of the complex to give rise to a conscious experience (Tononi 2005).

A parameter inspired by the main concepts underlying the IIT and needed for the evaluation of Φ is the Perturbational Complexity Index (PCI) (Casali et al. 2013). The PCI has been recently introduced in clinical practice as a tool to measure the loss and recovery of consciousness (Tononi et al. 2016, Storm et al. 2017). Practically, PCI measures the level of information integration of the cortico-thalamic system evaluating the complexity of the electroencephalographic (EEG) response to a direct perturbation with transcranical magnetic stimulation (TMS). To simplify, the EEG signal is analyzed with a nonparametric bootstrap-base statistics in order to extract a matrix containing the significant activations following the perturbation at different time samples. Then a Lempel-Ziv complexity algorithm (Lempel et al. 1976) scans the matrix and estimates the information content. The Lempel-Ziv measure is normalized by the source entropy obtaining the final PCI. In this way, the complexity value is minimally dependent on the amount of significant activations and maximally dependent on the spatio-temporal activations patterns present in the data. Interestingly, this parameter has been demonstrated to be representative of the level of consciousness in patients: the PCI is high only if brain responses are both integrated and differentiated, leading to an high complexity value. A lower PCI has been reported in cases of reduced connectivity among cortical areas (loss of integration) or in the presence of a stereotypical hypersynchronous activation (loss of differentiation), because in both these cases the perturbation response is not transmitted among interconnected areas and does not give rise to complex spatiotemporal patterns.

The clinical assessment of the PCI has been followed by micro-scale studies aiming to shed light on the neuronal mechanisms underlying the loss and recovery of complexity (Storm et al. 2017). In a

recent investigation (D'Andola et al. 2018), thalamo-cortical slices of rodent brains have been chosen as a simplified model, and an adapted version of the PCI, called slice PCI (sPCI) has been developed to measure network complexity. The sPCI has been computed directly from signals recorded *ex-vivo*, such as spikes and local field potentials. Interestingly, the sPCI proved to be sensitive to electrical and pharmacological perturbations of the system used to mimic different states of consciousness. These results might provide a link between macroscale measurements and microscale neuronal events.

Both the *in-vivo* (Casali et al. 2013) and *ex-vivo* (D'Andola et al. 2018) evaluations of complexity support the pivotal role played by the cortico-thalamic system in consciousness generation, excluding a possible cerebellar involvement. According to the IIT, the contribution of cerebellum to conscious experience should be minimal, due to its modular organization. Actually, this theory does not take into account inter-modular cerebellar connections, but considers cerebellar micro-zones as largely independent, without possible interactions between distant patches (Tononi 2005). Therefore, in striking contrast to the cortico-thalamic system and its high Φ value (Fig. 1.12A), cerebellar connections are not considered as an high Φ complex, but rather as many small complexes each presenting a low Φ value (Fig. 1.12B).

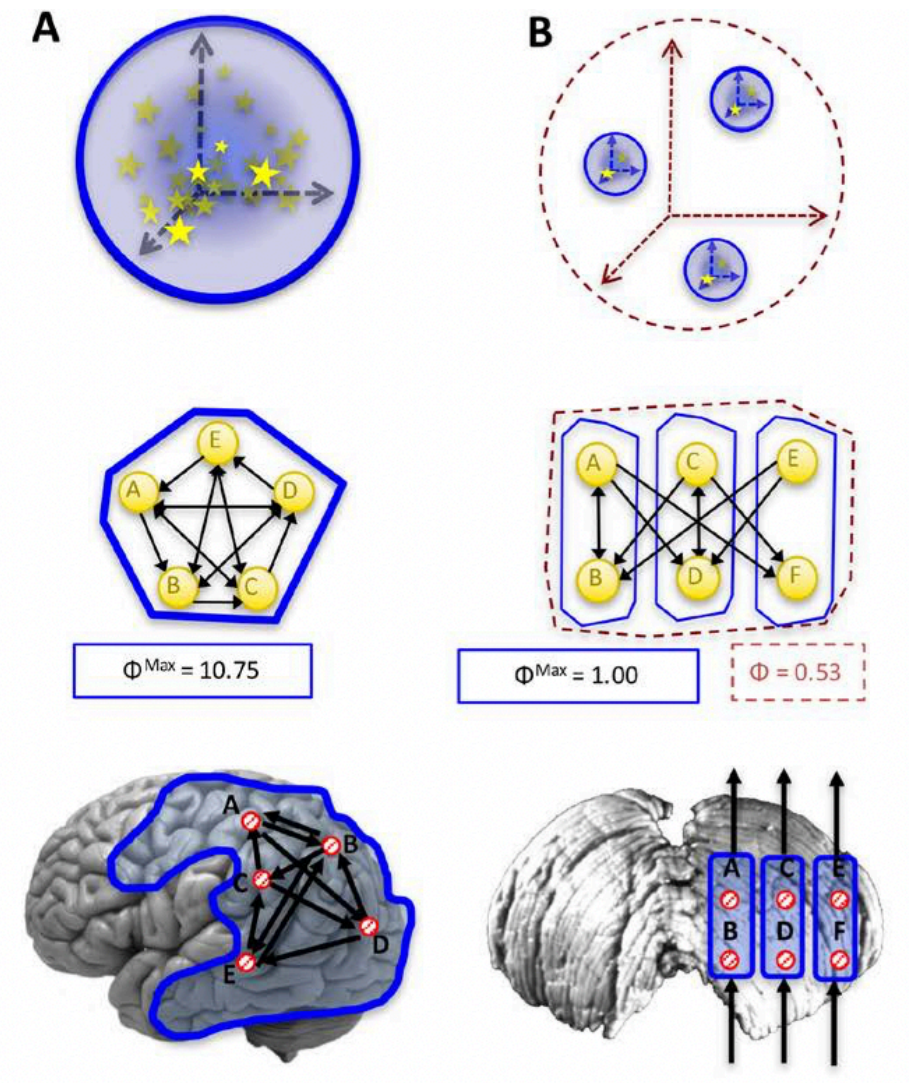

Fig. 1.12| Information integration for different neural architectures (Tononi et al. 2016). **A)** Incoming and outgoing connections are heterogeneously arranged in the cortical network and elements are highly connected to each other. This kind of organization maximizes functional integration and differentiation leading to an high Φ value. **B)** Cerebellar modular organization according to the IIT. The elements belonging to a cerebellar module appear to be connected to each other, but each module is considered as independent, presenting input and outputs different from other modules. This arrangement results in several small complexes with an overall low Φ value.

Nevertheless, a pure parallel information processing performed by cerebellar modules is unlikely (Apps et al. 2018). Besides the classical projection of individual modules to different targets, modular cooperation has been recently demonstrated observing that information coming from different modules can converge to the same brain area. Moreover, modular information processing needs to be considered as extremely dynamic, and different modules can operate independently or interact with others achieving a coordinated Purkinje cells output (Valera et al. 2016).

The cerebellum seems not to behave as a static and single operational machine, as considered in the IIT. Therefore, the estimation of the PCI value for the cerebellar network appears to be particularly interesting. Since cerebellar activity in humans cannot be reliably assessed with non-invasive measures, an *ex-vivo* evaluation of complexity needs to be taken into account, using the sPCI as a new tool to explore cerebellar network complexity. The computation of sPCI would provide a deeper understanding of cerebellar input processing and shed new light on its possible contribution to conscious experience.

References

Adamaszek, M., F. D'Agata, R. Ferrucci, C. Habas, S. Keulen, K. C. Kirkby, M. Leggio, P. Mariën, M. Molinari, E. Moulton, L. Orsi, F. Van Overwalle, C. Papadelis, A. Priori, B. Sacchetti, D. J. Schutter, C. Styliadis & J. Verhoeven (2017) Consensus Paper: Cerebellum and Emotion. *Cerebellum,* 16**,** 552-576.

Alahmadi, A. A., M. Pardini, R. S. Samson, K. J. Friston, A. T. Toosy, E. D'Angelo & C. A. Gandini Wheeler-Kingshott (2017) Cerebellar lobules and dentate nuclei mirror cortical force-related-BOLD responses: Beyond all (linear) expectations. *Hum Brain Mapp,* 38**,** 2566-2579.

Apps, R., R. Hawkes, S. Aoki, F. Bengtsson, A. M. Brown, G. Chen, T. J. Ebner, P. Isope, H. Jörntell, E. P. Lackey, C. Lawrenson, B. Lumb, M. Schonewille, R. V. Sillitoe, L. Spaeth, I. Sugihara, A. Valera, J. Voogd, D. R. Wylie & T. J. H. Ruigrok (2018) Cerebellar Modules and Their Role as Operational Cerebellar Processing Units: A Consensus paper [corrected]. *Cerebellum,* 17**,** 654-682.

Arleo, A., T. Nieus, M. Bezzi, A. D'Errico, E. D'Angelo & O. J. Coenen (2010) How synaptic release probability shapes neuronal transmission: information-theoretic analysis in a cerebellar granule cell. *Neural Comput,* 22**,** 2031-58.

Atluri, P. P. & W. G. Regehr (1996) Determinants of the time course of facilitation at the granule cell to Purkinje cell synapse. *J Neurosci,* 16**,** 5661-71.

Attwell, D., A. M. Buchan, S. Charpak, M. Lauritzen, B. A. Macvicar & E. A. Newman (2010) Glial and neuronal control of brain blood flow. *Nature,* 468**,** 232-43.

Bao, J., K. Reim & T. Sakaba (2010) Target-dependent feedforward inhibition mediated by short-term synaptic plasticity in the cerebellum. *J Neurosci,* 30**,** 8171-9.

Batchelor, A. M., K. Bartus, C. Reynell, S. Constantinou, E. J. Halvey, K. F. Held, W. R. Dostmann, J. Vernon & J. Garthwaite (2010) Exquisite sensitivity to subsecond, picomolar nitric oxide transients conferred on cells by guanylyl cyclase-coupled receptors. *Proc Natl Acad Sci U S A,* 107**,** 22060-5.

Batchelor, A. M. & J. Garthwaite (1997) Frequency detection and temporally dispersed synaptic signal association through a metabotropic glutamate receptor pathway. *Nature,* 385**,** 74-7.

Beierlein, M., D. Fioravante & W. G. Regehr (2007) Differential expression of posttetanic potentiation and retrograde signaling mediate target-dependent short-term synaptic plasticity. *Neuron,* 54**,** 949-59.

Beierlein, M. & W. G. Regehr (2006) Local interneurons regulate synaptic strength by retrograde release of endocannabinoids. *J Neurosci,* 26**,** 9935-43.

Bower, J. M. (2010) Model-founded explorations of the roles of molecular layer inhibition in regulating purkinje cell responses in cerebellar cortex: more trouble for the beam hypothesis. *Front Cell Neurosci,* 4.

Brenowitz, S. D. & W. G. Regehr (2005) Associative short-term synaptic plasticity mediated by endocannabinoids. *Neuron,* 45**,** 419-31.

Brown, S. P., S. D. Brenowitz & W. G. Regehr (2003) Brief presynaptic bursts evoke synapse-specific retrograde inhibition mediated by endogenous cannabinoids. *Nat Neurosci,* 6**,** 1048-57.

Buzsáki, G., C. A. Anastassiou & C. Koch (2012) The origin of extracellular fields and currents--EEG, ECoG, LFP and spikes. *Nat Rev Neurosci,* 13**,** 407-20.

Carter, A. G. & W. G. Regehr (2000) Prolonged synaptic currents and glutamate spillover at the parallel fiber to stellate cell synapse. *J Neurosci,* 20**,** 4423-34.

Casali, A. G., O. Gosseries, M. Rosanova, M. Boly, S. Sarasso, K. R. Casali, S. Casarotto, M. A. Bruno, S. Laureys, G. Tononi & M. Massimini (2013) A theoretically based index of consciousness independent of sensory processing and behavior. *Sci Transl Med,* 5**,** 198ra105.

Casali, S., M. Tognolina, E. D'Angelo (2020) Cellular resolution mapping uncovers spatial adaptive filtering at the cerebellum input stage. bioRxiv 2020.03.14.991794

Casiraghi, L., A. A. S. Alahmadi, A. Monteverdi, F. Palesi, G. Castellazzi, G. Savini, K. Friston, C. A. M. Gandini Wheeler-Kingshott & E. D'Angelo (2019) I See Your Effort: Force-Related BOLD Effects in an Extended Action Execution-Observation Network Involving the Cerebellum. *Cereb Cortex,* 29**,** 1351-1368.

Cerminara, N. L., E. J. Lang, R. V. Sillitoe & R. Apps (2015) Redefining the cerebellar cortex as an assembly of non-uniform Purkinje cell microcircuits. *Nat Rev Neurosci,* 16**,** 79-93.

Chabrol, F. P., A. Arenz, M. T. Wiechert, T. W. Margrie & D. A. DiGregorio (2015) Synaptic diversity enables temporal coding of coincident multisensory inputs in single neurons. *Nat Neurosci,* 18**,** 718-27.

Chadderton, P., T. W. Margrie & M. Häusser (2004) Integration of quanta in cerebellar granule cells during sensory processing. *Nature,* 428**,** 856-60.

Courtemanche, R., P. Chabaud & Y. Lamarre (2009) Synchronization in primate cerebellar granule cell layer local field potentials: basic anisotropy and dynamic changes during active expectancy. *Front Cell Neurosci,* 3**,** 6.

Courtemanche, R. & Y. Lamarre (2005) Local field potential oscillations in primate cerebellar cortex: synchronization with cerebral cortex during active and passive expectancy. *J Neurophysiol,* 93**,** 2039-52.

Courtemanche, R., J. C. Robinson & D. I. Aponte (2013) Linking oscillations in cerebellar circuits. *Front Neural Circuits,* 7**,** 125.

Cramer, S. C., R. M. Weisskoff, J. D. Schaechter, G. Nelles, M. Foley, S. P. Finklestein & B. R. Rosen (2002) Motor cortex activation is related to force of squeezing. *Hum Brain Mapp,* 16**,** 197-205.

D'Andola, M., B. Rebollo, A. G. Casali, J. F. Weinert, A. Pigorini, R. Villa, M. Massimini & M. V. Sanchez-Vives (2018) Bistability, Causality, and Complexity in Cortical Networks: An In Vitro Perturbational Study. *Cereb Cortex,* 28**,** 2233-2242.

D'Angelo, E. (2008) The critical role of Golgi cells in regulating spatio-temporal integration and plasticity at the cerebellum input stage. *Front Neurosci,* 2**,** 35-46.

--- (2011) Neural circuits of the cerebellum: hypothesis for function. *J Integr Neurosci,* 10**,** 317-52.

--- (2014) The organization of plasticity in the cerebellar cortex: from synapses to control. *Prog Brain Res,* 210**,** 31-58.

--- (2018) Physiology of the cerebellum. *Handb Clin Neurol,* 154**,** 85-108.

--- (2019) The cerebellum gets social. *Science,* 363**,** 229.

D'Angelo, E. & S. Casali (2012) Seeking a unified framework for cerebellar function and dysfunction: from circuit operations to cognition. *Front Neural Circuits,* 6**,** 116.

D'Angelo, E., G. De Filippi, P. Rossi & V. Taglietti (1995) Synaptic excitation of individual rat cerebellar granule cells in situ: evidence for the role of NMDA receptors. *J Physiol,* 484 (Pt 2)**,** 397-413.

D'Angelo, E. & C. I. De Zeeuw (2009) Timing and plasticity in the cerebellum: focus on the granular layer. *Trends Neurosci,* 32**,** 30-40.

D'Angelo, E., S. K. Koekkoek, P. Lombardo, S. Solinas, E. Ros, J. Garrido, M. Schonewille & C. I. De Zeeuw (2009) Timing in the cerebellum: oscillations and resonance in the granular layer. *Neuroscience,* 162**,** 805-15.

D'Angelo, E., L. Mapelli, C. Casellato, J. A. Garrido, N. Luque, J. Monaco, F. Prestori, A. Pedrocchi & E. Ros (2016) Distributed Circuit Plasticity: New Clues for the Cerebellar Mechanisms of Learning. *Cerebellum,* 15**,** 139-51.

D'Angelo, E., P. Mazzarello, F. Prestori, J. Mapelli, S. Solinas, P. Lombardo, E. Cesana, D. Gandolfi & L. Congi (2011) The cerebellar network: from structure to function and dynamics. *Brain Res Rev,* 66**,** 5-15.

D'Angelo, E., T. Nieus, A. Maffei, S. Armano, P. Rossi, V. Taglietti, A. Fontana & G. Naldi (2001) Theta-frequency bursting and resonance in cerebellar granule cells: experimental evidence and modeling of a slow k+-dependent mechanism. *J Neurosci,* 21**,** 759-70.

D'Angelo, E. & P. Rossi (1998) Integrated regulation of signal coding and plasticity by NMDA receptors at a central synapse. *Neural Plast,* 6**,** 8-16.

D'Angelo, E., S. Solinas, J. Mapelli, D. Gandolfi, L. Mapelli & F. Prestori (2013) The cerebellar Golgi cell and spatiotemporal organization of granular layer activity. *Front Neural Circuits,* 7**,** 93.

D'Errico, A., F. Prestori & E. D'Angelo (2009) Differential induction of bidirectional long-term changes in neurotransmitter release by frequency-coded patterns at the cerebellar input. *J Physiol,* 587**,** 5843-57.

de Solages, C., G. Szapiro, N. Brunel, V. Hakim, P. Isope, P. Buisseret, C. Rousseau, B. Barbour & C. Léna (2008) High-frequency organization and synchrony of activity in the purkinje cell layer of the cerebellum. *Neuron,* 58**,** 775-88.

De Zeeuw, C. I., F. E. Hoebeek, L. W. Bosman, M. Schonewille, L. Witter & S. K. Koekkoek (2011) Spatiotemporal firing patterns in the cerebellum. *Nat Rev Neurosci,* 12**,** 327-44.

De Zeeuw, C. I., F. E. Hoebeek & M. Schonewille (2008) Causes and consequences of oscillations in the cerebellar cortex. *Neuron,* 58**,** 655-8.

DiGregorio, D. A., Z. Nusser & R. A. Silver (2002) Spillover of glutamate onto synaptic AMPA receptors enhances fast transmission at a cerebellar synapse. *Neuron,* 35**,** 521-33.

DiGregorio, D. A., J. S. Rothman, T. A. Nielsen & R. A. Silver (2007) Desensitization properties of AMPA receptors at the cerebellar mossy fiber granule cell synapse. *J Neurosci,* 27**,** 8344-57.

Dittman, J. S., A. C. Kreitzer & W. G. Regehr (2000) Interplay between facilitation, depression, and residual calcium at three presynaptic terminals. *J Neurosci,* 20**,** 1374-85.

Dittman, J. S. & W. G. Regehr (1996) Contributions of calcium-dependent and calcium-independent mechanisms to presynaptic inhibition at a cerebellar synapse. *J Neurosci,* 16**,** 1623-33.

--- (1997) Mechanism and kinetics of heterosynaptic depression at a cerebellar synapse. *J Neurosci,* 17**,** 9048-59.

--- (1998) Calcium dependence and recovery kinetics of presynaptic depression at the climbing fiber to Purkinje cell synapse. *J Neurosci,* 18**,** 6147-62.

Diwakar, S., P. Lombardo, S. Solinas, G. Naldi & E. D'Angelo (2011) Local field potential modeling predicts dense activation in cerebellar granule cells clusters under LTP and LTD control. *PLoS One,* 6**,** e21928.

Dorgans, K., V. Demais, Y. Bailly, B. Poulain, P. Isope & F. Doussau (2019) Short-term plasticity at cerebellar granule cell to molecular layer interneuron synapses expands information processing. *Elife,* 8.

Doussau, F., H. Schmidt, K. Dorgans, A. M. Valera, B. Poulain & P. Isope (2017) Frequency-dependent mobilization of heterogeneous pools of synaptic vesicles shapes presynaptic plasticity. *Elife,* 6.

Dugué, G. P., N. Brunel, V. Hakim, E. Schwartz, M. Chat, M. Lévesque, R. Courtemanche, C. Léna & S. Dieudonné (2009) Electrical coupling mediates tunable low-frequency oscillations and resonance in the cerebellar Golgi cell network. *Neuron,* 61**,** 126-39.

Einevoll, G. T., C. Kayser, N. K. Logothetis & S. Panzeri (2013) Modelling and analysis of local field potentials for studying the function of cortical circuits. *Nat Rev Neurosci,* 14**,** 770-85.
Forti, L., E. Cesana, J. Mapelli & E. D'Angelo (2006) Ionic mechanisms of autorhythmic firing in rat cerebellar Golgi cells. *J Physiol,* 574**,** 711-29.
Foster, K. A., J. J. Crowley & W. G. Regehr (2005) The influence of multivesicular release and postsynaptic receptor saturation on transmission at granule cell to Purkinje cell synapses. *J Neurosci,* 25**,** 11655-65.
Gagliano, G., A. Monteverdi, T. Soda, U. Laforenza, F. Moccia, L. Mapelli, E. D'Angelo (*in preparation*) Neurovascular coupling in the granular layer of cerebellum.
Gall, D., F. Prestori, E. Sola, A. D'Errico, C. Roussel, L. Forti, P. Rossi & E. D'Angelo (2005) Intracellular calcium regulation by burst discharge determines bidirectional long-term synaptic plasticity at the cerebellum input stage. *J Neurosci,* 25**,** 4813-22.
Gandolfi, D., P. Lombardo, J. Mapelli, S. Solinas & E. D'Angelo (2013) θ-Frequency resonance at the cerebellum input stage improves spike timing on the millisecond time-scale. *Front Neural Circuits,* 7**,** 64.
Gandolfi, D., P. Pozzi, M. Tognolina, G. Chirico, J. Mapelli & E. D'Angelo (2014) The spatiotemporal organization of cerebellar network activity resolved by two-photon imaging of multiple single neurons. *Front Cell Neurosci,* 8**,** 92.
Gao, Z., B. J. van Beugen & C. I. De Zeeuw (2012) Distributed synergistic plasticity and cerebellar learning. *Nat Rev Neurosci,* 13**,** 619-35.
Grangeray-Vilmint, A., A. M. Valera, A. Kumar & P. Isope (2018) Short-Term Plasticity Combines with Excitation-Inhibition Balance to Expand Cerebellar Purkinje Cell Dynamic Range. *J Neurosci,* 38**,** 5153-5167.
Hawkes, R. (2014) Purkinje cell stripes and long-term depression at the parallel fiber-Purkinje cell synapse. *Front Syst Neurosci,* 8**,** 41.
Herculano-Houzel, S. (2009) The human brain in numbers: a linearly scaled-up primate brain. *Front Hum Neurosci,* 3**,** 31.
--- (2010) Coordinated scaling of cortical and cerebellar numbers of neurons. *Front Neuroanat,* 4**,** 12.
Heinricher MM. Principles of Extracellular Single-Unit Recording. Thieme Verlagsgruppe, Stuttgart, New York, Delhi, Rio, 2004.
Howarth, C., C. M. Peppiatt-Wildman & D. Attwell (2010) The energy use associated with neural computation in the cerebellum. *J Cereb Blood Flow Metab,* 30**,** 403-14.
Hoxha, E., F. Tempia, P. Lippiello & M. C. Miniaci (2016) Modulation, Plasticity and Pathophysiology of the Parallel Fiber-Purkinje Cell Synapse. *Front Synaptic Neurosci,* 8**,** 35.
Häusser, M. & A. Roth (1997) Dendritic and somatic glutamate receptor channels in rat cerebellar Purkinje cells. *J Physiol,* 501 (Pt 1)**,** 77-95.
Isope, P. & B. Barbour (2002) Properties of unitary granule cell-->Purkinje cell synapses in adult rat cerebellar slices. *J Neurosci,* 22**,** 9668-78.
Ito, M. (2006) Cerebellar circuitry as a neuronal machine. *Prog Neurobiol,* 78**,** 272-303.
--- (2008) Control of mental activities by internal models in the cerebellum. *Nat Rev Neurosci,* 9**,** 304-13.
Kanichay, R. T. & R. A. Silver (2008) Synaptic and cellular properties of the feedforward inhibitory circuit within the input layer of the cerebellar cortex. *J Neurosci,* 28**,** 8955-67.
Kelly, R. M. & P. L. Strick (2003) Cerebellar loops with motor cortex and prefrontal cortex of a nonhuman primate. *J Neurosci,* 23**,** 8432-44.

Kim, S. J., Y. Jin, J. Kim, J. H. Shin, P. F. Worley & D. J. Linden (2008) Transient upregulation of postsynaptic IP3-gated Ca release underlies short-term potentiation of metabotropic glutamate receptor 1 signaling in cerebellar Purkinje cells. *J Neurosci,* 28**,** 4350-5.

Klein, A. P., J. L. Ulmer, S. A. Quinet, V. Mathews & L. P. Mark (2016) Nonmotor Functions of the Cerebellum: An Introduction. *AJNR Am J Neuroradiol,* 37**,** 1005-9.

Koziol, L. F., D. Budding, N. Andreasen, S. D'Arrigo, S. Bulgheroni, H. Imamizu, M. Ito, M. Manto, C. Marvel, K. Parker, G. Pezzulo, N. Ramnani, D. Riva, J. Schmahmann, L. Vandervert & T. Yamazaki (2014) Consensus paper: the cerebellum's role in movement and cognition. *Cerebellum,* 13**,** 151-77.

Kreitzer, A. C. & W. G. Regehr (2000) Modulation of transmission during trains at a cerebellar synapse. *J Neurosci,* 20**,** 1348-57.

Lackey, E. P., D. H. Heck & R. V. Sillitoe (2018) Recent advances in understanding the mechanisms of cerebellar granule cell development and function and their contribution to behavior. *F1000Res,* 7.

Lauritzen, M., C. Mathiesen, K. Schaefer & K. J. Thomsen (2012) Neuronal inhibition and excitation, and the dichotomic control of brain hemodynamic and oxygen responses. *Neuroimage,* 62**,** 1040-50.

Le Guen, M. C. & C. I. De Zeeuw (2010) Presynaptic plasticity at cerebellar parallel fiber terminals. *Funct Neurol,* 25**,** 141-51.

Lindén, H., K. H. Pettersen & G. T. Einevoll (2010) Intrinsic dendritic filtering gives low-pass power spectra of local field potentials. *J Comput Neurosci,* 29**,** 423-44.

Maffei, A., F. Prestori, P. Rossi, V. Taglietti & E. D'Angelo (2002) Presynaptic current changes at the mossy fiber-granule cell synapse of cerebellum during LTP. *J Neurophysiol,* 88**,** 627-38.

Maffei, A., F. Prestori, K. Shibuki, P. Rossi, V. Taglietti & E. D'Angelo (2003) NO enhances presynaptic currents during cerebellar mossy fiber-granule cell LTP. *J Neurophysiol,* 90**,** 2478-83.

Manto, M., J. M. Bower, A. B. Conforto, J. M. Delgado-García, S. N. da Guarda, M. Gerwig, C. Habas, N. Hagura, R. B. Ivry, P. Mariën, M. Molinari, E. Naito, D. A. Nowak, N. Oulad Ben Taib, D. Pelisson, C. D. Tesche, C. Tilikete & D. Timmann (2012) Consensus paper: roles of the cerebellum in motor control--the diversity of ideas on cerebellar involvement in movement. *Cerebellum,* 11**,** 457-87.

Mapelli, J. & E. D'Angelo (2007) The spatial organization of long-term synaptic plasticity at the input stage of cerebellum. *J Neurosci,* 27**,** 1285-96.

Mapelli, J., D. Gandolfi & E. D'Angelo (2010a) Combinatorial responses controlled by synaptic inhibition in the cerebellum granular layer. *J Neurophysiol,* 103**,** 250-61.

--- (2010b) High-Pass Filtering and Dynamic Gain Regulation Enhance Vertical Bursts Transmission along the Mossy Fiber Pathway of Cerebellum. *Front Cell Neurosci,* 4**,** 14.

Mapelli, L., G. Gagliano, T. Soda, U. Laforenza, F. Moccia & E. U. D'Angelo (2017) Granular Layer Neurons Control Cerebellar Neurovascular Coupling Through an NMDA Receptor/NO-Dependent System. *J Neurosci,* 37**,** 1340-1351.

Mapelli, L., M. Pagani, J. A. Garrido & E. D'Angelo (2015) Integrated plasticity at inhibitory and excitatory synapses in the cerebellar circuit. *Front Cell Neurosci,* 9**,** 169.

Mapelli, L., P. Rossi, T. Nieus & E. D'Angelo (2009) Tonic activation of GABAB receptors reduces release probability at inhibitory connections in the cerebellar glomerulus. *J Neurophysiol,* 101**,** 3089-99.

Mapelli, L., S. Solinas & E. D'Angelo (2014) Integration and regulation of glomerular inhibition in the cerebellar granular layer circuit. *Front Cell Neurosci,* 8**,** 55.

Mathiesen, C., K. Caesar, N. Akgören & M. Lauritzen (1998) Modification of activity-dependent increases of cerebral blood flow by excitatory synaptic activity and spikes in rat cerebellar cortex. *J Physiol,* 512 (Pt 2)**,** 555-66.

Mathiesen, C., K. Caesar & M. Lauritzen (2000) Temporal coupling between neuronal activity and blood flow in rat cerebellar cortex as indicated by field potential analysis. *J Physiol,* 523 Pt 1**,** 235-46.

Middleton, S. J., C. Racca, M. O. Cunningham, R. D. Traub, H. Monyer, T. Knöpfel, I. S. Schofield, A. Jenkins & M. A. Whittington (2008) High-frequency network oscillations in cerebellar cortex. *Neuron,* 58**,** 763-74.

Miller, S. M. (2007) On the correlation/constitution distinction problem (and other hard problems) in the scientific study of consciousness. *Acta Neuropsychiatr,* 19**,** 159-76.

Mitchell, S. J. & R. A. Silver (2000a) GABA spillover from single inhibitory axons suppresses low-frequency excitatory transmission at the cerebellar glomerulus. *J Neurosci,* 20**,** 8651-8.

--- (2000b) Glutamate spillover suppresses inhibition by activating presynaptic mGluRs. *Nature,* 404**,** 498-502.

--- (2003) Shunting inhibition modulates neuronal gain during synaptic excitation. *Neuron,* 38**,** 433-45.

Monaghan A, Anderson K (1991) Heterogeneity and organizaton of excitatory amino acid receptors and transporters. In: Excitatory amino acids and synaptic function (H W, A T, eds), pp 33- 54. London: Academic.

Nielsen, T. A., D. A. DiGregorio & R. A. Silver (2004) Modulation of glutamate mobility reveals the mechanism underlying slow-rising AMPAR EPSCs and the diffusion coefficient in the synaptic cleft. *Neuron,* 42**,** 757-71.

Nieus, T., E. Sola, J. Mapelli, E. Saftenku, P. Rossi & E. D'Angelo (2006) LTP regulates burst initiation and frequency at mossy fiber-granule cell synapses of rat cerebellum: experimental observations and theoretical predictions. *J Neurophysiol,* 95**,** 686-99.

Nieus, T. R., L. Mapelli & E. D'Angelo (2014) Regulation of output spike patterns by phasic inhibition in cerebellar granule cells. *Front Cell Neurosci,* 8**,** 246.

O'Connor, S. M., R. W. Berg & D. Kleinfeld (2002) Coherent electrical activity between vibrissa sensory areas of cerebellum and neocortex is enhanced during free whisking. *J Neurophysiol,* 87**,** 2137-48.

Obien, M. E., K. Deligkaris, T. Bullmann, D. J. Bakkum & U. Frey (2014) Revealing neuronal function through microelectrode array recordings. *Front Neurosci,* 8**,** 423.

Öner, M., & Kocakoç, İ. D. (2017). JMASM 49: A Compilation of Some Popular Goodness of Fit Tests for Normal Distribution: Their Algorithms and MATLAB Codes (MATLAB). Journal of Modern Applied Statistical Methods, 16(2), 547-575. doi: 10.22237/jmasm/1509496200

Palesi, F., J. D. Tournier, F. Calamante, N. Muhlert, G. Castellazzi, D. Chard, E. D'Angelo & C. A. Wheeler-Kingshott (2015) Contralateral cerebello-thalamo-cortical pathways with prominent involvement of associative areas in humans in vivo. *Brain Struct Funct,* 220**,** 3369-84.

Pellerin, J. P. & Y. Lamarre (1997) Local field potential oscillations in primate cerebellar cortex during voluntary movement. *J Neurophysiol,* 78**,** 3502-7.

Popa, D., M. Spolidoro, R. D. Proville, N. Guyon, L. Belliveau & C. Léna (2013) Functional role of the cerebellum in gamma-band synchronization of the sensory and motor cortices. *J Neurosci,* 33**,** 6552-6.

Prestori, F., L. Mapelli & E. D'Angelo (2019) Diverse Neuron Properties and Complex Network Dynamics in the Cerebellar Cortical Inhibitory Circuit. *Front Mol Neurosci,* 12**,** 267.

Ramnani, N. (2006) The primate cortico-cerebellar system: anatomy and function. *Nat Rev Neurosci,* 7**,** 511-22.
Rancz, E. A., T. Ishikawa, I. Duguid, P. Chadderton, S. Mahon & M. Häusser (2007) High-fidelity transmission of sensory information by single cerebellar mossy fibre boutons. *Nature,* 450**,** 1245-8.
Rizza, M. F., F. Locatelli, S. Masoli, D. Sanchez Ponce, A. Munoz, F. Prestori, E. D'Angelo (2020) Stellate computational modelling predicts signal filtering in the molecular layer circuit of cerebellum bioRxiv 2020.08.25.266429.
Roostaei, T., A. Nazeri, M. A. Sahraian & A. Minagar (2014) The human cerebellum: a review of physiologic neuroanatomy. *Neurol Clin,* 32**,** 859-69.
Ros, H., R. N. Sachdev, Y. Yu, N. Sestan & D. A. McCormick (2009) Neocortical networks entrain neuronal circuits in cerebellar cortex. *J Neurosci,* 29**,** 10309-20.
Rössert, C., S. Solinas, E. D'Angelo, P. Dean & J. Porrill (2014) Model cerebellar granule cells can faithfully transmit modulated firing rate signals. *Front Cell Neurosci,* 8**,** 304.
Sargent, P. B., C. Saviane, T. A. Nielsen, D. A. DiGregorio & R. A. Silver (2005) Rapid vesicular release, quantal variability, and spillover contribute to the precision and reliability of transmission at a glomerular synapse. *J Neurosci,* 25**,** 8173-87.
Satake, S., F. Saitow, D. Rusakov & S. Konishi (2004) AMPA receptor-mediated presynaptic inhibition at cerebellar GABAergic synapses: a characterization of molecular mechanisms. *Eur J Neurosci,* 19**,** 2464-74.
Saviane, C. & R. A. Silver (2006) Fast vesicle reloading and a large pool sustain high bandwidth transmission at a central synapse. *Nature,* 439**,** 983-7.
Schmahmann, J. D. (2019) The cerebellum and cognition. *Neurosci Lett,* 688**,** 62-75.
Sims, R. E. & N. A. Hartell (2005) Differences in transmission properties and susceptibility to long-term depression reveal functional specialization of ascending axon and parallel fiber synapses to Purkinje cells. *J Neurosci,* 25**,** 3246-57.
--- (2006) Differential susceptibility to synaptic plasticity reveals a functional specialization of ascending axon and parallel fiber synapses to cerebellar Purkinje cells. *J Neurosci,* 26**,** 5153-9.
Sola, E., F. Prestori, P. Rossi, V. Taglietti & E. D'Angelo (2004) Increased neurotransmitter release during long-term potentiation at mossy fibre-granule cell synapses in rat cerebellum. *J Physiol,* 557**,** 843-61.
Solinas, S., L. Forti, E. Cesana, J. Mapelli, E. De Schutter & E. D'Angelo (2007) Fast-reset of pacemaking and theta-frequency resonance patterns in cerebellar golgi cells: simulations of their impact in vivo. *Front Cell Neurosci,* 1**,** 4.
Solinas, S., T. Nieus & E. D'Angelo (2010) A realistic large-scale model of the cerebellum granular layer predicts circuit spatio-temporal filtering properties. *Front Cell Neurosci,* 4**,** 12.
Southam, E., R. Morris & J. Garthwaite (1992) Sources and targets of nitric oxide in rat cerebellum. *Neurosci Lett,* 137**,** 241-4.
Stoodley, C. J. & J. D. Schmahmann (2009) Functional topography in the human cerebellum: a meta-analysis of neuroimaging studies. *Neuroimage,* 44**,** 489-501.
--- (2010) Evidence for topographic organization in the cerebellum of motor control versus cognitive and affective processing. *Cortex,* 46**,** 831-44.
Storm, J. F., M. Boly, A. G. Casali, M. Massimini, U. Olcese, C. M. A. Pennartz & M. Wilke (2017) Consciousness Regained: Disentangling Mechanisms, Brain Systems, and Behavioral Responses. *J Neurosci,* 37**,** 10882-10893.
Szapiro, G. & B. Barbour (2007) Multiple climbing fibers signal to molecular layer interneurons exclusively via glutamate spillover. *Nat Neurosci,* 10**,** 735-42.

Tabuchi, S., J. I. Gilmer, K. Purba & A. L. Person (2019) Pathway-Specific Drive of Cerebellar Golgi Cells Reveals Integrative Rules of Cortical Inhibition. *J Neurosci,* 39**,** 1169-1181.

Timmann, D., J. Drepper, M. Frings, M. Maschke, S. Richter, M. Gerwig & F. P. Kolb (2010) The human cerebellum contributes to motor, emotional and cognitive associative learning. A review. *Cortex,* 46**,** 845-57.

Tononi, G. (2005) Consciousness, information integration, and the brain. *Prog Brain Res,* 150**,** 109-26.

Tononi, G., M. Boly, M. Massimini & C. Koch (2016) Integrated information theory: from consciousness to its physical substrate. *Nat Rev Neurosci,* 17**,** 450-61.

Tononi, G. & G. M. Edelman (1998) Consciousness and complexity. *Science,* 282**,** 1846-51.

Tononi, G. & C. Koch (2008) The neural correlates of consciousness: an update. *Ann N Y Acad Sci,* 1124**,** 239-61.

--- (2015) Consciousness: here, there and everywhere? *Philos Trans R Soc Lond B Biol Sci,* 370.

Valera, A. M., F. Binda, S. A. Pawlowski, J. L. Dupont, J. F. Casella, J. D. Rothstein, B. Poulain & P. Isope (2016) Stereotyped spatial patterns of functional synaptic connectivity in the cerebellar cortex. *Elife,* 5.

Valera, A. M., F. Doussau, B. Poulain, B. Barbour & P. Isope (2012) Adaptation of granule cell to Purkinje cell synapses to high-frequency transmission. *J Neurosci,* 32**,** 3267-80.

Vyazovskiy Vladyslav V., Olcese Umberto & Tononi Giulio. 2012. Investigating Sleep Homeostasis with Extracellular Recording of Multiunit Activity from the Neocortex in Freely Behaving Rats. In *Neuronal Network Analysis,* ed. S. Protocols.

Wadiche, J. I. & C. E. Jahr (2001) Multivesicular release at climbing fiber-Purkinje cell synapses. *Neuron,* 32**,** 301-13.

Wall, M. J. (2005) Short-term synaptic plasticity during development of rat mossy fibre to granule cell synapses. *Eur J Neurosci,* 21**,** 2149-58.

Walter, J. T., M. J. Dizon & K. Khodakhah (2009) The functional equivalence of ascending and parallel fiber inputs in cerebellar computation. *J Neurosci,* 29**,** 8462-73.

Xu-Friedman, M. A., K. M. Harris & W. G. Regehr (2001) Three-dimensional comparison of ultrastructural characteristics at depressing and facilitating synapses onto cerebellar Purkinje cells. *J Neurosci,* 21**,** 6666-72.

Xu-Friedman, M. A. & W. G. Regehr (2003) Ultrastructural contributions to desensitization at cerebellar mossy fiber to granule cell synapses. *J Neurosci,* 23**,** 2182-92.

Zhou, H., Z. Lin, K. Voges, C. Ju, Z. Gao, L. W. Bosman, T. J. Ruigrok, F. E. Hoebeek, C. I. De Zeeuw & M. Schonewille (2014) Cerebellar modules operate at different frequencies. *Elife,* 3**,** e02536.

Zucker, R. S. & W. G. Regehr (2002) Short-term synaptic plasticity. *Annu Rev Physiol,* 64**,** 355-405.

Acknowledgments

Thank you to Professor Egidio D'Angelo for the opportunity to enter in this lab and increase my interest and my knowledge in neuroscience.
Thank you to Lisa Mapelli for the supervision of this work.
Thank you to all the people in the lab that lived with me these intense three years of adventures: to Giuseppe for being my preferred "MAESTRO" at the beginning and for all the hours passed arguing in front of tables and data; to Stefano M., for the most precious help received aiming to make the computer work and for giving me the permission to use his photo as a real "holy card"; to Stefano C., for all the teachings in matlab and coding and the patience in explaining me how to do some parts of my crazy analysis; to Danila, words can't fully explain all the reasons; to Teresa and Mary, for all the time spent laughing and talking and for being a real psychologist especially in the first years; to Ileana, for all the songs we've listened to overcome desperation; to all the people that I met in these years and that contributed to this experience.
Thank you to Alessandro, for all the explanations given, for all the time spent teaching me something about data analysis and for all the hours passed working together on the HD-MEA and learning every time something completely new.
Thank you to Gabriele, Gianfranca and Maurizio, for all the jokes and laughs of these years, I will never forget our time together.
Grazie a mamma e papà, per avermi sempre ascoltata e supportata anche quando ho visto tutto nero…siete voi per me "la molecola su un milione".
Grazie a Matteo, più passano gli anni più dovrei scrivere un libro che contenga tutti i perché.
Thank you to all the people that during this PhD experience supported me and to all the ones that did not believe in my ability in this work, because both contributed to convince me to never give up and always keep my enthusiasm high.